ISTANBUL TECHNICAL UNIVERSITY ★ GRADUATE SCHOOL

DEVELOPMENT OF E-TEXTILE BASED RFID ENABLED MOISTURE SENSOR FOR WEARABLE TECHNOLOGIES

Ph.D. THESIS

Meltem TEKÇİN

Department of Textile Engineering

Textile Engineering Programme

JANUARY 2024

ISTANBUL TECHNICAL UNIVERSITY ★ GRADUATE SCHOOL

DEVELOPMENT OF E-TEXTILE BASED RFID ENABLED MOISTURE SENSOR FOR WEARABLE TECHNOLOGIES

Ph.D. THESIS

Meltem TEKÇİN
(503162801)

Department of Textile Engineering

Textile Engineering Programme

Thesis Advisor: Assoc. Prof. Dr. Senem KURŞUN
Thesis Co-Advisor: Prof. Dr. Selçuk PAKER

JANUARY 2024

ISTANBUL TEKNİK ÜNİVERSİTESİ ★ LİSANSÜSTÜ EĞİTİM ENSTİTÜSÜ

GİYİLEBİLİR TEKNOLOJİLER İÇİN E-TEKSTİL TABANLI RFID İŞLEVLİ NEM SENSÖRÜ GELİŞTİRİLMESİ

DOKTORA TEZİ

Meltem TEKÇİN
(503162801)

Tekstil Mühendisliği Anabilim Dalı

Tekstil Mühendisliği Programı

Tez Danışmanı: Doç. Dr. Senem KURŞUN
Eş Danışman: Prof. Dr. Selçuk PAKER

OCAK 2024

Meltem Tekçin, a Ph.D. student of İTU Graduate School student ID 503162801, successfully defended the thesis/dissertation entitled "DEVELOPMENT OF E-TEXTILE BASED RFID ENABLED MOISTURE SENSOR FOR WEARABLE TECHNOLOGIES", which she prepared after fulfilling the requirements specified in the associated legislations, before the jury whose signatures are below.

Thesis Advisor :	**Assoc. Prof. Dr. Senem KURŞUN** İstanbul Technical University	.....
Co-advisor :	**Prof. Dr. Selçuk PAKER** İstanbul Technical University	.....
Jury Members :	**Assoc. Prof. Dr. Umut Kıvanç ŞAHİN** İstanbul Technical University	.....
	Assist. Prof. Dr. Mehmet Kürşat YALÇIN Niğde Ömer Halisdemir University	.....
	Assist. Prof. Dr. Egemen BİLGİN MEF University	.....
	Assoc. Prof. Dr. Ersin SAYAR İstanbul Technical University	.....
	Prof. Dr. Merih PALANDÖKEN İzmir Katip Çelebi University	.....

Date of Submission : 1 December 2023
Date of Defense : 12 January 2024

To my family,

FOREWORD

First of all, I would like to express my deepest gratitude to my esteemed thesis advisor, Assoc. Prof. Dr. Senem KURŞUN, for her academic guidance, continuous support, valuable advice and efforts throughout my PhD. She taught me all the steps required to be a good researcher, and while teaching, she was much closer than an advisor, and constantly enlightened my work with her motivating, energetic and positive attitude.

I would like to express my special thanks to my co-advisor, Prof. Dr. Selçuk PAKER, for his contributions to my thesis, his time, his valuable comments, suggestions and help.

I would like to thank Prof. Dr. Merih PALANDÖKEN for guiding my study, his time, understanding and support at all times.

Deepest thanks also to my thesis committee members, Assoc. Prof. Dr. Umut Kıvanç ŞAHİN, Assist. Prof. Dr. Mehmet Kürşat YALÇIN and Assist. Prof. Dr. Egemen BİLGİN, for their time, support and valuable comments that improved my thesis study.

I would like to thank The Scientific and Technological Research Council of Turkey (TÜBİTAK; Project no: 119M976) for funding the research work presented in the thesis.

I also would like to thank Assoc. Prof. Dr. Ersin SAYAR for his support, encouragement and contribution to my thesis.

I also want to thank Dr. Burcu ARMAN KUZUBAŞOĞLU and İsmail AKDAĞ for their support and help during my thesis study.

Finally, I would like to express my gratitude to my mother, father and brother, Yasemin, Mehmet and Kemal Onur TEKÇİN, who have always been by my side, for their endless support, encouragement and motivation.

December 2023

Meltem TEKÇİN
(M.Sc. Textile Engineer)

TABLE OF CONTENTS

Page

FOREWORD ..... **ix**
TABLE OF CONTENTS ..... **xi**
ABBREVIATIONS ..... **xiii**
SYMBOLS ..... **xv**
LIST OF TABLES ..... **xvii**
LIST OF FIGURES ..... **xix**
SUMMARY ..... **xxi**
ÖZET ..... **xxiii**
1. INTRODUCTION **1**
2. WEARABLE AND FLEXIBLE HUMIDITY SENSOR INTEGRATED TO DISPOSABLE DIAPERS FOR WETNESS MONITORING AND URINARY INCONTINENCE **5**
2.1 Introduction 6
2.2 Materials and Methods 9
2.2.1 Chemicals and materials 9
2.2.2 Ink formulation for inkjet printing 10
2.2.3 Humidity sensor design and fabrication 11
2.2.4 Measurement of the humidity sensor behavior 13
2.3 Results 14
2.3.1 Conductive polymer ink (PEDOT:PSS) characterization 14
2.3.2 Humidity sensor characterization 15
2.3.3 Application of the humidity sensor to disposable diapers for urinary incontinence 18
2.4 Conclusions 21
2.5 Author Contributions 22
2.6 Funding 22
2.7 Data Availability Statement 23
2.8 Conflicts of Interest 23
3. UHF-RFID ENABLED WEARABLE FLEXIBLE PRINTED SENSOR WITH ANTENNA PERFORMANCE **25**
3.1 Introduction 26
3.2 Materials and Methods 29
3.2.1 Chemicals-materials and ink formulation 29
3.2.2 UHF-RFID enabled wearable sensor design and fabrication 30
3.2.3 Impedance measurement method 32
3.2.4 Gain measurement method 33
3.2.5 Bending measurement method 33
3.3 Results and Discussion 34
3.3.1 Impedance measurement results of the non-sintered textile antennas 34
3.3.2 Impedance measurement results of the sintered textile antennas 35
3.3.3 Gain measurement results of the sintered textile antennas 37
3.3.4 Bending measurement results of the sintered textile antennas 37

3.4 Conclusion 38
3.5 Declaration of Competing Interest 39
3.6 Acknowledgement 39
3.7 Data availability 39
4. WEARABLE UHF-RFID SENSOR FOR WETNESS DETECTION 41
4.1 Introduction 42
4.2 Materials and Methods 45
4.2.1 Chemicals, materials and ink formulation 45
4.2.2 UHF-RFID wetness sensor design, simulation and fabrication 46
4.2.3 Integration of the RFID sensor onto adult diaper for RSSI measurements 49
4.2.4 Bending simulation and bending measurement of RFID sensor structure 52
4.3 Results and Discussion 53
4.4 Conclusion 62
5. CONCLUSIONS AND RECOMMENDATIONS 63
REFERENCES 69
CURRICULUM VITAE 81

ABBREVIATIONS

3D	**:** Three Dimensional
ADL	**:** Acquisition/Distribution Layer
CST	**:** Computer Simulation Technology
EDANA	**:** European Disposable and Nonwoven Association
E-Textile	**:** Electronic Textile
IAD	**:** Incontinence Associated Dermatitis
IC	**:** Integrated Circuit
IDE	**:** Interdigitated Electrode
NaCl	**:** Sodium Chloride
PE	**:** Polyethylene
PEDOT:PSS	**:** Poly(3,4-ethylenedioxythiophene): Polystyrene Sulfonate
pH	**:** Potential Hydrogen
PP	**:** Polypropylene
PU	**:** Polyurethane
PVA	**:** Polyvinyl Acetate
RF	**:** Radio Frequency
RFID	**:** Radio Frequency Identification
RH	**:** Relative Humidity
RSSI	**:** Received Signal Strength Indicator
SAP	**:** Superabsorbent Polymer
SIW	**:** Substrate Integrated Waveguide
SRR	**:** Split-ring Resonator
Triton X-100	**:** 2-[4-(2,4,4-trimethylpentan-2-yl)phenoxy]ethanol
TUBITAK	**:** The Scientific and Technological Research Council of Turkey
UI	**:** Urinary Incontinence
UHF	**:** Ultra High Frequency
USB	**:** Universal Serial Bus
VNA	**:** Vector Network Analyzer
WiFi	**:** Wireless Fiber

SYMBOLS

cm	**:** Centimeter
cP	**:** Centipoise
dB	**:** Decibel
dBi	**:** Decibels relative to isotropic
dBm	**:** Decibel milliwatts
g	**:** Gram
kHz	**:** Kilohertz
mg	**:** Milligram
min	**:** Minutes
mL	**:** Milliliter
mm	**:** Millimeter
mm^2	**:** Square Millimeter
mm^3	**:** Cubic Millimeter
MHz	**:** Megahertz
MΩ	**:** Megaohm
pF	**:** Picofarad
s	**:** Seconds
µS	**:** Microsiemens
^{o}	**:** Degree
^oC	**:** Celsius
%	**:** Percentage
Ω	**:** Ohm
$\|S_{11}\|$	**:** Reflection Coefficient
σ	**:** Conductivity
ε	**:** Relative Permitivity

LIST OF TABLES

Page

Table 3.1 : Comparison of the proposed RFID antenna with the other textile-based flexible RFID antennas..... **28**
Table 4.1 : Dimensions of proposed RFID sensor structure. **47**
Table 4.2 : RSSI levels for different situations on RFID sensor structure. **55**
Table 4.3 : Near field RSSI measurement results of RFID sensor structure before and after deformation test. **58**
Table 4.4 : RSSI values of RFID sensor structure with diaper for different bending angles at 30 cm. **59**
Table 4.5 : Comparison of passive RFID diaper wetness sensors. **60**

LIST OF FIGURES

Page

Figure 2.1 : Schematic view of inkjet-printed humidity sensor fabrication, and integration into an adult diaper. **10**
Figure 2.2 : Dimensions of the humidity sensor design. **12**
Figure 2.3 : Printed humidity sensor and conductive yarns connected to its ends. .. **12**
Figure 2.4 : Humidity chamber. **13**
Figure 2.5 : Graph of the resistance change of the sensor against relative humidity..... **16**
Figure 2.6 : Graph of fabric moisture change against relative humidity. **17**
Figure 2.7 : Graph of repeatability test of the sensor while working at the interval of 35–100% RH (from 35% RH to 100% RH and then 100% RH to 35% RH). (a) For five cycles, (b) for 50 cycles. **18**
Figure 2.8 : Graph of wrist bending test of the sensor. **19**
Figure 2.9 : The test setup for urinary incontinence detection. **19**
Figure 2.10 : Graph of the resistance change of the humidity sensor against different amounts of water. **20**
Figure 2.11 : Graph of the resistance values of the humidity sensor against different amounts of water. **21**
Figure 3.1 : Schematic view of the UHF-RFID enabled wearable sensor fabrication, and impedance measurement..... **29**
Figure 3.2 : Image of the designed UHF-RFID enabled wearable sensor. **30**
Figure 3.3 : Pad printing machine. **31**
Figure 3.4 : Printed UHF-RFID enabled wearable sensor. **31**
Figure 3.5 : Experiment setup for the impedance measurement. **32**
Figure 3.6 : Gain measurement setup. **33**
Figure 3.7 : (a) Bending test setup, (b) Bending test of antenna with x direction, (c) Bending test of antenna with y direction. 33
Figure 3.8 : Antenna impedance graph of the non-sintered textile antennas. **34**
Figure 3.9 : Reflection coefficients of the non-sintered textile antennas. **35**
Figure 3.10 : Antenna impedance graph of the sintered textile antennas. **36**
Figure 3.11 : Reflection coefficients of the sintered textile antennas. **36**
Figure 3.12 : S21 measurements of the reference antenna and textile antenna. **38**
Figure 3.13 : Reflection coefficients of the textile antenna in different bending directions. **38**
Figure 4.1 : Proposed RFID sensor structure..... **47**
Figure 4.2 : $|S_{11}|$ parameter of RFID sensor structure at 867 MHz. **47**
Figure 4.3 : 2D polar radiation patterns for RFID sensor structure. **48**
Figure 4.4 : Surface current distribution at 867 MHz. **48**
Figure 4.5 : a) Printed RFID sensor structure (b) Printed RFID sensor structure with chip integration. **49**
Figure 4.6 : Schematic view of the integration of the RFID sensor into the diaper. **50**
Figure 4.7 : RSSI near field measurement setup. **50**

Figure 4.8 : RSSI measurement setup with highly directive 2 × 2 antenna array at practical separation distances emulating the real life..... **51**
Figure 4.9 : Four layered human body phantom model. **53**
Figure 4.10 : RSSI levels for different salt water amounts on RFID sensor structure..... **54**
Figure 4.11 : RSSI values of RFID sensor structure for different orientation angles with the separation distance of 32 cm, 40 cm, and 50 cm. **56**
Figure 4.12 : $|S_{11}|$ values of RFID sensor structure placed on the human body model against different bending angles. **57**
Figure 4.13 : (a) $|S_{11}|$ values of RFID sensor structure against positive bending angles (b) $|S_{11}|$ values of RFID sensor structure against negative bending angles. **58**

DEVELOPMENT OF E-TEXTILE BASED RFID ENABLED MOISTURE SENSOR FOR WEARABLE TECHNOLOGIES

SUMMARY

The applications of e-textiles are progressively expanding with the advancements in technology on a daily basis. Particularly versatile, wearable, flexible, light, thin and small electronic structures can be seamlessly employed across diverse domains, owing to the incorporation of textile materials. It is noteworthy that the sensors used in heart rate, respiratory rate monitoring, sweat and wetness detection used in health monitoring areas have recently consisted of textile-based electronic structures. Although there are many sensor structures used for wetness detection, the disadvantages of their usage are that these structures are generally rigid, hard, large and uncomfortable. Instead of these sensors, thin, flexible, light, textile-based sensors that are compatible with the user's movement are needed. On the other hand, studies indicate that the world population is gradually aging and urinary incontinence is becoming more common health problem in aging people. For these reasons, structures that detect urinary incontinence on time are needed for sick elderly individuals in terms of both personal comfort and health of users, and to alleviate the workload of their caregivers.

This thesis aims to develop a textile-based, wearable, flexible, lightweight and comfortable RFID enabled moisture sensor structures that detects moisture and wetness while transmitting RF signals. Furthermore, the objective lies on printing techniques and ink formulations for crafting these sensors.

This thesis consists of three articles, arranged by paying attention to the integrity of the scope. All of the articles given within the scope of the thesis are original and add innovation to the literature. In the articles, important and unique results of the thesis topic are discussed.

In the first article, the design of a humidity sensor for wetness detection with respect to design criteria found in the literature research, was presented. The designed humidity sensor was printed on a polyamide-based taffeta label fabric using PEDOT:PSS conductive polymer by inkjet printing method. Ink characterizations were carried out to make PEDOT:PSS polymer suitable for inkjet printing. Sensor performance was measured in a closed humidity chamber where the relative humidity is controlled by an automatic humidifier against change in electrical resistance values of the sensor. Response and recovery times, sensitivity and repeatability of the sensor sensor were also measured. The humidity sensor was integrated onto the diaper to detect urinary incontinence. The variations in electrical resistance values of the sensor were analyzed by exposing it to varying quantities of an urine-like water solution, applied to the sensor integrated onto the diaper.

The second article examines the UHF-RFID antenna performance of the proposed sensor structure. The sensor structure designed in this article was printed on polyamide-based taffeta label fabric using silver nanoparticle ink by pad printing

method with different print passes. The importance of the sintering process was investigated and its effect on the results presented in the article was discussed. While the sintering process was applied to one group of sensor samples, the sintering process was not applied to the other group for comparison. UHF-RFID antenna performance of all samples was examined using a vector network analyzer. In addition to impedance measurements, gain and bending measurements of the textile antennas were carried out in order to show the antennas' flexibility. It has been determined that the sensor samples exposed to the sintering process operate as antennas.

Finally, the third article encompassed the execution of an RFID sensor design capable of serving dual roles as both a sensor and an antenna. The proposed structure was designed using the CST Studio program, aiming to operate at 867 MHz according to European band. The RFID sensor was printed on polyamide-based taffeta label fabric by pad printing method using silver nanoparticle ink. A chip was integrated onto the structure so that the RFID sensor operates at the targeted frequency. The RFID sensor was integrated onto the diaper considering the real usage environment. RSSI measurements were made using both near-field RSSI measurement setup and highly antenna arrays. Additionally, the strength of the proposed structure was investigated by applying bending simulation and deformation tests. RSSI changes of the structure were examined by dropping distilled water, salt water and artificial urine solutions to simulate urinary incontinence. In addition, the maximum reliable reading range was determined by changing the distances between the RFID sensor and the reader antenna.

In summary, all three articles presented within the scope of the thesis contribute to the literature separately. The articles reveal that the thesis topic and the results obtained as a result of the studies are original and innovative. The fact that the thesis topic is up-to-date and coupled with its relevance to personal health monitoring makes the results of the study important for everyone. The outcomes delineated in the articles and the devised sensors carry profound significance in addressing the contemporary issue of urinary incontinence-wetness detection. Moreover, it is anticipated that the findings of this thesis will serve as a guiding source for researchers in this field.

GİYİLEBİLİR TEKNOLOJİLER İÇİN E-TEKSTİL TABANLI RFID İŞLEVLİ NEM SENSÖRÜ GELİŞTİRİLMESİ

ÖZET

Gelişen teknolojiyle birlikte e-tekstillerin kullanım alanları her geçen gün daha da yaygınlaşmaktadır. Özellikle esnek, giyilebilir, hafif, ince ve küçük elektronik yapılar, tekstil malzemeleri sayesinde farklı alanlarda rahatlıkla kullanılabilmektedir. Sağlık izleme alanlarında kullanılan kalp atış hızı, solunum hızı, terleme izleme, ıslaklık tespitinde kullanılan sensörlerin son dönemlerde tekstil tabanlı elektronik yapılardan oluşması dikkat çekmektedir. Islaklık tespiti için kullanılan birçok sensör yapısı olduğu halde genellikle bu yapıların katı, sert, büyük ve rahatsız edici olması kullanımlarındaki dezavantajlardandır. Bu sensörlerin yerine ince, esnek, kullanıcının hareketine uyumlu, konforlu tekstil tabanlı sensörlere ihtiyaç duyulmaktadır.

Üriner inkontinans istem dışı idrar kaçırma olarak bilinmekle birlikte yaşlı bireylerde, özellikle de kadınlarda en sık görülen sağlık sorunlarından biridir. Uyku, öksürme, hapşırma, fiziksel efor sırasında, vücut pozisyonunun değişmesiyle veya hiçbir sebep yokken ortaya çıkabilir. Üriner inkontinans hijyen ve cilt sorunları gibi fiziksel etkilere neden olurken; utanç, kaygı, depresyon, uyku bozuklukları gibi psikolojik sorunlar da yaratmaktadır. İdrar kaçırma sorununu çözmek için davranışsal müdahale, ilaç tedavisi veya cerrahi prosedürler kullanılmaktadır. Ancak, literatürdeki çalışmalara göre tedaviler sonucunda kesin başarıya ulaşılamamaktadır. Bu nedenle, üriner inkontinans sorunu yaşayan kişiler çoğunlukla tek kullanımlık bezleri tercih etmektedir.

Öte yandan, yapılan çalışmalarda dünya nüfusunun giderek yaşlandığı ve yaşlanan kişilerde üriner inkontinansın daha sık görüldüğü belirtmektedir. Yetişkin bezi kullanan yaşlı hastaların çoğunda demans ya da bilişsel bozukluk olduğu için idrar kaçırmalarını anlamakta ve bunu bakıcılarına ya da sağlık personeline bildirmekte zorluk çekmektedir. Bu nedenle bakıcıların belirli aralıklarla hastaların bezlerini kontrol etmesi gerekir. Ancak bu kontrollerle ideal zamanda bezinin değiştirilmesi mümkün değildir. Ayrıca rutin bez kontrollerinin özellikle geceleri hastaları rahatsız etmesi uykularını bölmektedir. Gereksiz rutin kontroller bakım hizmeti verenler için oldukça zahmetli olup iş yüklerini artırmaktadır. Tüm bu olumsuz durumlardan kurtulmak, yaşlı ve hasta bireylerin hem kişisel rahatlığı ve sağlığı hem de bakıcılarının iş yükünün hafifletilmesi için hasta bezi ıslandığında bakıcıyı veya sağlık personelini anında uyaran sensör ve sistemlere ihtiyaç duyulmaktadır.

Bu tez, nem ve ıslaklığı algılayabilen aynı zamanda RF sinyalleri iletimini gerçekleştiren tekstil tabanlı, giyilebilir, esnek, hafif ve konforlu RFID entegre nem sensör yapılarını geliştirmeyi amaçlamaktadır. Ayrıca, bu sensörlerin oluşturulması için baskı teknikleri ve mürekkep formülasyon çalışmalarına da odaklanmaktadır.

Bu tez konu bütünlüğüne dikkat edilerek sıralanmış 3 makaleden oluşmaktadır. Tez kapsamında verilen makalelerin tümü özgün olup literatüre yenilik katmaktadır. Makalelerde tez konusunun önemli ve özgün sonuçları tartışılmaktadır.

Birinci makalede, ıslaklık tespiti için literatür araştırmaları sonucu tasarım kriterleri belirlenen nem sensörü sunulmuştur. Tasarlanan nem sensörü inkjet baskı yöntemi ile PEDOT:PSS iletken polimer kullanılarak poliamid tabanlı tafta etiket kumaşa basılmıştır. PEDOT:PSS polimerin inkjet baskıya uygun hale gelmesi için mürekkep karakterizasyonları yapılmıştır. Önerilen nem sensörünün performansı, oluşturulan

kapalı bir kabin içerisinde değişen bağıl neme karşı sensörün direnç değerlerindeki değişim gözlenerek ölçülmüştür. PEDOT:PSS iletken polimer neme duyarlı bir yapıda olduğu için oda şartlarında ölçülen (%35 RH) bağıl nemde bile sensörde direnç değeri elde edilmiştir. Kapalı kabin içerisindeki bağıl nem %35'ten %100'e arttırıldığında sensörün direnci 17.05 ± 0.05 MΩ'dan 2.09 ± 0.06 MΩ'a düşerken, kumaş üzerindeki nem miktarı ise %4.8'den %23'e çıkmıştır. Nem sensörünün hassasiyetini belirleyen yanıt süresi ve tepki süresi sırasıyla, 42 sn ve 82 sn olarak ölçülmüştür. Üriner inkontinans tespiti için ise nem sensörü beze entegre edilmiştir. Sensör üzerine farklı miktarlarda su damlatılarak sensörün direnç değerlerindeki değişimler incelenmiştir. Sensörün oda koşullarında kuru haldeki direnç değeri 15.52 MΩ olarak ölçülürken, sensör entegre edilmiş bezin üzerine 0.1 mL ve 100 mL tuzlu su damlatıldığında elde edilen direnç değerleri sırasıyla 13.62 MΩ ve 3.81 MΩ'dur. Böylece, 0.1 mL'lik su miktarında bile nem sensöründe direnç değişimi elde edilmiş olup önerilen nem sensörünün küçük idrar sızıntılarını dahi tespit edebileceği gösterilmiştir. Ayrıca, giyilebilir nem sensörü, esnek yapısı ve kumaş üzerine düşük maliyetli basılabilirliği nedeniyle, başta idrar kaçırma ve bezlerdeki ıslaklığın tespit edilmesi olmak üzere sağlık uygulamaları için tek kullanımlık bir sensör olarak kullanılma potansiyeline sahiptir.

Sunulan ilk makalede, kullanılan mürekkebin neme duyarlı bir polimer olması nedeniyle oda koşullarındaki mevcut bağıl nem altında bile nem sensörünün iki elektrodu arasında direnç elde edilebilmiştir. PEDOT:PSS polimerinin iletkenliğinin düşük olması ölçülen direnç değerlerinin yüksek olmasına neden olmaktadır. Ayrıca, kullanılan baskı tekniği incelendiğinde inkjet baskının hızlı ve kolay olması bir avantaj sağlarken kullanılan mürekkeplerin inkjet baskıya uygun hale getirilebilme zorluğu (inkjet baskı için hazır satılan mürekkepler hariç) bir dezavantaj olarak karşımıza çıkmaktadır. Birinci makalede kullanılan mürekkep, eletriksel iletkenliğinin düşük olması nedeniyle anten performansını sergileyemeyeceği düşünülerek ikinci makalede değiştirilmiştir. Öncellikle, gümüş nanopartikül içeren mürekkebin inkjet baskı tekniği ile basılması için denemeler yapılmıştır. Fakat nanopartiküllerin baskı düzelerini tıkaması nedeniyle baskı tekniği değiştirilerek tampon baskı yöntemi ile çalışmaya devam edilmiştir.

İkinci makale, birinci makalede önerilen sensör yapısının UHF-RFID anten performansını incelemektedir. Bu makalede, tasarlanan sensör yapısı, poliamid bazlı tafta etiket kumaşı üzerine 1'den 5'e kadar değişen farklı baskı sayıları ile gümüş nanopartikül mürekkep kullanılarak tampon baskı yöntemiyle basılmıştır. Gümüş mürekkebin tampon baskı yönteminde kullanılabilmesi için mürekkebin karakterizasyon ve formülasyon çalışmaları yapılmıştır. Kullanılan mürekkebin nanopartikül içermesi nedeniyle sinterleme işleminin önemi araştırılmış ve makalede sunulan sonuçlara etkisi tartışılmıştır. Farklı baskı sayılarına sahip bir grup sensör numunesine sinterleme işlemi uygulanırken diğer gruba karşılaştırma yapmak amacıyla sinterleme işlemi uygulanmamıştır. Tüm numunelerin UHF-RFID anten performansı bir vektör ağ analizörü kullanılarak incelenmiştir. Sinterleme yapılmamış ve farklı baskı sayılarına sahip sensörlerin yansıma katsayısı grafiğinin yansıma katsayısı frekansı 254 MHz iken, sensörlerin sinterleme sonrası yansıma katsayısı grafiğinin çökme noktası 943 MHz olmuştur. Ölçümler, sinterleme işleminin giyilebilir sensörlerin anten performansları üzerinde önemli bir etkiye sahip olduğunu göstermektedir ve sinterlenmiş giyilebilir ve tekstil tabanlı sensör örneklerinin kısa mesafede kablosuz olarak veri aktarımına olanak sağladığı sonucuna varılmıştır. Ayrıca empedans ölçüm sonuçlarına göre en iyi performansa sahip olan giyilebilir

sensöre bükülme ve kazanç ölçümleri uygulanmıştır. Bu nedenle, anten performansına sahip bu UHF-RFID özellikli giyilebilir sensörler, RFID ve giyilebilir teknolojiler için pasif etkileşimli sensör mimarisi ağı oluşturmak için iyi bir seçenek olabilir.

Birinci ve ikinci makalelerde sunulan nem sensörü tasarımları aynı olup, üretim yöntemi ve sensörleri basmak için kullanılan mürekkepler farklılık göstermekteydi. Nem sensörü tasarımının gümüş mürekkep ile basılması ve dolayısıyla iletkenliğinin daha fazla olması sensör yapısının anten işlevi görüp göremeyeceği konusunun araştırılmasına olanak sağlamıştır. İkinci makalede, sunulan yapının anten işlevi göstermesi hakkında detaylı incelemeler yapılmıştır. Ancak, birinci ve ikinci makalede önerilen yapıların kablosuz olarak ıslaklığı tespit edebilmesi ile ilgili bir araştırma yapılmamıştır. Üçüncü makalede, bu eksiklik giderilerek tez konusu ile örtüşecek şekilde kablosuz ıslaklık tespitine yönelik incelemeler yapılmıştır.

Son olarak, üçüncü makalede, birinci ve ikinci makalelerde kullanılan sensör tasarımı değiştirilerek hem sensör hem de anten işlevi gören RFID sensör tasarımı yapılmıştır. Önerilen yapı CST programı kullanılarak Avrupa bandına göre 867 MHz'de çalışması hedeflenerek tasarlanmıştır. RFID sensör, ikinci makalede olduğu gibi gümüş nanopartikül mürekkep kullanılarak tampon baskı yöntemi ile poliamid bazlı tafta etiket kumaşa basılmıştır. RFID sensör için 3 baskı sayısı kullanılmıştır. Çalışmada nanopartikül içeren mürekkep kullanıldığından numune, baskı işleminden sonra 150°C'de 30 dakika boyunca etüv kullanılarak sinterlenmiştir. RFID sensörün hedeflenen frekansta çalışması için yapıya çip entegre edilmiştir. RFID sensör, gerçek kullanım ortamı göz önünde bulundurularak beze entegre edilmiştir. Önerilen sensörün uygulanabilirliğini test etmek ve doğrulamak için yakın alan bölgesinde ve daha uzak mesafelerinde daha gerçekçi çevre koşullarını taklit eden iki farklı tipte Alınan Sinyal Gücü Göstergesi (RSSI) ölçüm kurulumu gerçekleştirilmiştir. RFID sensör entegreli bebek bezi üzerine farklı solüsyonlar damlatılarak yakın alan RSSI ölçümlerinde farklı ıslatma koşullarının değerlendirilmesi için su, tuzlu su ve yapay idrar solüsyonları kullanılmıştır. Önerilen ıslaklık algılama sensörünün ıslak ve kuru durumları arasında en az 17 dBm'lik bir sinyal farkı tespit edilmiştir. Önerilen RFID sensörünün performansı, ikili ıslaklık durumlarının güvenilir bir şekilde belirlenmesi için maksimum okuma mesafesinin 50 cm olduğu pratik sonucu ile 32 cm, 40 cm ve 50 cm'lik farklı okuma mesafeleri kullanılarak değerlendirilmiştir. Ayrıca, RFID ıslaklık sensörünün farklı bükülme ve deformasyon koşullarına karşı performansı neredeyse sağlamdır. Önerilen sensör yapısının, uzaktan sağlık izleme sistemlerinde idrar kaçırma gibi durumlarda ıslaklık durumlarının güvenilir bir şekilde tespit edilmesini kolaylaştırmak için hasta bezlerine entegre edilebileceği sonucuna varılmıştır.

Özetle, tez kapsamında sunulan üç makale de ayrı ayrı literatüre katkı sunmaktadır. Makaleler tez konusunun ve çalışmaların sonucunda elde edilen çıktıların, özgün ve yenilikçi olduğunu ortaya koymaktadır. Tez konusunun güncel ve kişisel sağlık izleme ile ilgili olması çalışmanın sonuçlarını herkes için önemli hale getirmektedir. Makalelerde sunulan sonuçlar, geliştirilen sensör ve sistemler günümüzde yaşanan idrar kaçırma-ıslaklık tespiti sorununun çözümü için oldukça önemlidir. Ayrıca, bu tezin sonuçlarının araştırmacılara yol göstereceği düşünülmektedir.

1. INTRODUCTION

As technology advances, there is a growing fascination with wearable and textile-based electronics designed to enhance people's daily lives. Care is taken to ensure that the structures developed on the basis of the studies carried out in this field are flexible, low-cost, lightweight and can be easily integrated into clothing. Structures such as sensors, electrodes, antennas and batteries developed within the framework of wearable electronics stand out in many critical areas such as sport, automotive, military, and health fields. Wearable technologies developed especially for the field of health, such as physical activity, health monitoring, and disease recognition, provide the life of both patients and healthcare personnel easier. Flexible and wearable humidity sensors, which are widely used in the field of health monitoring, are especially used for sweating, respiratory monitoring, and urinary incontinence detection.

Urinary incontinence is known as the involuntary leakage of urea during physical activity, under stress or without any reason. Urinary incontinence is seen in babies as well as in adults and elderly individuals. Although there are different treatments for urinary incontinence, none of these treatments provide definitive results. In this case, people suffering from urinary incontinence use disposable diapers as a solution. In nursing homes, caregivers change the diapers of individuals with urinary incontinence problems. Diapers that are not changed on time cause bacterial infections, wounds and skin irritations in patients. Therefore, it is very important to change diapers on time. On the other hand, caregivers have to wake up the patient and change the lying position periodically in order to check the diapers. These checks both disturb the patient and create an extra workload for the staff. For these reasons, a wearable and flexible structure that detects urinary incontinence on time and provides information to the caregiver is needed.

In this thesis, based on the above-mentioned need, it is aimed to develop a flexible and wearable RFID-enabled moisture sensor embedded in textiles, capable of timely detection and transmission of wetness signals.

This thesis consists of three articles, listed taking into account the integrity of the thesis. These articles roughly include general information about wearable humidity sensors and antennas, current status in the relevant literature, general information about urinary incontinence, fabrication methods of wearable sensors and antennas, inkjet and pad printing techniques, PEDOT:PSS and silver conductive ink formulations and their characterizations according to the printing method, information about humidity sensor and RFID antenna types and design criteria, the importance of the sintering process and the number of print passes, determination and characterization of sensor and antenna behaviors, measurement of antenna performances of sensors, characteristic tests of wearable sensor and antenna structures, the integration of sensors and antennas onto diapers, and examination and evaluation of their performance in urinary incontinence simulations.

In the first article, the humidity sensor designed by researching the literature was printed on a polyamide-based taffeta label fabric using humidity sensitive PEDOT:PSS conductive polymer according to the inkjet printing technique. The sensitivity of the fabricated sensor was tested according to different relative humidity levels. The wetness detection performance of the sensor was evaluated by simulating urinary incontinence.

In the inkjet printing technique, ink is sprayed from nozzles and transferred to the substrate. Ink formulation studies were carried out in order to print easily. The ink formulation of PEDOT:PSS conductive polymer was studied and could be printed without any problems in inkjet printing technique. Silver ink prepared from silver nanoparticles was used in the rest of the study. Since the silver ink printed with inkjet printing technique clogged the nozzles of the inkjet printer after a few printings, a pad printing machine was used for the continuation of the study.

The second article involves the examination of the RFID antenna performance of the moisture sensor design presented in the first article. The humidity sensor was printed with a pad printing machine using silver ink with different print passes. Due to the presence of silver nanoparticles in the ink, the sintering process must be implemented

post-printing to guarantee the stability of the printed structures in relation to conductivity.The impedance and reflection coefficients of the sensor samples with and without the sintering process were measured using a vector network analyzer. When the reflection coefficients of the sensors were evaluated after sintering, it was determined that the sensors function as RFID antennas in the ultra-high frequency (UHF) band. This situation emphasizes the importance of the sintering process for inks containing nanoparticles. In the continuation of the article, bending tests were performed to show that the sensors were flexible and wearable.

Although the humidity sensor design used in the first and second articles was the same, the inks and printing techniques used were different. The humidity sensor proposed in the first article can detect wetness in case of urinary incontinence. However, the sensor could not sense the situation change (wetting) via wireless communication. In the second article, the antenna performance of the proposed humidity sensor was measured and it was shown that the sensor can also be used as a UHF RFID antenna with appropriate printing passes and sintering process. However, even if the sensor shows antenna performance, it cannot notify wirelessly about the wetness situation. Considering this situation, the design was changed in the third article.

Finally, UHF RFID sensor structure designed for wetness detection was printed with a pad printing machine using silver conductive ink in the third article. By integrating the RFID sensor onto the diaper, its application potential was tested more realistically. RFID sensor integrated diaper was tested with two different types of Received Signal Strength Indicator (RSSI) measurement setups. It was determined that there was a signal difference of at least 17 dBm between the wet and dry states of the RFID sensor, which was tested by dropping water, saline and urine solutions. The maximum reading range of the RFID sensor, which has been proven to be resistant to different bending and deformations, is 50 cm. The RFID sensor proposed in this article detects urinary incontinence with remote reading.

As a result, the three articles presented within the scope of the thesis show that the thesis is original and innovative. The humidity sensor and antenna structure proposed for wetness detection in the articles is flexible, wearable, lightweight, easily produced and integrated, and batteryless, making a significant contribution to the relevant literature. The fact that the structures introduced in the articles hold potential application in health monitoring, particularly in urinary incontinence detection as well

as in logistics, where moisture and wetness detection is crucial. Hence, the findings emphasize the potential of the thesis to contribute towards challenges encountered in everyday life.

2. WEARABLE AND FLEXIBLE HUMIDITY SENSOR INTEGRATED TO DISPOSABLE DIAPERS FOR WETNESS MONITORING AND URINARY INCONTINENCE[1]

Disposable diapers are widely used by individuals with urinary incontinence. Diapers should be checked frequently for elderly, disabled, and hospital patients. Wet diapers that are not changed properly can cause health problems. The importance of electronic devices that provide warning in case of wetness is increasing in health monitoring. A disposable and wearable printed humidity sensor was designed and fabricated to detect wetness. The sensor was printed on polyamide-based taffeta label fabric by the inkjet printing method using specifically formulated PEDOT:PSS-based conductive polymer ink. The sensor sensitivity was tested under different relative humidity levels inside a controlled chamber. The resistance of the sensor decreased from 17.05 ± 0.05 MΩ to 2.09 ± 0.06 MΩ as the relative humidity increased from 35 to 100%, while the moisture value of the fabric increased from 4.8 to 23%. The response and recovery times were 42 s and 82 s. This sensor was integrated into the adult diaper to evaluate wetness. The sensor resistance change comparing to the dry state resistance (15.52 MΩ) was determined as 3.81 MΩ to 13.62 MΩ by dripping 0.1 mL to 100 mL salty water on the diaper. Due to its flexible structure and low-cost printability onto fabric, the wearable printed humidity sensor has the potential to be used as a disposable sensor for healthcare applications, particularly for urinary incontinence and capturing wetness in diapers.

Keywords: inkjet printing, humidity sensor, conductive ink, wetness monitoring, diaper, wearable, urinary incontinence.

[1] This chapter is based on the paper "Tekcin, M., Sayar, E., Yalcin, M. K., and Bahadir, S. K. 2022. Wearable and Flexible Humidity Sensor Integrated to Disposable Diapers for Wetness Monitoring and Urinary Incontinence, *Electronics*, 11(7), 1025. DOI: 10.3390/electronics11071025."

2.1 Introduction

Urinary incontinence, which occurs as an involuntary loss of urine, is one of the most common health problems among elderly individuals, especially for women (Cho et al., 2021; Ueda et al., 2000). It can appear during sleeping, coughing, sneezing, physical exertion, or with a change of body position (Aoki et al., 2017). Urinary incontinence causes hygiene and skin problems. In addition, it creates psychological problems such as embarrassment, anxiety, depression, asociality, and sleep disturbances. Urinary incontinence decreases the quality of life (Jerez-Roig et al., 2016; Karakaya et al., 2019). As a result of studies conducted in different countries, urinary incontinence is seen between 25% and 45% in a population on average (Cho et al., 2021; Milsom & Gyhagen, 2019). In addition, more than 50% of nursing home residents experience urinary incontinence in a nursing home (Karakaya et al., 2019; Kim et al., 2017; Milsom & Gyhagen, 2019; Skotnes et al., 2012). Behavioral intervention, drug therapy, and surgical procedures can be used to solve urinary incontinence. These treatments may cause challenges for older individuals. Considering this situation, the most appropriate option for these individuals is to use absorbent products and urinary catheters (Cho et al., 2021; Skotnes et al., 2012). In a study, it was stated that more than 85% of people with urinary incontinence prefer diapers (Johnson et al., 2001). According to the diaper market report, in 2020, the global diaper market reached $69.5 billion, while the adult diaper market is expected to grow by $3.01 billion in the period 2020–2024 (*Diaper Market: Global Industry Trends, Share, Size, Growth, Opportunity and Forecast 2021-2026*, 2021; *Global Adult Diaper Market 2020-2024*, 2020). However, there are some risks in the use of such a preferred product. For example, wet diapers that are not changed promptly can lead to incontinence-associated dermatitis (IAD) and infections caused by exposure to urine or feces. Particular attention should be paid to the diapers of bedridden patients with bedsores. This is because these infections cause bedsores to worsen (Gray, 2010).

Adult diapers, which are one of the liquid absorbent hygiene products, are frequently used in daily life. Most absorbent incontinence materials consist of cover stock, acquisition/distribution layer, absorbent core typically composed of fluff pulp, cellulose wadding, and a superabsorbent polymer (SAP). The cover stock also called the top sheet, is the most important part of the incontinence pads since this part is in direct contact with the skin of the user. Using low-quality products or harmful

chemicals on this layer may cause skin rash or dermatitis. For these reasons, the pores on the top sheet of the adult diaper should be large enough for the diaper to breathe, but small enough to prevent urine from flowing out. ADL (Acquisition/Distribution Layer) is located between the top sheet and the absorbent core. It is used in the form of a patch or in the length of the core. This layer is especially necessary for diapers where the absorbent core is very thin. The layer absorbs, transfers, and distributes the liquid quickly. In addition, ADL maintains a feeling of dryness on the skin by providing separation between the wet surface and the skin (Ajmeri & Ajmeri, 2016). The absorbent core is an essential part of the absorbent hygiene product. This part holds urine and other bodily wastes. This layer consists of a combination of cellulose fluff pulp and superabsorbent polymers (SAP). The use of only cellulose fluff pulp in the incontinence pads produced previously could not provide sufficient protection for the diapers due to the decrease in the liquid absorption capacity of the fluff pulp under pressure. This situation is eliminated by adding SAP to the absorbent core, and the production of ultra-thin diapers is made possible. The average weight of the absorbent core can vary from 0.003 to 0.015 g/cm. The main task of the back sheet is to prevent the absorbed liquid from leaking. The back sheet of the diaper is in the structure of a liquid impermeable polyethylene film. A breathable surface is created by allowing water vapor to pass through the micropores on the polyethylene film. Sometimes, a fabric appearance is given by adding polypropylene nonwoven structure to the back sheet film (Ajmeri & Ajmeri, 2016; Das, 2014). The efficiency of the diaper depends on the structure of the layers around the absorbent core, while the cover stock, the acquisition layer, and the back sheet allow the skin to dry and prevent leakage. Adult incontinence products can be divided into three groups as light, moderate, or heavy incontinence according to the severity of the incontinence problem (Ajmeri & Ajmeri, 2016). According to EDANA, European Disposable and Nonwoven Association, the product composition offered for typical incontinence includes 62% fluff pulp, 12% SAP, 10% PE (polyethylene) film, 15% nonwoven PP (polypropylene), 3% adhesives, and 1% elastics (*EDANA*, 2021). The first step in the production of incontinence products is the fiberization of the fluff pulp. Next, SAP is added and filled with nonwoven substrates and laminated with elastic elements and tapes to form the absorbent core. The wetness indicator and traceability marks are printed, thereafter. The forming, cutting, folding, and packaging processes are carried out, respectively, in the final stage (Ajmeri & Ajmeri, 2016).

Elderly patients who wear adult diapers have difficulty understanding their urinary incontinence and reporting it to their caregivers or health personnel because most of them have dementia or cognitive impairment. Therefore, caregivers need to check the diapers of patients at certain intervals. However, with these controls, it is not possible to change the diaper at the ideal time. In addition, routine diaper checks disturb patients, especially at night, interrupting their sleep. Unnecessary routine checks are very troublesome for caregivers and increase their workload. To get rid of all these negative situations, systems that warn the caregiver or health personnel as soon as the diaper gets wet, are very necessary. In the study (Cho et al., 2021), a smart diaper system consisting of two carbon conductive lines embedded in the diaper, a sensing device, and a smartphone was presented. Bluetooth technology was used to automatically detect incontinence and its volume. In another study, a smart gadget attached to the outside of the diaper for urine detection determined the temperature increase and sent a notification to the caregiver's smartphone (Khan, 2019). However, the external, inflexible, and rigid devices used in these studies may cause urinary incontinence patients to be uncomfortable with the presence of these devices. The use of flexible and small wearable sensors instead of these hard and externally integrated additional devices contributes positively to the comfort of the patients. In a study, a wearable humidity sensor was used to detect urinary incontinence. This capacitive humidity sensor was embroidered onto the textile substrate. The wearable system detected urine leaks on a bed sheet or underwear (Marc et al., 2021). The system consisted of a humidity sensor, a control unit, and a remote server in reference (Marc et al., 2021).

Methods such as embroidery, knitting, weaving, coating/lamination, chemical treatment, and printing are used to integrate sensors onto textile substrates (Stoppa & Chiolerio, 2014). The printing method is one of the most used methods in sensors' integration onto textile substrates and it includes a wide range of application techniques. These are inkjet printing (Gaspar et al., 2017), screen printing (Kutzner et al., 2013), and gravure printing (Zhang et al., 2020). Among these techniques, the inkjet printing method is one of the most preferred techniques in terms of being both fast and low cost.

Many polymer-based materials and their combinations are used in the production of sensors. Among polymer-based materials, poly(3,4-ethylenedioxythiophene):

polystyrene sulfonate) (PEDOT:PSS) draws attention. PEDOT:PSS polymer has many advantages such as high conductivity, low price, and easy processability at room temperature (Aziz et al., 2015; Seekaew et al., 2014). Hassan et al. produced a humidity sensor using the PEDOT:PSS, which is known to be a humidity-sensitive polymer. In addition to PEDOT:PSS polymer, methyl red, and graphene oxide were used to increase the sensitivity range and to improve the response and recovery times of the humidity sensor in this study (G. Hassan et al., 2019). In another study, a real-time humidity sensor based on a microwave resonator was designed using PEDOT:PSS conductive polymer (Park et al., 2018). Two humidity sensors (interdigitated electrode structure) were printed on glossy photo paper using PEDOT:PSS polymer and silver ink with the inkjet printing method. Relative humidity, temperature, compressive, and tensile bending tests were applied to the produced sensors. However, it was found that the PEDOT:PSS humidity sensor did not show good performance for the long-term bending test (Barmpakos et al., 2020).

In this study, a wearable humidity sensor was designed to detect urinary incontinence and printed on polyamide-based taffeta label fabric using PEDOT:PSS conductive polymer with inkjet printing method. The behavior of the printed humidity sensor against humidity was tested by fixing the sensor inside of a closed chamber at different humidity levels. Finally, the printed humidity sensor was integrated into the adult diaper to simulate the incontinence situation. The performance of the sensor against wetness was observed.

2.2 Materials and Methods

2.2.1 Chemicals and materials

In the study, humidity-sensitive PEDOT:PSS (poly(3,4-ethylenedioxythiophene): polystyrene sulfonate) conductive polymer was used to print the humidity sensor. The concentration of this conductive polymer from Sigma-Aldrich (CAS No: 0155090838, San Diego, CA, USA) is 3–4% by weight in water. Triton X-100 surfactant was purchased from Merck Millipore (CAS No: 9036-19-5, San Diego, CA, USA) to adjust the surface tension of the ink. Ethylene glycol used in the study was purchased from Sigma-Aldrich. The polyamide-based taffeta label fabric with a thickness of 0.105–0.115 mm, and an average weight of 62 ± 5 g/m² on which the sensor was printed, was purchased from Huzhou Hengxin Label Manufacture Co. (Huzhou, China). Silver-

plated polyamide yarn was purchased from Shieldex (Bremen, Germany). Its yarn count was 235f × 34 × 2, and it had a linear electrical resistance <85 Ω/m. This yarn was placed at the electrodes of the humidity sensor for easier measurement. A translucent polyurethane welding tape (ST 604) purchased from Bemis (Shirley, NY, USA) is used to attach the silver-plated polyamide yarns to the two electrodes on the humidity sensor. The softening temperature of this elastic and washable tape is 105°C. The softening process can be carried out under moderate pressure and temperature conditions.

2.2.2 Ink formulation for inkjet printing

A schematic diagram of the sensor fabrication and its integration was shown in Figure 2.1. Firstly, a polymer solution was obtained by mixing PEDOT:PSS, and distilled water. After the mixing procedure, ethylene glycol was added to adjust the ink viscosity, and Triton X-100 was added to adjust the surface tension of the ink where both chemicals are added simultaneously. Details of the formulation study are given (Tekcin et al., 2021). In the end, a homogeneous printing ink was obtained suitable for the inkjet printing method.

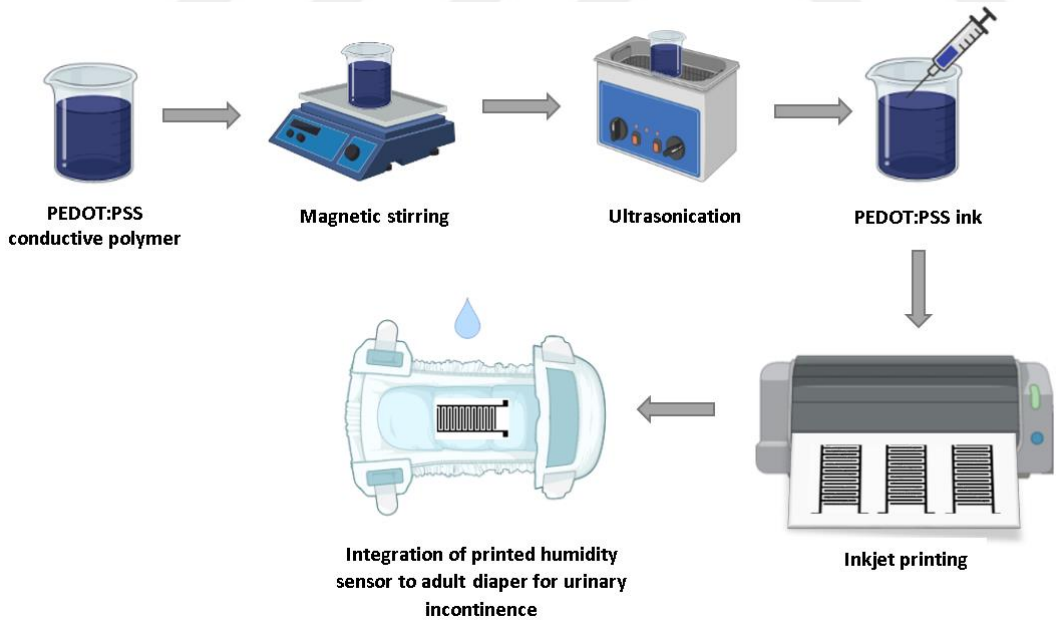

Figure 2.1 : Schematic view of inkjet-printed humidity sensor fabrication, and integration into an adult diaper.

To print the prepared printing ink with the inkjet printing method, many ink parameters need to be examined. These parameters are expected to be within certain ranges. Otherwise, inkjet printing is not possible.

The most important of these ink parameters are the viscosity, surface tension, and contact angle of the ink (Tekcin et al., 2021). The dynamic viscosity of the prepared printing ink was measured with the Fungilab alpha device (L model, İstanbul, Turkey). Theta Lite optical tensiometer (Ontario, ON, Canada) was used to measure the surface tension of the prepared ink. This measurement was done using the pendant drop method (Marmur, 2006; Stauffer, 1965). In addition to these measurements, the contact angles at the points where the ink comes into contact with the fabric surface were made with the Theta Lite optical tensiometer device using the sessile drop method (Stauffer, 1965).

2.2.3 Humidity sensor design and fabrication

There are two types of sensors which are capacitive and resistive. The sensor presented in this study is a resistive humidity sensor. The operating principle of this humidity sensor is based on the measurement of changes in electrical impedance. The sensors usually consist of metal electrodes. These metal electrodes are obtained by placing conductive polymer, salt, or different hygroscopic chemicals on the substrate. As the hygroscopic material absorbs water, the ionic groups dissociate. This causes an increase in conductivity. As the humidity in the environment increases, the conductivity increases and the resistance of the material decreases. Resistive sensors provide a linear response to humidity changes (Mecnika et al., 2015; Najeeb et al., 2018; Su & Wang, 2007). The humidity sensor in the study was designed according to the interdigitated electrode (IDE) structure. The humidity sensor design was made larger for easier urinary incontinence detection following the purpose of the study. The total area of the sensor was 46.74 × 24.13 mm. Inkscape commercial software was used to draw the designed sensor. The sensor consists of 20 IDEs, with each electrode 1 mm wide and 15 mm long. The gap between the electrodes was determined as 1 mm. Figure 2.2 indicates the dimensions of the designed sensor.

Dimatix inkjet printer, which is frequently used in studies, is quite expensive. In this study, the printing process was done with Canon office-type printer. Thus, more cost-effective fabrication was realized. Polyamide-based taffeta label fabric was chosen as the substrate. The prepared printing ink was injected directly into the cartridge and rested for 5 min prior to printing to spread the ink properly in the cartridge.

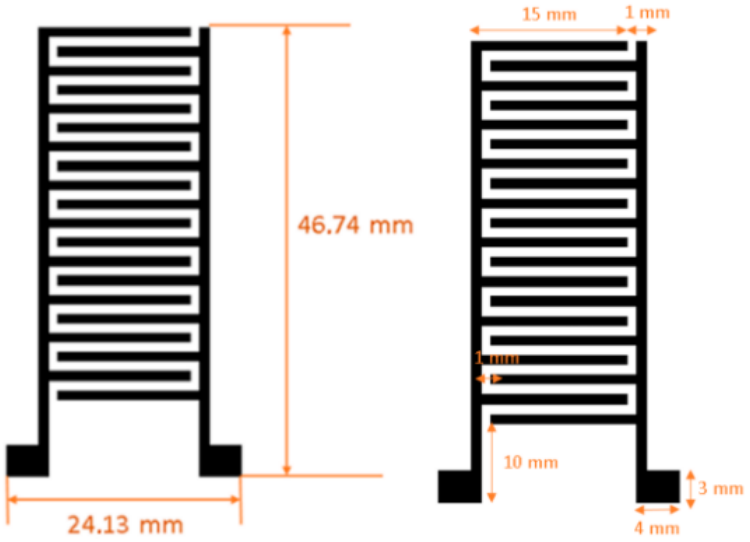

Figure 2.2 : Dimensions of the humidity sensor design.

Preprint and printing processes were carried out at room conditions. Multiple printing processes were applied onto the polyamide-based taffeta label fabric to increase the conductivity and to have more uniform printing lines. The number of passes applied was 15. After each printing, a drying process was applied at 120 °C for 2 min to prevent slipping and dispersion (Tekcin et al., 2021). After the printing process, silver-plated polyamide yarn was placed at both ends of the humidity sensor. Then, a polyurethane tape was placed on the ends of the humidity sensor where it only came into contact with the conductive yarns. To activate the tape, 5.5 bar pressure was applied at 80 °C for 10 s in the hot-press machine. The printed humidity sensor and conductive yarns connected to its ends were indicated in Figure 2.3.

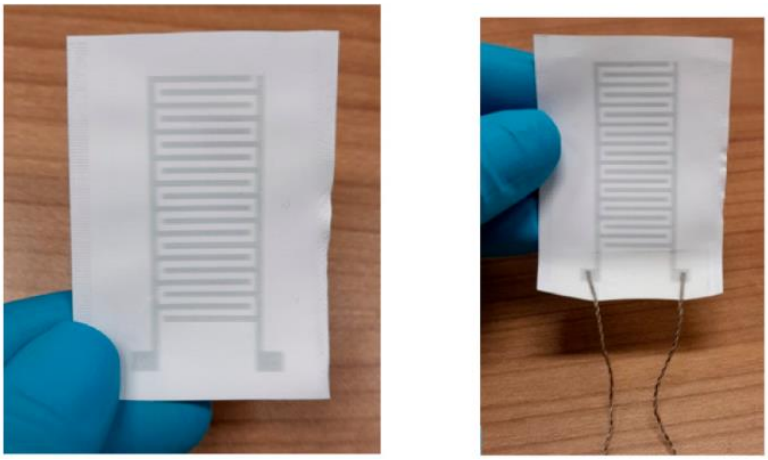

Figure 2.3 : Printed humidity sensor and conductive yarns connected to its ends.

2.2.4 Measurement of the humidity sensor behavior

To perform the humidity tests, a closed humidity chamber was designed and built. The resistance variations of the printed humidity sensor were measured with a Keithley 2700 multimeter according to the four-wire measurement method. The four-wire method ensures more accurate measurement results than the two-wire method. The measured resistance values were transferred from Keithley 2700 Data Acquisition System to the computer with Excelinx software via the universal serial bus (USB) converter cable through RS232 terminal. While the humidifier placed in the chamber increased the humidity of the chamber inside, the commercial humidity and temperature meter (Achem HTC-1, İstanbul, Turkey) measured the relative humidity and temperature in the chamber. Humidity and temperature in the chamber were also checked by another commercial humidity sensor (SHT30 V1.0, İstanbul, Turkey) connected to the Keithley 2700 Data Acquisition System to ensure accurate measurement of humidity and temperature inside the chamber. A clip-on fixing tool was used to prevent the cables from slipping and to improve stability while measuring the resistance. A Trotec T510 moisture meter (İstanbul, Turkey) was used to measure the moisture content on the fabric surface. Figure 2.4 shows the closed humidity chamber and the devices in it.

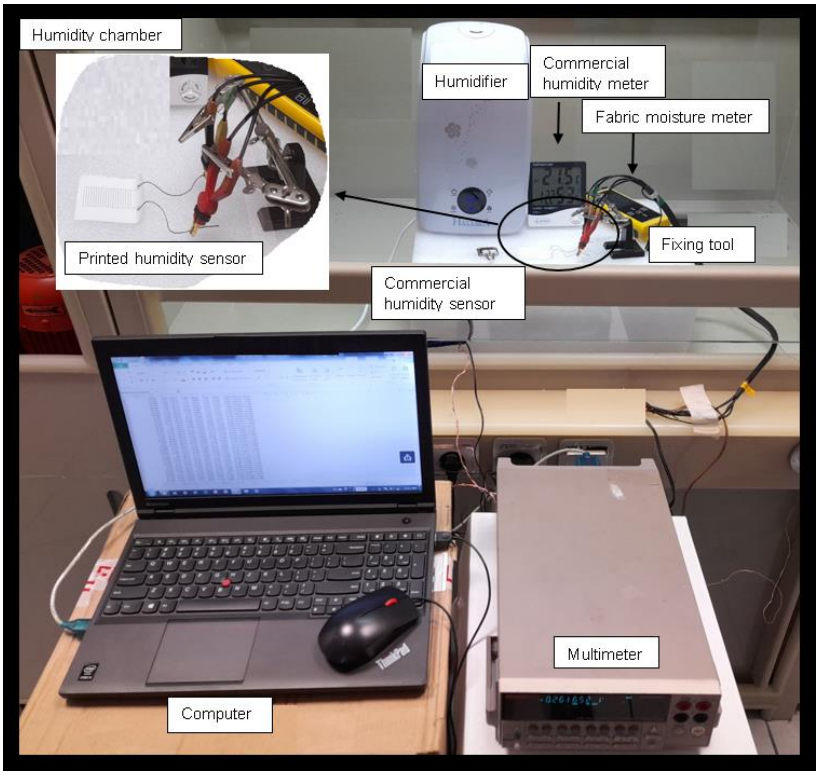

Figure 2.4 : Humidity chamber.

The humidity inside the chamber was fixed at relative humidity ranging from 40 to 100% in 5% RH increments. To show a stable structure for the printed humidity sensor against humidity, the sensor was kept in the chamber for 5 min at each fixed humidity level. Then, the resistance values were measured at the predefined relative humidity level for 3 min with the automatic measurement system and the recordings were directed to the computer. In addition, fabric moisture values were measured with a moisture meter in response to the varying humidity values in the chamber.

2.3 Results

2.3.1 Conductive polymer ink (PEDOT:PSS) characterization

Dynamic viscosity, surface tension, and contact angle measurements of the ink were made to investigate whether the developed PEDOT:PSS conductive polymer ink is suitable for the inkjet printing method or not. Conductive polymer ink formulation studies were also carried out. Since the rheological behavior of the ink used in the inkjet printing method is very important, the viscosity and surface tension values of the ink have been well defined in the literature. While the viscosity value specified in the literature is between 1–25 mPa·s, the surface tension is between 25–50 mN/m(Cummins et al., 2012; Tekcin et al., 2021). The viscosity and surface tension of the prepared PEDOT:PSS ink were measured as 6.53 mPa·s, and 25.83 mN/m, respectively. They are coherent with the specifications given in the literature. The sample volume for viscosity measurement was 20 mL. All measurements were done at room conditions and by taking the average of five measurement results. Thus, the measured values of the prepared ink are compatible with the inkjet printing method according to the literature (Tekcin et al., 2021).

One of the measured values of the prepared ink was the contact angle. The contact angle is defined in the literature as the angles measured at the point where the solid surface and the liquid come into contact after a liquid is dropped on a solid surface. Near zero contact angle for full wetting, contact angle below 90° for partial wetting, and contact angle values above 90° for hydrophobic structures are seen (Bracco & Holst, 2013). The measured contact angle values were 27.8° on the left, 27° on the right, and 27.4° on average. Therefore, when the prepared ink comes into contact with the substrate (polyamide-based taffeta label fabric), it makes partial wetting. This case is suitable for the inkjet printing method (Tekcin et al., 2021).

2.3.2 Humidity sensor characterization

The humidity sensor produced with conductive polymer measures the resistance according to changing relative humidity. Since PEDOT:PSS conductive polymer is a humidity-sensitive polymer, first of all, the resistance value of the printed humidity sensor was measured at room conditions (21 °C, 35% RH). Then, the humidity sensor was placed in the humidity chamber and a silver-plated polyamide yarn, which was fixed to the ends of the humidity sensor, was connected to the clamp cables of the multimeter. A fixing tool was used to prevent any movement on the yarns while taking measurements. The humidity inside the chamber was fixed at 40%, 45%, 50%, 55%, 60%, 65%, 70%, 75%, 80%, 85%, 90%, 95%, and 100% RH. The sensor was kept in the chamber for a while without taking measurements to let the sensor satisfy a mass concentration balance with the ambient moisture content and to equalize to the ambient temperature, satisfying a complete local thermodynamic equilibrium. The behavior of the sensor against humidity did not change after waiting in the chamber for more than 5 min. Therefore, the conditioning time of the sensor in the chamber has been determined as 5 min. The resistance measurements of the humidity sensor were conducted with the Keithley 2700 Data Acquisition System using the four-probe method. The experiments were repeated 10 times and each one of the experimental measurement results was recorded covering a three minute time interval. The results were averaged and presented with error bars. The graph showing the change in resistance of the sensor in the chamber against increasing relative humidity is shown in Figure 2.5.

The increase of the relative humidity in the chamber caused the resistance of the sensor to decrease (Figure 2.5). The resistance value of the sensor at room conditions (21 °C, 35% RH) was measured as 17.05 ± 0.05 MΩ. When the humidity chamber reached 100% RH, the resistance of the sensor decreased to 2.09 ± 0.06 MΩ. The decrease in resistance is expected to be linear as the relative humidity increases for resistive sensors. When the graph in Figure 2.5 is examined, it is seen that the resistance-relative humidity relationship is almost linear. In addition, resistance values can be found for certain relative humidity from the given equation in Figure 2.5. Fabric moisture was measured with a fabric moisture meter to understand how the changing relative humidity in the chamber affects the fabric moisture values.

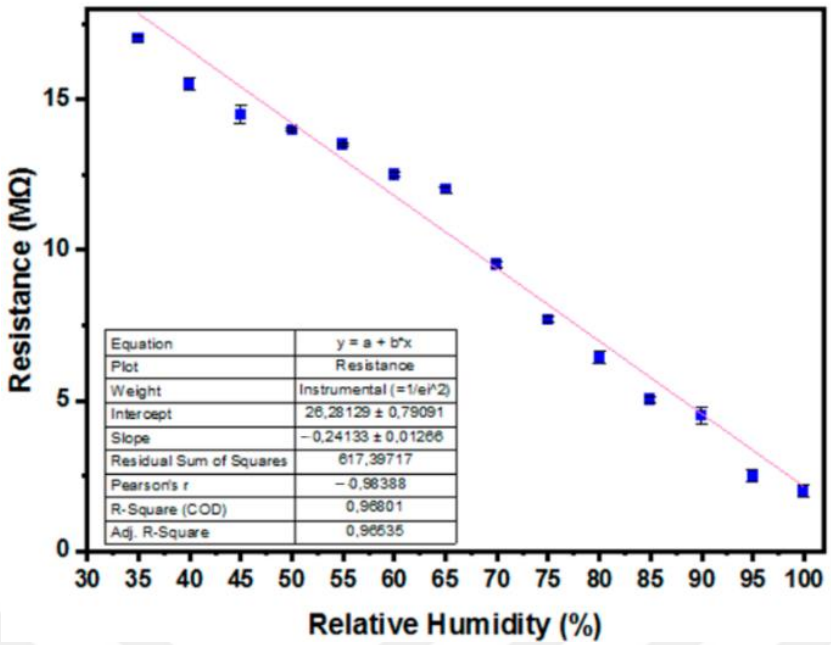

Figure 2.5 : Graph of the resistance change of the sensor against relative humidity.

The fabric moisture meter uses the resistance measurement method to determine the moisture of the material. While the moisture of the fabric was 4.8% at room conditions, it was measured as 23% when the inside of the chamber was increased to 100% RH. As the relative humidity in the chamber increased, the moisture of the fabric increased as expected (Figure 2.6). However, moisture on the fabric did not increase linearly with increasing humidity in the chamber. This situation may be related to the ability of the textile material to absorb moisture in the air. Herewith, it has been proven that fabric moisture increases with the relative humidity of the surrounding environment while the resistance of the sensor decreases due to its conductive polymer.

Humidity sensors produced are expected to have many potential applications in various application areas. Two of these characteristics are response time and recovery time (Rittersma, 2002). Response time is defined as the required time from the initial value of the resistance to a stable value, while recovery time is defined as the inverse of the response time. The response time and the recovery time of the produced humidity sensor were measured 42 s and 82 s, respectively. While measuring the response time of the sensor, the sensor was taken into the humidity chamber (100% RH) from the room conditions (35% RH) and then the required time from the initial value at room conditions to a stable value at 100% RH was measured. Conversely, the recovery time of the sensor was measured as the time taken when the sensor was removed from the chamber at 100% RH and brought to room conditions (35% RH).

In the study (G. Hassan et al., 2019), the response time and recovery time of the humidity sensor created using PEDOT:PSS, methyl red, and graphene oxide were measured as 1.0 s, and 3.5 s, respectively. In another study, the response time of the humidity sensor created using PEDOT:PSS and PVA composite ink was measured as 0.625 s, while the recovery time was measured as 0.53 s (Choi et al., 2015). Therefore, the response time and recovery time of the humidity sensor presented in this study are low compared to other studies. It is thought that the response and recovery times of the sensor will be shortened by adding different materials to PEDOT:PSS polymer, as in other studies. However, since our sensor is designed to integrate a disposable diaper for single usage, the response time of the sensor would be also quite acceptable.

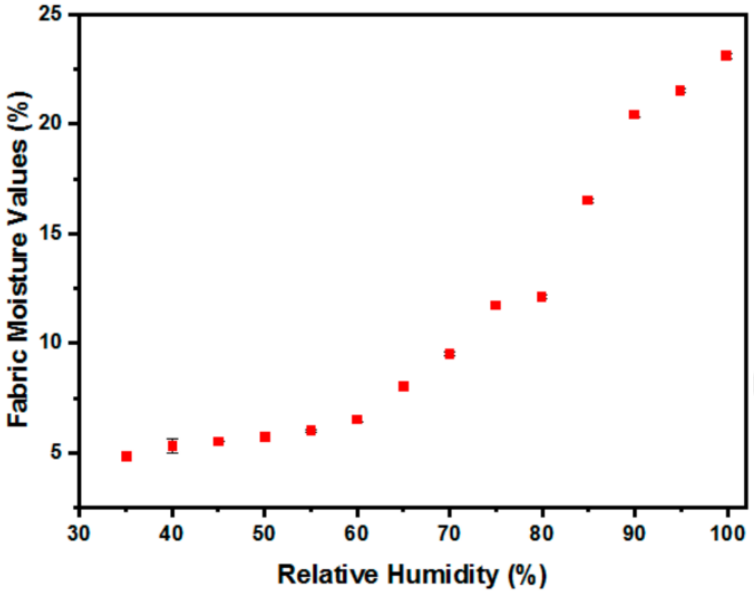

Figure 2.6 : Graph of fabric moisture change against relative humidity.

Moreover, a repeatability test was applied to the humidity sensor. The room ambient conditions where the sensor was located were 30.9% RH and 23.5 °C before the test. Then, a repeatability cycle was completed by measuring the resistance change of the sensor between 35% chamber indoor air relative humidity and 100% RH. Altering the relative humidity between 35 to 100% and back to 35% is considered a cycle. This cycle was repeated for 50 consecutive cycles. At first, the cabin RH was increased from 35 to 100% RH and then it was decreased to 35% RH to 100% RH. To observe the changes clearly, sensor repeatability for five cycles is depicted in Figure 2.7a, while 50 cycles are given in Figure 2.7b. It can be seen from Figure 7 that the printed humidity sensor shows good repeatability. For the humidity test and repeatability test

performed in the chamber, different resistances were measured at the same humidity levels. It is thought that this difference is due to the difference in humidity and temperature on the days of the tests.

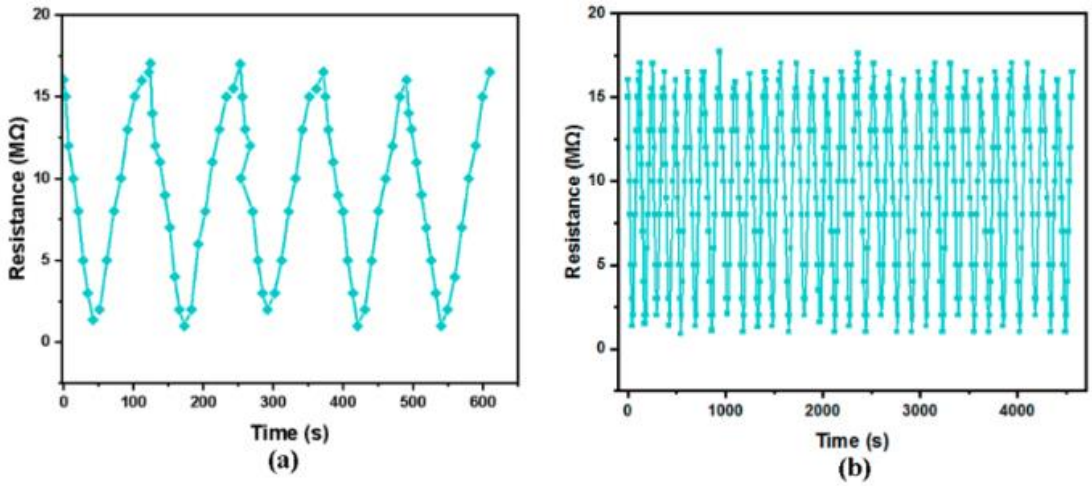

Figure 2.7 : Graph of repeatability test of the sensor while working at the interval of 35–100% RH (from 35% RH to 100% RH and then 100% RH to 35% RH). (a) For five cycles, (b) for 50 cycles.

The humidity sensor to be integrated into the adult diaper for urinary incontinence is expected to be wearable and flexible. At the same time, it should maintain its mechanical stability and conductivity in cases such as bending or twisting. Therefore, multiple bending cycles should be applied to wearable sensors (Gao et al., 2017; Kuzubasoglu et al., 2021). Wrist joint bending was applied to the sensor to understand how bending movements alter sensor electrical resistance values. Figure 2.8 indicates the resistance change of the sensor when applied to repeated wrist bending movements. The maximum resistance change measured between the initial state of the sensor and its state after 16 bending cycles was 1%. According to the bending test result, the resistance change measured between the initial state of the sensor and its state after 10 bending cycles was 0.41%, while the measured maximum resistance change after 16 bending cycles was 1%. Accordingly, it can be said that the electrical conductivity and mechanical resistance of the sensor slightly change after 10 bending cycles.

2.3.3 Application of the humidity sensor to disposable diapers for urinary incontinence

The humidity sensor was printed onto the adhesive polyamide-based taffeta label fabric in order to integrate easily it into the adult diaper.

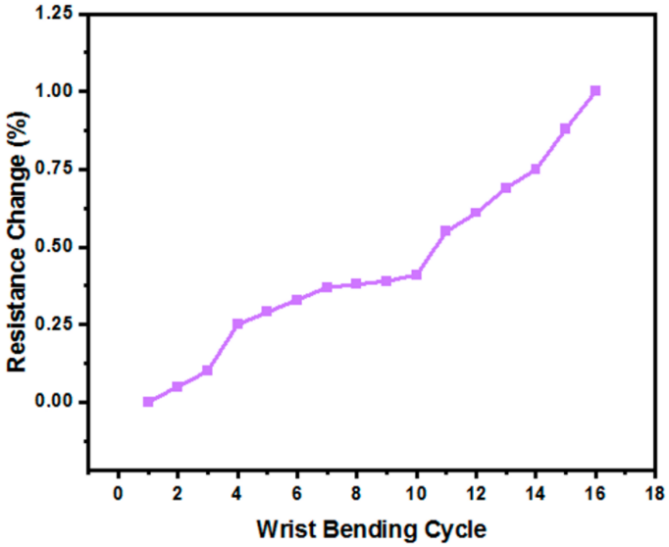

Figure 2.8 : Graph of wrist bending test of the sensor.

Firstly, the top layer of the adult incontinence diaper, the cover stock, has been completely removed. The length of the absorbent part of the diaper was measured as 36 cm where the sensor was attached to the 16–22 cm part. Then, the cover stock was put back to prevent the sensor from coming into direct contact with the skin. As a result, the sensor was placed between the ADL and the cover stock. Silver-plated polyamide yarns, which are located at both ends of the sensor (providing easier measurements) were passed through the cover stock of the adult diaper, employing a needle hole to attach to multimeter probes.

Salty water was used to simulate urinary incontinence. While the conductivity of the water was 340 µS/cm, its pH was measured as 7.05. Five different amounts of water, 0.1 mL, 0.5 mL, 1 mL, 10 mL, and 100 mL, were used for the incontinence test with a micropipette. The distance of the micropipette to the adult diaper was determined as 2 cm. The test setup for the urinary incontinence simulation is shown in Figure 2.9.

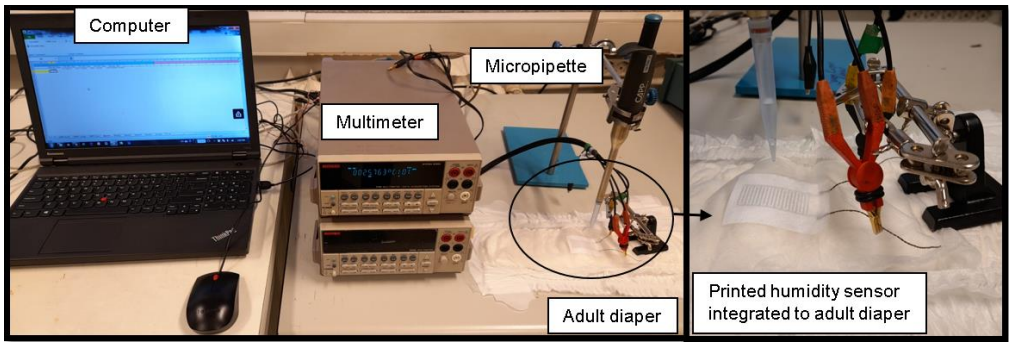

Figure 2.9 : The test setup for urinary incontinence detection.

Resistance measurements were carried out with the Keithley 2700 Data Acquisition System using the four-probe method. There were in total six resistance measurement reference points. Out of the six points, one was conducted at room conditions (24.5 °C, 42% RH) without any added water and the other five points were considered at five different amounts of water dripping (0.1 mL, 0.5 mL, 1 mL, 10 mL, and 100 mL) at the same room conditions. The clamped ends of the multimeter cables connected to the fixing tool were attached to the conductive yarns placed at the ends of the sensor. Thus, a possible move that would affect the measurement result while taking a measurement was prevented. Data were recorded for 60 s for each measurement condition (room conditions, 0.1 mL, 0.5 mL, 1 mL, 10 mL, and 100 mL). The graph of the resistance change of the humidity sensor integrated into the adult diaper for different amounts of water is given in Figure 2.10.

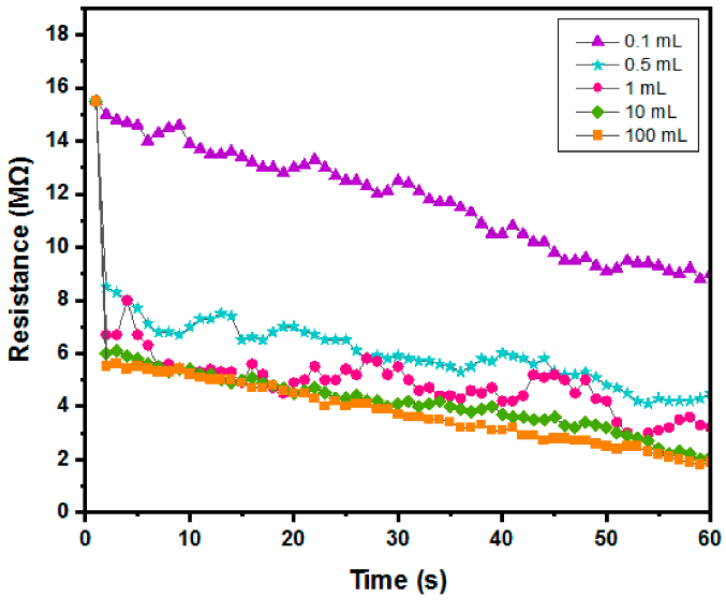

Figure 2.10 : Graph of the resistance change of the humidity sensor against different amounts of water.

Firstly, the resistance values were recorded while the sensor was dry. Then, a determined amount of water was dropped on the sensor and the resistance values were recorded for 1 min. When the resistance change graph in Figure 2.10 is examined, it is seen that very small urinary incontinences of 0.1 mL were even detected by the sensor. When 0.1 mL of water was dropped, the least resistance change was observed according to the dry condition of the sensor. As the amount of dripped water increases, the measured resistance value decreases. The intensity of urinary incontinence can be understood from the resistance changes of the sensor (Figure 2.10).

The graph of the measured average resistance values of the sensor against different amounts of water is indicated in Figure 2.11. While the resistance value of the dry state of the sensor was measured as 15.52 ± 0.01 MΩ at room conditions (24.5 °C, 40% RH), the average resistance decreased to 11.71 ± 0.04 MΩ when 0.1 mL of water was dropped on the sensor. The average resistance values measured were 5.96 MΩ ± 0.03, 4.81 MΩ ± 0.04, 2.12 ± 0.06, and 1.90 MΩ ± 0.07 when 0.5 mL, 1 mL, 10 mL, and 100 mL water were dripped, respectively. The inset graph shows the resistance values of the dry sensor after dripping 0.1 mL, 0.5 mL, and 1 mL water amounts on the sensor. When the graph is examined, there is no great difference in the resistance change of the sensor at water amounts above 0.5 mL.

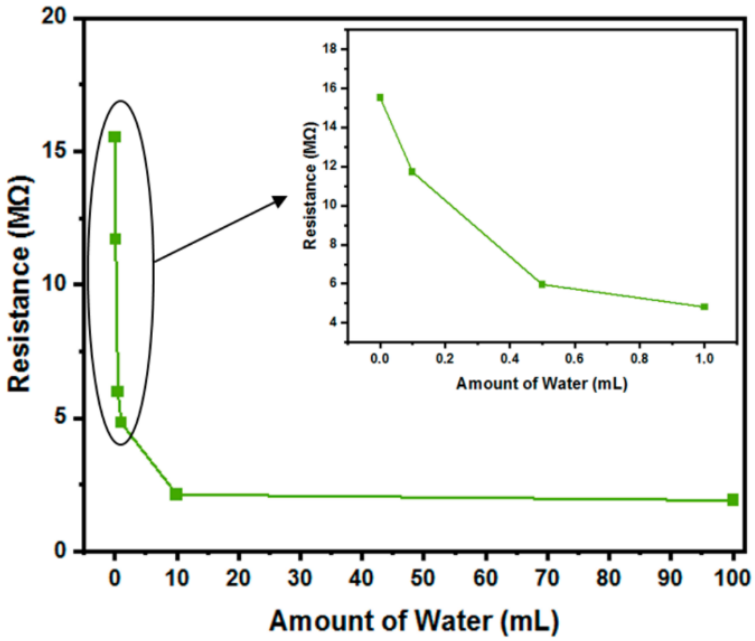

Figure 2.11 : Graph of the resistance values of the humidity sensor against different amounts of water.

2.4 Conclusions

In this study, a wearable and flexible humidity sensor was designed to be used in wetness monitoring and urinary incontinence detection. Conductive PEDOT:PSS polymer was used in the production of the humidity sensor. Formulation studies were carried out to make PEDOT:PSS polymer suitable for inkjet printing method. Using an office-type inkjet printer, conductive polymer ink was printed on polyamide-based taffeta label fabric. In order to determine the sensitivity of the printed and disposable humidity sensor, a closed humidity chamber was designed and the resistance change

of the sensor was monitored against the relative humidity varying from 40 to 100%. The resistance of the sensor decreased from 17.05 ± 0.05 MΩ to 2.09 ± 0.06 MΩ as the relative humidity increased from 35 to 100%, while the moisture value of the fabric increased from 4.8 to 23% as the relative humidity increased. The response time and recovery time of the humidity sensor were found to be 42 s and 82 s, respectively, which are sufficient for the proposed applications. The sensor was then integrated into the adult diaper between the cover stock of the adult diaper, and ADL for urinary incontinence detection. Thus, the sensor was positioned close to the surface, although direct contact with the skin was prevented. The resistance change of the humidity sensor comparing to the dry state resistance (15.52 MΩ) was determined as 3.81 MΩ to 13.62 MΩ by dripping 0.1 mL to 100 mL salty water on the adult diaper to simulate urinary incontinence detection. The results showed that the resistance changes of the sensor differ depending on the amount of water. Even the information on very small incontinence status (solution of 0.1 mL) can be obtained easily and the intensity of urinary incontinence can also be detected with the developed humidity sensor. Making urinary incontinence detection by using a wearable and flexible sensor instead of solid, large, and uncomfortable gadgets is the innovative and promising part of the study. In future studies, it is planned to transform the developed sensors' output into a system that wirelessly communicates with the caregiver or the user in cases of urinary incontinence.

2.5 Author Contributions

Conceptualization, M.T. and S.K.B.; methodology, M.T. and S.K.B.; software, E.S.; validation, M.T., S.K.B., and E.S.; formal analysis, M.T.; investigation, M.T., S.K.B.; resources, M.T.; data curation, E.S. and M.K.Y.; writing—original draft preparation, M.T.; writing—review and editing, S.K.B.; visualization, M.T.; supervision, S.K.B.; project administration, S.K.B.; funding acquisition, S.K.B. All authors have read and agreed to the published version of the manuscript.

2.6 Funding

This research was funded by the scientific, and technological research council of Turkey (TUBITAK), grant number 119M976.

2.7 Data Availability Statement

The data presented in this study will be available on request from the corresponding author when the whole project (119M976) is completed.

2.8 Conflicts of Interest

The authors declare no conflict of interest.

3. UHF-RFID ENABLED WEARABLE FLEXIBLE PRINTED SENSOR WITH ANTENNA PERFORMANCE[2]

Many different parameters affect the antenna performance of the wearable sensors. In this study, antenna performances of textile based sensors which have different pass numbers from 1 to 5 printed using conductive ink with pad printing method were investigated. Moreover, the effect of sintering process after printing on the RF antenna performances of wearable sensors was examined. For this, antenna impedances, and reflection coefficients of the sintered, and non-sintered printed sensors were measured using a vector network analyzer. While the frequency at the collapse point of the reflection coefficient graph of the sensors without sintering and with different pass numbers was 254 MHz, the collapse point of the reflection coefficient graph of the sensors was 943 MHz after sintering. The measurements indicate that the sintering process has a significant effect on the antenna performances of wearable sensors, and it is concluded that the sintered printed wearable sensor samples enable data transmission wirelessly in short range. In addition, bending, and gain measurements was applied to wearable sensor which has the best performance according to the impedance measurement results. Thus, these UHF-RFID enabled wearable sensors with antenna performance might be good option to form a network of passive interactive sensor architecture for RFID and wearable technologies. In addition, considering the designed wearable sensor structure, it is foreseen that the potential usage areas of this structure may be moisture sensitive areas (such as supply chains and transportation of moisture-sensitive products).

Keywords: wearable, printed sensor, printed antenna, antenna performance, sintering process, pad printing.

[2] This chapter is based on the paper "Tekcin, M., Paker, S., and Bahadir, S. K. 2022. UHF-RFID Enabled Wearable Flexible Printed Sensor with Antenna Performance, *AEU - Int. J. Electron. Commun.*, 157, 154410. DOI: 10.1016/j.aeue.2022.154410".

3.1 Introduction

UHF-RFID (Ultra High Frequency- Radio Frequency Identification) enabled wearable sensor studies, which can be used in many different areas and facilitate the lives and work of users, are increasing day by day. In particular, wearable sensors, and antennas, which are preferred in the areas of health monitoring, medical, and tracking systems, have many advantages (Cheng et al., 2021). These advantages include being light, flexible, low cost, and easy to manufacture (S. Hassan & Shehab, 2016; Yalduz et al., 2020). Considering the advantages of wearable antennas and the developments in RFID technology, the use of wearable antennas in RFID technology in the above-mentioned areas becomes inevitable. In a study, UHF RFID tag antenna was produced by using electrically conductive polymer fibers in an elastic polymer for automotive tire applications. It has been emphasized that the produced antenna can operate in broadband, a wide variety of dielectric materials and various environments compared to traditional RFID tag antennas (Shao et al., 2015). In the study of Long et al., RFID strain sensor tag application for textile antennas was presented. For the main antenna part, the high conductivity non-stretchable copper-coated fabric was used, and it was combined with the stretchable conductive fabric via an embroidery machine (Long et al., 2015). Textile UHF-RFID antennas produced for many different application areas, especially surgical masks, were combined with an integrated circuit (IC) chip (Rocky 100). It was stated that the resonance curves measured with the simulation results are compatible and that various improvements have been made in the study to increase the maximum reading range (Luo, Gil, & Fernandez-Garcia, 2022b). In another study, a wearable textile RFID tag for the European UHF band (865–870 MHz) was designed using Substrate Integrated Waveguide (SIW) technology (Casula et al., 2020). In the study where textile-based wearable UHF RFID slotted patch, and split ring resonator reader antennas integrated onto work gloves were presented, the gains of the slotted patch antenna, and SRR antenna were −2.16 dBi, and −4 dBi, respectively (Ahmed et al., 2019). In another study, a passive RFID moisture detection system was produced for UHF RFID technology by using embroidery, and three-dimensional (3D) printing methods. It is emphasized that this system consists of a flexible sensor tag, and a stable reference tag (Chen et al., 2020).

Sintering technologies are progressively used in many different fields, especially in the automotive, military, electronics, and medical (El Hajjaji et al., 2021). Heat

treatment is a 2-step process that is frequently applied especially in printed electronics. The first step which is drying process, is applied to evaporate the different solvents in the inks (El Hajjaji et al., 2021; Z. Wang et al., 2017). The second step is sintering. Sintering helps to increase conductivity by providing the bonding between metal particles (El Hajjaji et al., 2021; Moon et al., 2005). The sintering parameters (such as sintering temperature, and duration) of metal particles in the conductive inks affect the behavior of electronic structures such as sensors, antennas, and filters (Lukacs et al., 2022; Pietrikova et al., 2015).

Today, printing technologies are preferred rather than conventional production methods for the production of low-cost, and high-performance wearable electronics (Htwe & Mariatti, 2022; Kamyshny & Magdassi, 2019). The substrate, and conductive ink have great importance in order to produce flexible printed electronics with the required properties according to the field of use. The properties of the substrate materials used in the production of RFID enabled wearable sensor affect the antenna behavior. The low dielectric constant of the textiles reduces the surface wave losses, and increases the impedance bandwidth of the antenna. This feature enables textiles to be used as a substrate for the production of wearable antennas (Mersani et al., 2018; Salvado et al., 2012; Yalduz et al., 2020). In addition, it is very important to choose the optimum printing method (Htwe et al., 2021; Htwe & Mariatti, 2022). Different printing techniques such as flexography (Tafoya et al., 2022), screen printing (Brooke et al., 2022), gravure printing (A. M. et al., 2022), inkjet printing (Sun et al., 2022) and pad printing (Bodenstein et al., 2019) can be used for the production of wearable electronics.

The pad printing method, which was first used to transfer ink to porcelain surfaces, is one of the oldest printing techniques. Despite it is the oldest printing technique, scientific studies on pad printing are extremely rare (Bodenstein et al., 2019). The main parts of the pad printing machine are an engraved printing plate called the cliché and a silicone rubber pad. The printing pattern is transferred from the printing plate to the substrate by a silicone rubber pad. First of all, the cliché is filled with a lot of ink. Then, the excess ink is scraped off and the silicone pad lifts the ink from the plate. Finally, the ink on the pad is printed onto the substrate (Merilampi et al., 2011). The absence of ink wetting problems in pad printing, the ability to print with high quality, the simple and low cost of the printing process show that this method is advantageous

to be used in printed electronics as well. In addition, inks with solid particles, and inks which have wide viscosity ranges can be used in pad printing without any problems (Bodenstein et al., 2019; Izdebska & Thomas, 2015). The comparison of the textile-based RFID antenna presented in the study and the flexible textile-based RFID antennas found in the literature is shown in Table 3.1.

Table 3.1 : Comparison of the proposed RFID antenna with the other textile-based flexible RFID antennas.

Reference	Operating Frequency (MHz)	Antenna Area (mm^2)	Thickness (mm)	Substrate	Fabrication Method
(Shao et al., 2015)	263 (Free space)	1023	1	Textile	Embedding in a polymer
(Luo, Gil, & Fernandez-Garcia, 2022c)	868	896	0.62	Textile	Embroidery
(Casula et al., 2020)	868	6790	4	Textile	Metallization
(Ahmed et al., 2019)	866	10.17	4	Textile	Adhesion
(Chen et al., 2020)	866-915	1876	-	Textile	Embroidery & 3D Printing
Proposed	943	1127.83	0.1	Textile	Pad printing

In this study, a wearable, and flexible textile sensor was designed, and produced. At the same time, they were tested whether the produced sensors can be used as an antenna for UHF RFID technology. Silver conductive ink was used as an electrode while polyamide-based taffeta label fabric was used as a substrate. Silver conductive ink was printed on polyamide-based taffeta label fabric via pad printing machine with different pass numbers. In order to show the effect of the sintering process on the antenna performance, sintering was performed on one sample group while the other sample group was not sintered. Then, the impedance, and magnitude of the textile antennas was measured with a vector network analyzer. As far as known, it is the first study to examine the effect of sintering process on wearable textile antenna performance.

3.2 Materials and Methods

3.2.1 Chemicals-materials and ink formulation

Silver conductive ink was used to print wearable textile-based UHF-RFID enabled sensor. Silver conductive ink, which is highly durable, and highly flexible, was purchased from Engineered Conductive Materials, LLC (Product code: CI-1036, Ohio, OH, USA). Thinner was purchased from TRI Electronic (Batch no: 0000243578, İstanbul, Turkey) to adjust the viscosity of the ink. Polyamide-based taffeta label fabric was selected as a substrate for wearable antenna, and this fabric, whose technical specifications were given in the previous study (Tekcin, Sayar, et al., 2022), was purchased from Huzhou Hengxin Label Manufacture Co. (Huzhou, China). Silver conductive ink which has 10.000 cP viscosity was mixed with the thinner at a ratio of 5:1 by weight on a magnetic stirrer for 30 min. Thus, homogeneous ink was obtained and the viscosity of the ink was ensured to reach the optimum value for the pad printing machine. A schematic diagram of the UHF-RFID enabled wearable sensor fabrication, and impedance measurement is shown in Figure 3.1.

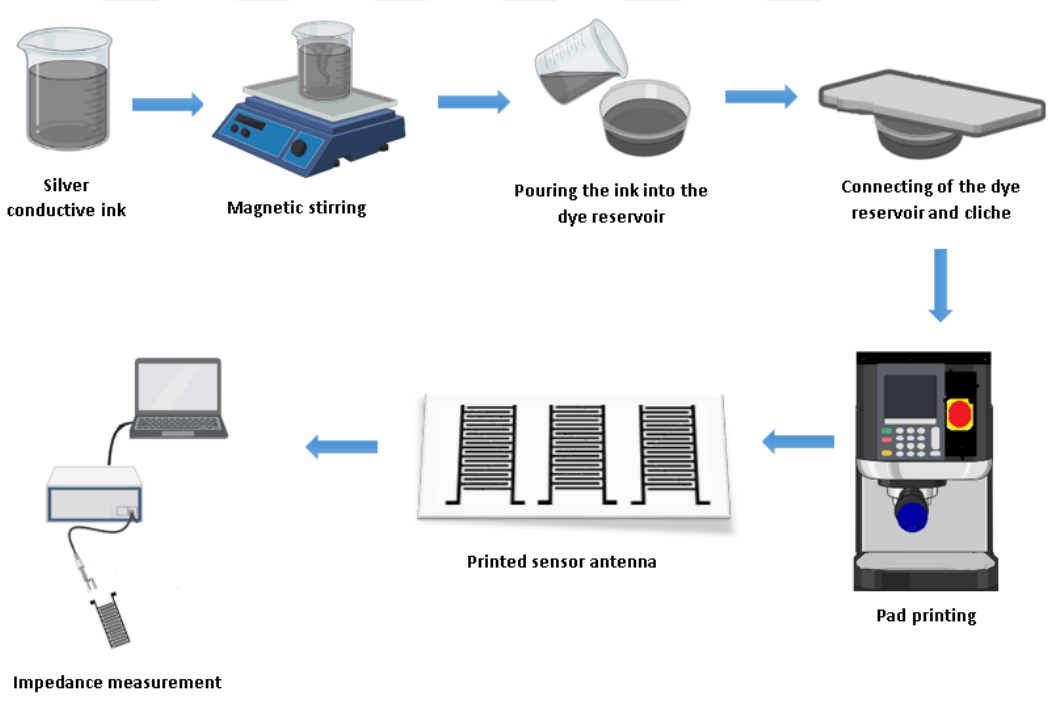

Figure 3.1 : Schematic view of the UHF-RFID enabled wearable sensor fabrication, and impedance measurement.

3.2.2 UHF-RFID enabled wearable sensor design and fabrication

The design of the UHF-RFID enabled wearable sensor, whose dimensions were given in detail in the previous study (Tekcin, Sayar, et al., 2022), was carried out with a vector drawing software called Inkscape. UHF-RFID enabled wearable sensor, which is 46.74 mm long, and 24.13 mm wide, consists of 20 interdigitated electrode (IDE) structures. The image of the designed UHF-RFID enabled wearable sensor is shown in Figure 3.2.

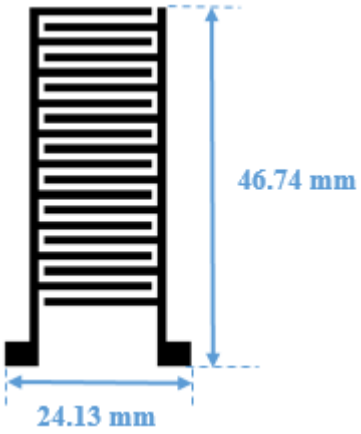

Figure 3.2 : Image of the designed UHF-RFID enabled wearable sensor.

Pad printing machine (COMEC, EAZY90) was used to print UHF-RFID enabled wearable sensor on the polyamide-based taffeta label fabric. The pattern of the antenna was engraved on the plate (cliché) which is made of stainless steel. Afterwards, the prepared ink was poured into the dye reservoir of the pad printing machine. The dye reservoir was turned upside down and placed on the cliché. Maximum adhesion of the dye reservoir to the cliché was ensured with the help of magnets in the dye reservoir. The tight contact between the dye reservoir, and the cliché prevented the ink and solvent in the dye reservoir from volatilizing. The inverted dye reservoir with the cliché was placed on the machine. The prepared ink in the dye reservoir covered the antenna pattern, and the sharp edges of the paint reservoir scraped off the excess ink on the antenna with the movement of the machine. Thus, only enough ink remained on the antenna. Then, the silicone pad contacted the cliché, and transferred the antenna pattern on the cliché. Finally, the silicone pad printed on the polyamide-based taffeta label fabric selected as the substrate, and printing process was completed. Figure 3.3 indicates the pad printing machine used in the study.

Figure 3.3 : Pad printing machine.

Ink preparation, and printing processes were carried out at room conditions. Different pass numbers from 1 to 5 were applied to increase the conductivity, and to interpret the change in the radiation behavior of the antenna. At the same time, sintering process was applied to one sample group while sintering process was not applied to the other sample group in order to examine the effect of sintering process on the radiation behavior of antennas. The sample group, which was applied sintering process, was cured in an oven at 150 °C for 15 min after printing. The printed UHF-RFID enabled wearable sensor was shown in Figure 3.4.

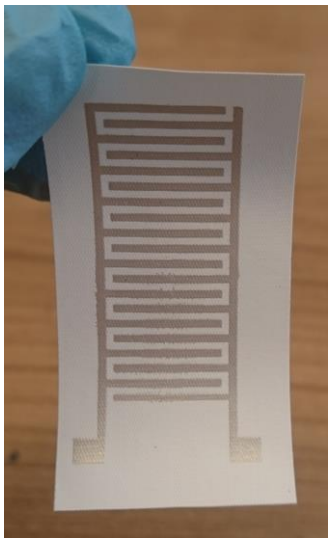

Figure 3.4 : Printed UHF-RFID enabled wearable sensor.

3.2.3 Impedance measurement method

Printed sensor, and RFID antenna structures are balanced form, and the impedance of these structures cannot be measured directly with unbalanced connections such as coaxial cables attached to the end of measurement devices (Shan & Xiao, 2015). In some studies, different from the methods presented for unbalanced antennas, methods that have proven to achieve accurate measurement results for symmetrical balanced antennas are presented (Luo, Gil, & Fernandez-Garcia, 2022b; Luo, Gil, & Fernández-García, 2022; Qing et al., 2009; Shan & Xiao, 2015; Zhu et al., 2010). Based on the studies carried out, Copper Mountain Vector Network Analyzer (TR1300/1) used for RF measurements, and the probes developed for the measurement are shown in Figure 3.5. Probe tips which are made of semi-rigid cables are soldered together. Firstly, the Vector Network Analyzer was calibrated using a standard calibration kit. Then, the probe tips produced were connected to the professional cable so that balanced antenna measurements could be made. In order to move the calibration to the produced probe tips, the device was recalibrated from the professional cable using the standard calibration kit. Finally, the probe tips were connected to the produced antenna electrodes, and the measurement was carried out with 50 Ω load.

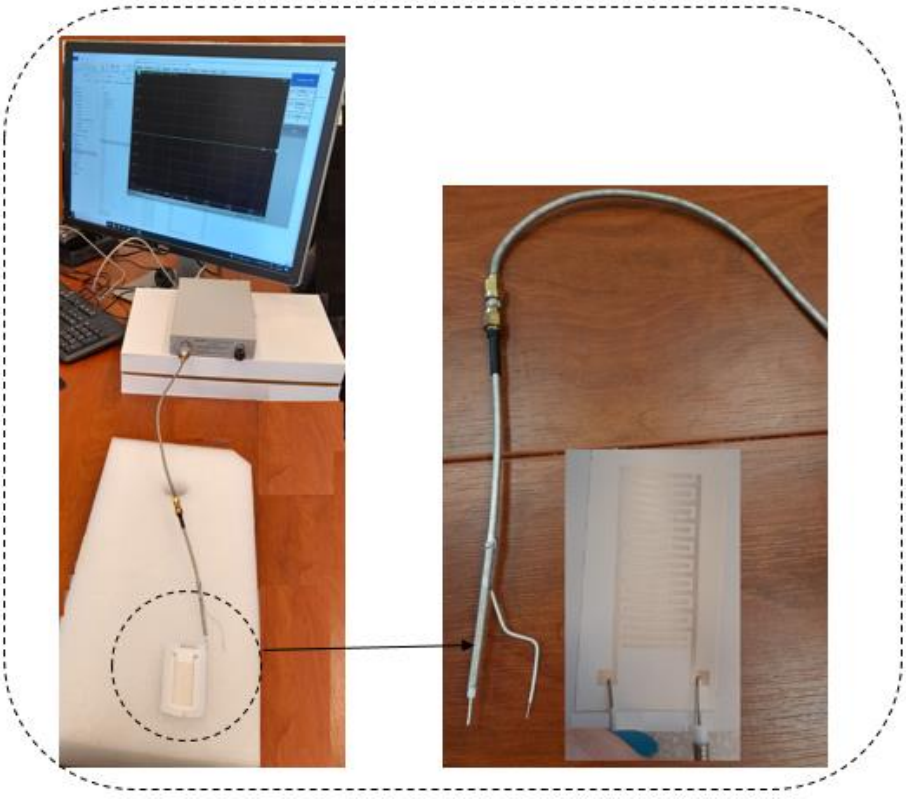

Figure 3.5 : Experiment setup for the impedance measurement.

3.2.4 Gain measurement method

Gain measurement was carried out with the sintered antenna which has 5 pass and the best conductivity (called sample 10). This measurement was made using a linear polarized broadband horn antenna (Schwarzbeck, BBHA 9120 D), and a reference antenna. Reference antenna has vertical polarization and its dimension 30 × 30 cm. Firstly, the broadband horn antenna was connected to the vector network analyzer. Then, the reference antenna was placed 60 cm away from the broadband horn antenna. The gain measurement test setup is shown in Figure 3.6.

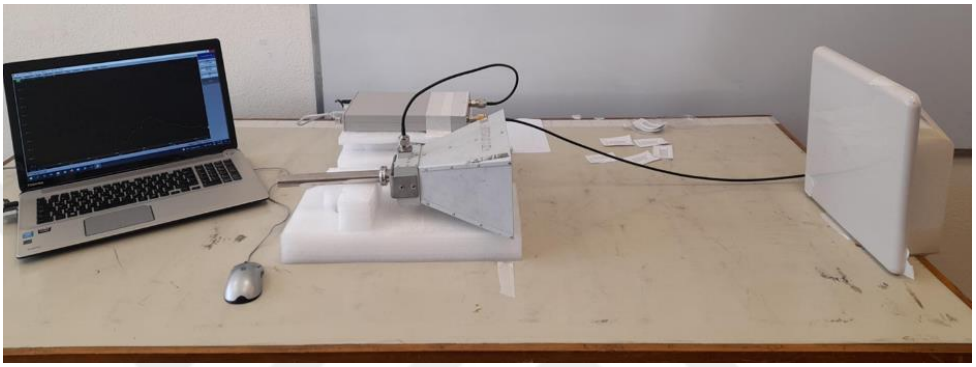

Figure 3.6 : Gain measurement setup.

3.2.5 Bending measurement method

Bending test was applied in the polarization direction (x direction), and opposite direction (y direction) of the sintered antenna which has 5 pass to measure its flexibility. The bending test setup, and different bending positions of the antenna are shown in Figure 3.7. Foam with a radius of 10 mm was used for the bending test. First, the test specimen was measured without bending. Then, it was placed around the foam and measurements were made in the directions of x and y.

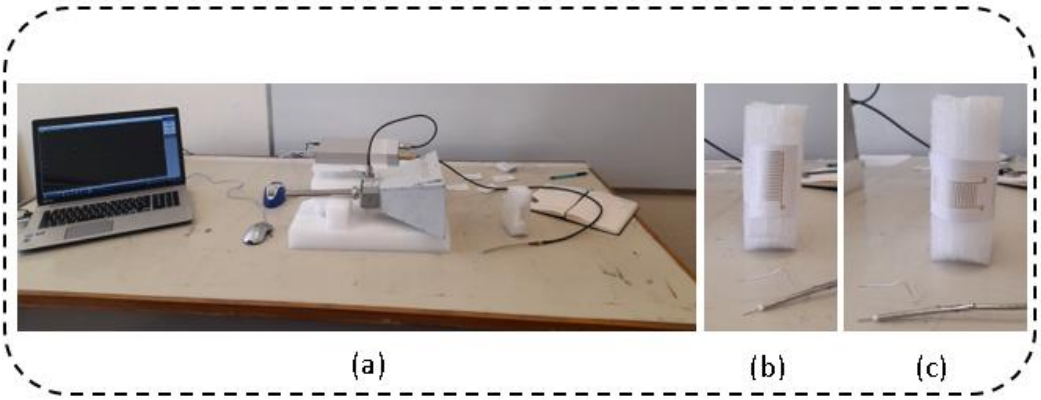

Figure 3.7 : (a) Bending test setup, (b) Bending test of antenna with x direction, (c) Bending test of antenna with y direction.

3.3 Results and Discussion

3.3.1 Impedance measurement results of the non-sintered textile antennas

Reflection coefficients, and impedances of the printed antennas (with different pass numbers from 1 to 5) were measured with a vector network analyzer as described above, without exposing the sintering process. The impedance–frequency graph of antennas including resistance, and reactance values is shown in Figure 3.8. Sample 1 indicates non-sintered antenna with 1 pass while sample 2 shows non-sintered antenna with 2 pass. The 3 pass non-sintered antenna is designated as sample 3, while the 4 pass non-sintered antenna, and the 5 pass non-sintered antenna are called as sample 4 and sample 5, respectively. When the graph in Figure 3.8 is examined, it is seen that the non-sintered samples with different pass numbers have similar resistance, and reactance curves. At the same time, a resonance around 720 MHz is observed in the impedance graph.

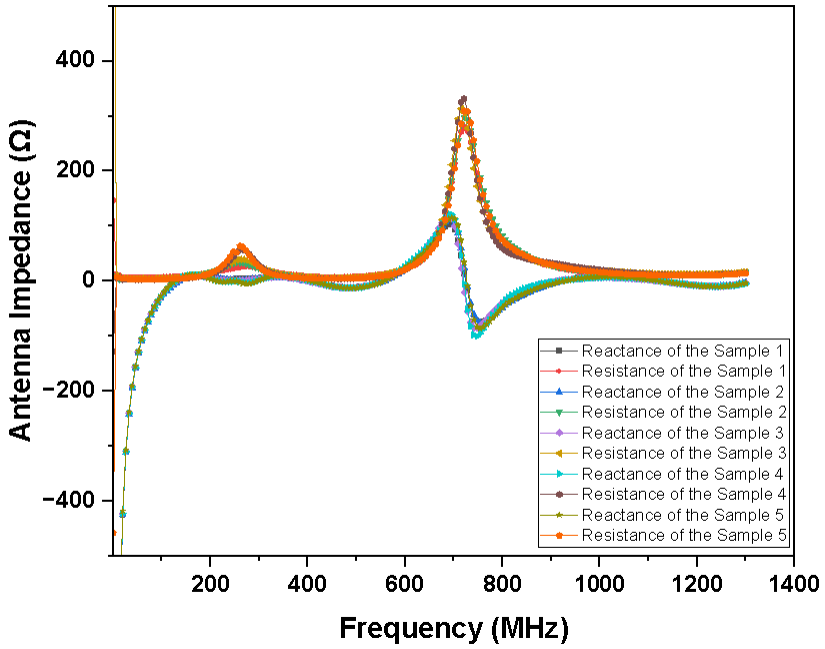

Figure 3.8 : Antenna impedance graph of the non-sintered textile antennas.

Figure 3.9 indicates the reflection coefficients (S parameters) of the non-sintered textile antennas. In terms of antenna efficiency, it is desired that the reflection coefficient of the antenna is lower than −10 dB. According to Figure 3.9, it is seen that all samples collapse at 254 MHz. The reflection coefficients of samples 1, 2, 3, 4, and 5 at 254 MHz were measured as −8.24 dB, −12.52 dB, −15 dB, −30.85 dB, and −34.87

dB, respectively. At the same time, it is understood that the different pass numbers make a significant difference in the reflection coefficient values of the antennas.

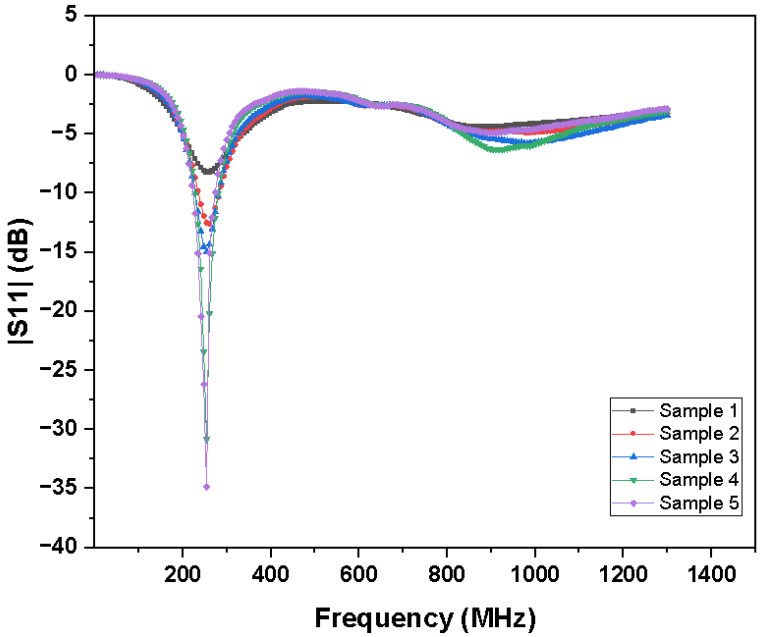

Figure 3.9 : Reflection coefficients of the non-sintered textile antennas.

3.3.2 Impedance measurement results of the sintered textile antennas

In order to understand the effect of the sintering process on the radiation behavior of the antennas, the samples produced in the same way with pass numbers from 1 to 5 were sintered in an oven at 150 °C for 15 min after the printing process. Samples with 1 pass 2 pass, 3 pass, 4 pass, and 5 pass were named as sample 6, sample 7, sample 8, sample 9, and sample 10, respectively. After the sintering process, the reflection coefficients, and impedances of the antennas were measured with a vector network analyzer as mentioned before. The impedance–frequency graph drawn according to the measurement results is shown in Figure 3.10. When Figure 3.10 is examined, it is seen that the resistance, and reactance curves of the non-sintered samples (Figure 3.8) show similar trends with the sintered samples. The reflection coefficients of the sintered textile antennas are shown in Figure 3.11. The reflection coefficients of samples 6, 7, 8, 9, and 10 at 943 MHz which is the resonance point, were measured as −8.25 dB, −8.45 dB, −9.52 dB, −9.57 dB, and −9.86 dB, respectively. If an external impedance matcher is used, the antenna may be usable more efficient at 943 MHz. According to the measurement results, the sample closest to −10 dB was the sample with the highest pass number. As the pass number decreases, the reflection coefficient

rises above −10 dB. This is thought to be due to the increase in conductivity as the number of passes increases.

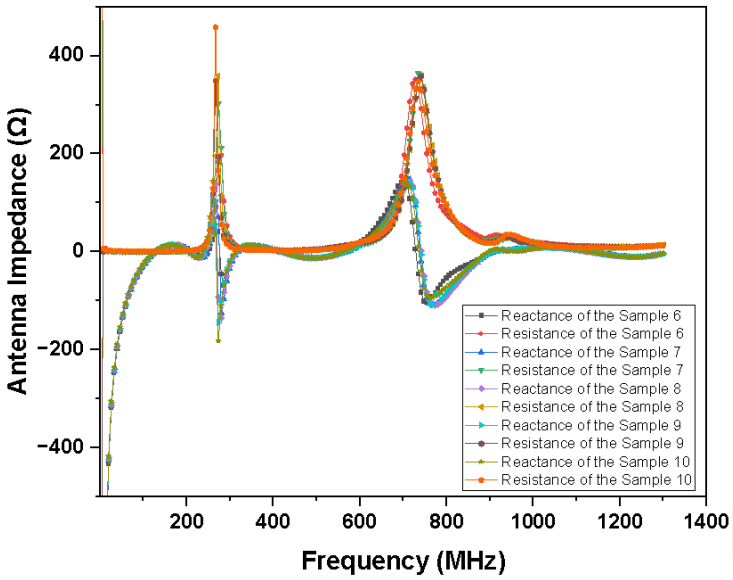

Figure 3.10 : Antenna impedance graph of the sintered textile antennas.

Therefore, it is seen that the difference in the pass number has an effect on the radiation behavior of the antenna. When the sintered samples are compared with the non-sintered samples, it is understood that the resonance point shifted from 254 MHz to 943 MHz. It is known that the frequency band of the UHF RFID is 860–960 MHz (Meng et al., 2022). Thus, flexible textile-based UHF-RFID enabled wearable sensors printed with pad printing method become suitable for UHF RFID technologies after sintering process.

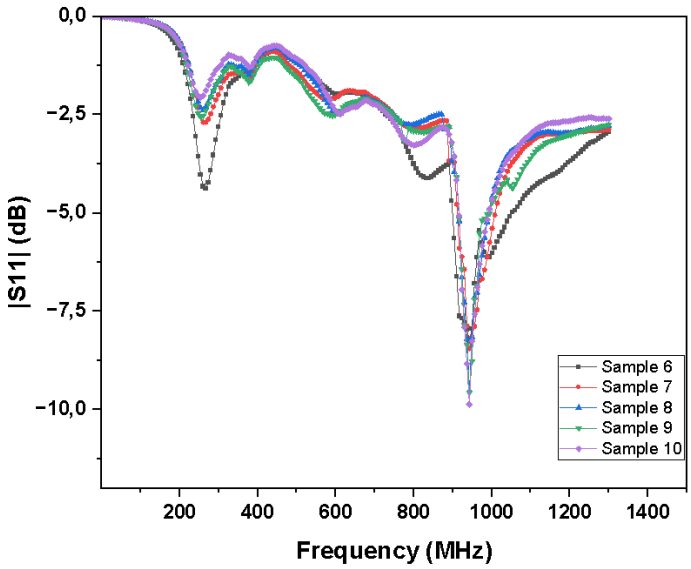

Figure 3.11 : Reflection coefficients of the sintered textile antennas.

3.3.3 Gain measurement results of the sintered textile antennas

S21 measurements were performed with a vector network analyzer for the reference antenna, and the sintered 5 pass textile antenna. The gain difference between the reference antenna, and the fabricated antenna is shown in Figure 3.12. According to Figure 3.11, S21 measurement of the reference antenna was −21.2 dB at 943 MHz, while the S21 measurement of the fabricated textile antenna was −31.0 dB at 943 MHz. The gain difference between the reference antenna, and the fabricated antenna was approximately −10 dB. However, considering that the dimension of the reference antenna is 30 × 30 cm and the dimension of the produced antenna is 24.13 × 46.74 mm, it is thought that this difference is due to the size difference, and the gain of the fabricated antenna is not bad.

3.3.4 Bending measurement results of the sintered textile antennas

The sintered 5 pass textile antenna was subjected to bending in different directions. Figure 3.13 indicates reflection coefficient graphs of the antenna according 3 different situation. According to Figure 3.13, there is no resonance frequency shift. When the S11 values are examined, the reflection coefficient in the flat state of the antenna was −9.85 dB at 943 MHz. When the antenna was bent in the x direction (polarization direction), the reflection coefficient value was measured as −8.81 dB at 943 MHz. In the last case, the reflection coefficient was measured as −5.76 dB at 943 MHz when the antenna is bent in the y direction. Therefore, the proposed textile UHF RFID antenna still performs well after bending in the polarization direction. In a study, bending test was applied with different radius to the flexible UHF RFID antenna embroidered on the surgical mask using conductive yarns. Antenna impedances, and reflection coefficients were measured for different radius. As a result, it was determined that the reflection coefficients increased with increasing bending angles, and there was a slight shift in the resonant frequency (below 20 MHz). Therefore, it is emphasized that the proposed UHF RFID textile antenna still works well (Luo, Gil, & Fernandez-Garcia, 2022b). When the results of the above-mentioned study are compared with the results in Figure 3.13, it is seen that the proposed RFID antenna performs better against bending. This shows that the textile antenna is wearable, and flexible.

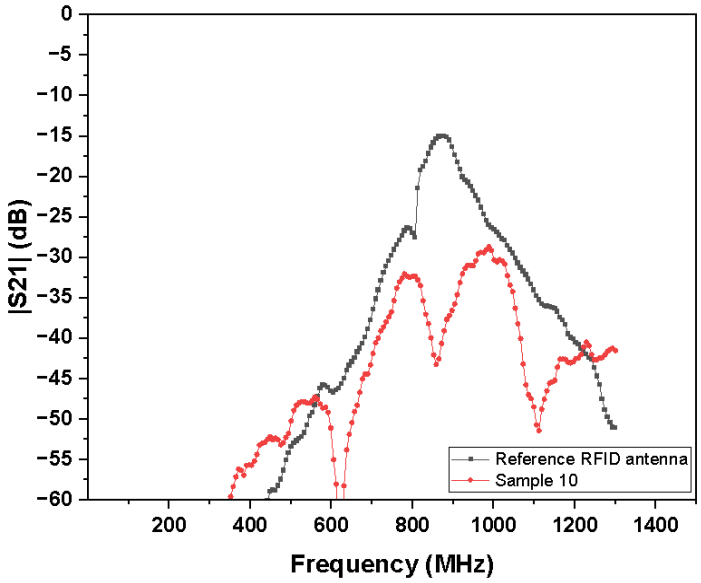

Figure 3.12 : S21 measurements of the reference antenna and textile antenna.

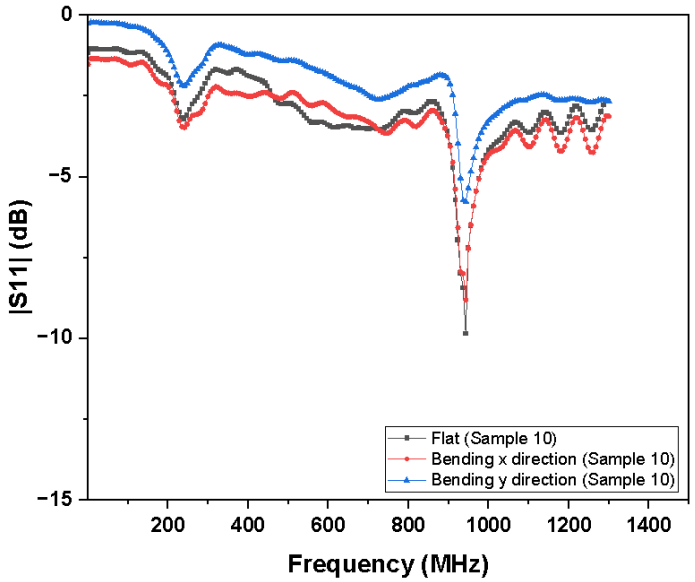

Figure 3.13 : Reflection coefficients of the textile antenna in different bending directions.

3.4 Conclusion

As a result, the designed UHF-RFID enabled wearable sensors were produced by pad printing method using silver conductive ink. In order to understand the effect of the sintering process on antenna performance, some of the antennas produced were sintered (150 °C, 15 min), while the other part was not. The impedances and reflection coefficients of the sintered, and non-sintered samples were measured using a vector network analyzer. When the impedances of the non-sintered, and sintered antennas

were compared, it was seen that quite similar curves were obtained, and the difference in the pass numbers did not make a remarkable difference on the antenna impedances. When the reflection coefficient graphs were examined, it was determined that the resonance point of the non-sintered samples was at 254 MHz and the reflection coefficient was −34.87 dB for the sample with 5 pass. After the samples were sintered, it was measured that the resonance point was at 943 MHz and the reflection coefficient of 5 pass sample was −9.86 dB. Therefore, it is thought that antennas with better performance can be produced by changing the sintering duration, and temperature, while it is determined that the antenna performance of the samples is suitable for the UHF RFID band, after the sintering process. In addition the impedance measurement of the fabricated sensors, bending tests was applied to the best sample to show the sensors wearable, and flexible. Moreover, gain measurements was carried out according to the reference antenna to make the antenna performance more understandable. As a result of all tests, it is predicted that the structure designed as a wearable sensor can be used as a UHF RFID antenna, especially humidity sensitive areas because of the proposed structure.

3.5 Declaration of Competing Interest

The authors declare that they have no known competing financial interests or personal relationships that could have appeared to influence the work reported in this paper.

3.6 Acknowledgement

This study was supported by the scientific, and technological research council of Turkey (TUBITAK) with the project number 119M976.

3.7 Data availability

Data will be made available on request.

4. WEARABLE UHF-RFID SENSOR FOR WETNESS DETECTION[3]

The use of wearable textile Radio Frequency Identification (RFID) sensors is becoming widespread in many different application areas because of their technical utilization advantages. In this study, a textile-based Ultra High Frequency (UHF) RFID sensor that can be used to detect wetness has been developed and fabricated with a pad printing machine using silver conductive ink. The overall physical dimension of the proposed sensor structure is 75.0 mm × 38.0 mm × 0.12 mm. Two different types of Received Signal Strength Indicator (RSSI) measurement setups in near field region and at practical separation distances emulating more realistic environmental conditions have been carried out to test and validate the applicability of the proposed sensor. Water, saline and urine solutions have been used to evaluate different wetting conditions in the near field RSSI measurements by dropping different solutions on the RFID sensor integrated diaper. A permissible signal difference of at least 17 dBm has been detected between the wet and dry states of the proposed wetness detection sensor. The performance of the proposed RFID sensor has been evaluated using different separation distances of 32 cm, 40 cm and 50 cm with the practical result of maximum reading range to be 50 cm for the reliable determination of the binary wetness states. In addition, the performance of the RFID wetness sensor against different bending and deformation conditions is almost robust. It is concluded that the proposed sensor structure can be integrated onto the patient's diapers to facilitate the reliable detection of wetness states in cases such as urinary incontinence in remote health monitoring systems.

Index Terms: diaper, printing, received signal strength indicator (RSSI), RFID sensor, textile based sensor, ultra high frequency (UHF), urinary incontinence, wearable, wetness detection.

[3] This chapter is based on the paper "Tekcin, M., Palandoken, M., and Kursun, S. 2023. Wearable UHF-RFID Sensor for Wetness Detection, IEEE Access, 11, 115179 - 115189. DOI: 10.1109/ACCESS.2023.3324816".

4.1 Introduction

Radio Frequency Identification (RFID) is defined as a low-cost wireless technology that is used in businesses to identify products, locate, and communicate, as well as establish connections between numerous objects (Costa et al., 2021). The use of RFID technology in many different application areas is becoming widespread. Health monitoring (Prather et al., 2019; Xie et al., 2022), goods (Shafiq et al., 2019) or patient tracking systems (Cao et al., 2014), and logistics (Caccami et al., 2019; Wanhua, 2020) are the areas where RFID technology is frequently used. The design and operating frequency of RFID sensors are determined according to the needs of their usage areas, and sensing functions (Luo, Gil, & Fernandez-Garcia, 2022a). Generally, there are three different frequency bands used for RFID tags. These frequency bands are the low frequency band (120–150 kHz), the high frequency band (13.56 MHz), and the ultra-high frequency band (433 MHz, 865–868 MHz in Europe, 917–922 MHz in China and 902–928 MHz in North America) (Gaspari & Quaranta, 2019; Luo et al., 2020). Recently, Ultra High Frequency (UHF) RFID tags and sensors are highly preferred due to several advantages. Among these advantages are the low cost, long-distance operation, and fast-easy identification of UHF-RFID devices (Luo, Gil, & Fernandez-Garcia, 2022a; Vena et al., 2019).

Textile UHF RFID sensors have emerged as a result of the combination of sensing data wirelessly with flexible, and wearable substrates. The signal strength indicator parameter is a typical method used to detect data wirelessly (Akdag et al., 2022; Luo, Gil, & Fernandez-Garcia, 2022a; Tajin, Amanatides, et al., 2021). Received Signal Strength Indicator (RSSI) is an important parameter which shows the signal strength received from RFID tag to RFID reader in RFID systems for communication to take place. There are limits that the reader, and chip used in the RFID system, and these limits show the sensitivity of the reader, and the chip. For communication to take place, the RSSI value must be within these limits. Although RSSI value changes depending on antenna gain, distance between antenna, and path loss, RFID tag can be designed to function as a sensor according to RSSI value, since it can also be affected by different conditions. In this study, it is aimed to design textile-based RFID structure to act as a sensor according to the received signal against different wetness levels.

Wetness detection systems for individuals are generally developed for sweat, blood, skin wetness sensing and urinary incontinence situations. In this study, urinary incontinence was chosen for wetness detection. Urinary incontinence is the involuntary leakage of urea during exertion and in situations such as coughing and sneezing (Frigerio et al., 2023). Urinary incontinence can affect many conditions such as social, psychological, physical and family life of the patient, and this situation reduces the life quality of people and limits their social lives (Alizadeh, Mohammah-Alizadeh-Charandabi, et al., 2023; Alizadeh, Montazeri, et al., 2023). Although there are many treatments for urinary incontinence, none of these treatments are completely curative (Michel et al., 2023). For this reason, urinary incontinence patients have to use diapers. Diaper changes of urinary incontinence patients in hospitals and nursing homes are done by caregivers and health personnel. Caregivers check these individuals very often, as wet diapers on patients and the elderly cause various diseases such as dermatitis and infection (Cho et al., 2021; Jaekel et al., 2023). While these controls are an extra workload for the caregiver, they also cause the patients to be awakened and disturbed (Cho et al., 2021). For these reasons, there is a need wetness detection system that detect when diaper changes are necessary.

Textile-based UHF-RFID sensors are lightweight, washable, flexible, and wearable compared to conventional UHF-RFID sensors. This situation ensures the use of textile-based RFID sensors to increase day by day (Luo et al., 2020). In a study, a wearable knitted UHF-RFID compression sensor antenna has been proposed for respiratory monitoring. As a result of the tests performed on the reusable UHF-RFID sensor, the radiation efficiency on the body has shown good values with permissible sensitivity to the compression (Tajin, Amanatides, et al., 2021). In another study, textile-based UHF-RFID antennas produced by embroidery method have been applied to surgical masks. The maximum reading distance of the UHF-RFID antenna placed on the surgical mask has been measured as 1.1 meters. It has been emphasized that the proposed design can provide identification or safe distance warning in case of an epidemic (Luo, Gil, & Fernandez-Garcia, 2022b). In another study using the embroidery method, the moisture sensing performance of the textile-based UHF-RFID antenna has been investigated. As a result, it has been shown that the use of RFID technology in moisture sensing studies is very advantageous (Shuaib et al., 2017). UHF-RFID antenna performance has been investigated by applying different heat

treatments to the wearable sensor produced using the printing method. According to the results obtained, it is stated that the proposed sensor structure can be used as a UHF-RFID antenna, especially in areas sensitive to humidity (Tekcin et al., 2022). In the study of Sen et al., moisture detection has been made with UHF RFID moisture monitoring by utilizing absorbent polymers in diapers. The proposed sensor structure has been designed using metal and hydrogel in accordance with the diaper geometry (Sen et al., 2020). Bluetooth-based detector developed for babies and the elderly detects wetness and bleeding. The wetness sensor consisting of two or four conductive thin wires has been connected to pressing studs which placed in the diaper or bandage. When the wires inside the diaper or bandage come into contact with blood or urine, the conductivity of the pressing studs exceeds the predetermined threshold value, informing its wetness status (Simik et al., 2019). A sensor mat that can be placed under the sheets was recommended to detect urinary incontinence and bed occupancy. This sensor consists of embroidered conductive yarns. While the wetness is detected by looking at the resistance change of the sensor, the occupancy status was determined by the capacitance change. An external unit consisting of radio frequency (RF) connection or WiFi module has been used for recording and transferring the obtained data (Fischer et al., 2019).

There are many printing methods available today and it is extremely important to select the appropriate printing method for printed electronic structures to perform at their best. Printing technologies consist of two main groups; contact, and non-contact methods. In contact printing method, the surface with ink is in direct contact with the substrate, while in non-contact printing method, the ink prepared in solution is dispersed or sprayed onto the substrate (Beltrão et al., 2022). Inkjet (Tekcin et al., 2021; Tekcin et al., 2022), and aerosol jet printing (Cooper & Hughes, 2020) techniques are the examples of non-contact printing methods. On the other hand, some kinds of contact printing techniques are screen printing (Qi et al., 2020), gravure printing (Bariya et al., 2018), flexographic (Y. Wang et al., 2021), and pad printing (Tekcin et al., 2022) methods. Pad printing, which is a versatile offset printing technique, is one of the oldest printing techniques. Thanks to the developments in pad printing, the application areas of pad printing have expanded from conventional textiles to sensors, biosensors, RFID tags, and photovoltaic cells (Jaafar et al., 2021; Xiong & Qu, 2011). The first step in the pad printing method is to create the desired

pattern on the printing plate called cliché. Then, the ink reservoir comes over this pattern and the ink covers the pattern. At this point, the important thing is to remove the excess ink from the cliché very well. Finally, the silicone pad first takes the pattern onto itself and then transfers it to the substrate (Merilampi et al., 2011; Tekcin et al., 2022; Xiong & Qu, 2011). Pad printing becomes advantageous when compared to other printing methods due to its low cost, simplicity, fastness, ability to work even with high viscosity inks, printing on a wide variety of substrates like flexible, curved, and rough surfaces, and printing layer by layer (Jaafar et al., 2021).

Literature reveals that many textile-based sensors and antennas have been introduced. However, the difference of the current study compared to the alternative sensor designs in the literature is that it proposes a novel sensor design that senses through the RSSI level for the wetness detection. Thus, in this study, textile-based wearable and flexible UHF-RFID sensor is designed, numerically computed, and printed on polyamide-based taffeta label fabric according to the pad printing method using silver conductive ink. After RFID chip is integrated onto the printed RFID sensor, water, saline and urine solution have been dropped onto the fabricated RFID sensor for wetness detection measurements. Wetness performance of the produced RFID sensor structure is determined by detecting the RSSI changes in the RFID sensor with the help of RFID reader antenna. RFID sensor structure used in the study can also be integrated onto baby diapers to detect urinary incontinence in babies. However, the study targets urinary incontinence in adults, as diaper changes are easier in infants than in elderly and sick adults. The presented study is one of the rare studies that uses the RSSI sensing principle to detect urinary incontinence through the pad printed RFID sensor geometric model with the chip integration. The novelty of the study is that the disposable, flexible, textile-based RFID sensor to be designed and fabricated for this application can be produced by a very simple printing method, and it is very thin and small to provide users' comfort with the biocompatible feature.

4.2 Materials and Methods

4.2.1 Chemicals, materials and ink formulation

In this study, silver conductive ink has been used to produce e-textile based UHF-RFID wetness sensor. To adapt the viscosity of silver conductive ink having 10.000 cP dynamic viscosity to the pad printing method, a thinner from TRI Electronic is used.

Polyamide-based taffeta label fabric supplied by Huzhou Hengxin Label Manufacture Co. (Huzhou, China) is used as a substrate for printing the UHF-RFID wetness sensor. The technical characteristics of the substrate have been detailed in the previous study (Tekcin et al., 2022). Impinj Monza R6-P tag chip was purchased to connect the UHF-RFID wetness sensor with the RFID reader. The optimum ink formulation for pad printing is given in (Tekcin et al., 2022).

4.2.2 UHF-RFID wetness sensor design, simulation and fabrication

While RFID sensor circuit performance is greatly influenced by the frequency-dependent complex impedance of the chip to be integrated after the fabrication of the sensor model, the input impedance of whole sensor geometric model has to be determined through the parametric analysis and optimizations. Therefore, the input impedance of the chip is firstly obtained from the datasheet after the RFID chip to be integrated has been determined. In this study, Impinj Monza R6-P RFID chip is selected. The complex chip impedance at 867 MHz is nearly equal to 18.27 - j146.7Ω, which is additionally checked through the fabricated directional coupler. After the chip impedance is obtained, the impedance of RFID sensor structure is designed to be complex conjugated with the impedance of the chip to be integrated. The RFID sensor model is shown in Figure 4.1 along with the geometric parameters in Table 4.1. The proposed sensor model is composed of E-shaped resonator and modified U-shaped resonator loaded with the T-shaped extended stub where the RFID chip is to be connected in between. The structural model of the proposed sensor has been designed and numerically calculated in Microwave CST Studio. The discrete port impedance has been set to 18.27Ω and the required amount of capacitance representing the reactive part of RFID chip has been modelled through the capacitance lumped element of 1.25 pF in the numerical model as shown in Figure 4.1. Therefore, the discrete port representing the RFID chip has been completely modelled through the series combination of discrete capacitance and port resistance with the respective values of 1.25 pF and 18.27Ω . The substrate material has been selected as polyamide based taffeta with the relative permittivity and loss tangent of 2 and 0.02, respectively. The metal parts have been selected as silver. The overall dimensions of the proposed sensor structure are 75.0 mm × 38.0 mm × 0.12 mm.

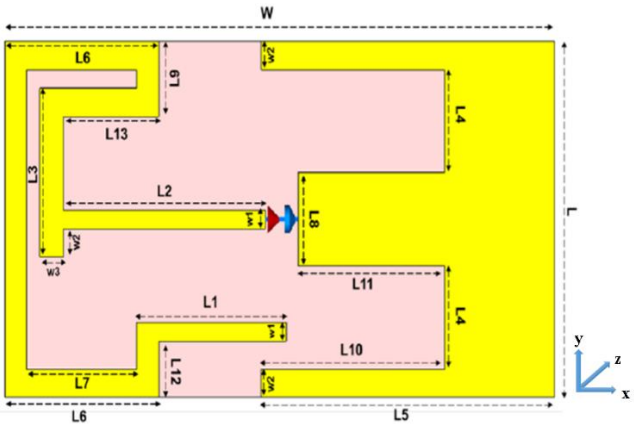

Figure 4.1 : Proposed RFID sensor structure.

Table 4.1 : Dimensions of proposed RFID sensor structure.

Symbol	Size	Symbol	Size
L	75 mm	L5	40 mm
W	38 mm	L6	21 mm
W1	2 mm	L7	15 mm
W2	3 mm	L8	10 mm
W3	3.25 mm	L9	8 mm
L1	20.40 mm	L10	25 mm
L2	27.50 mm	L11	20 mm
L3	18 mm	L12	6 mm
L4	11 mm	L13	13 mm

As deduced from Figure 4.2, the RFID sensor structure operates in the frequency band of 857 MHz and 872 MHz with the resonance frequency of 867 MHz. The polar radiation patterns for X-Y, X-Z, and Y-Z planes, and surface current distribution of RFID sensor structure at 867 MHz have been shown in Figure 4.3 and Figure 4.4, respectively.

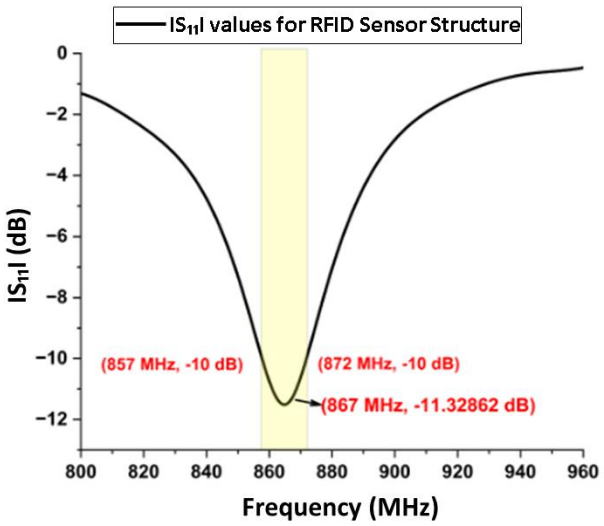

Figure 4.2 : $|S_{11}|$ parameter of RFID sensor structure at 867 MHz.

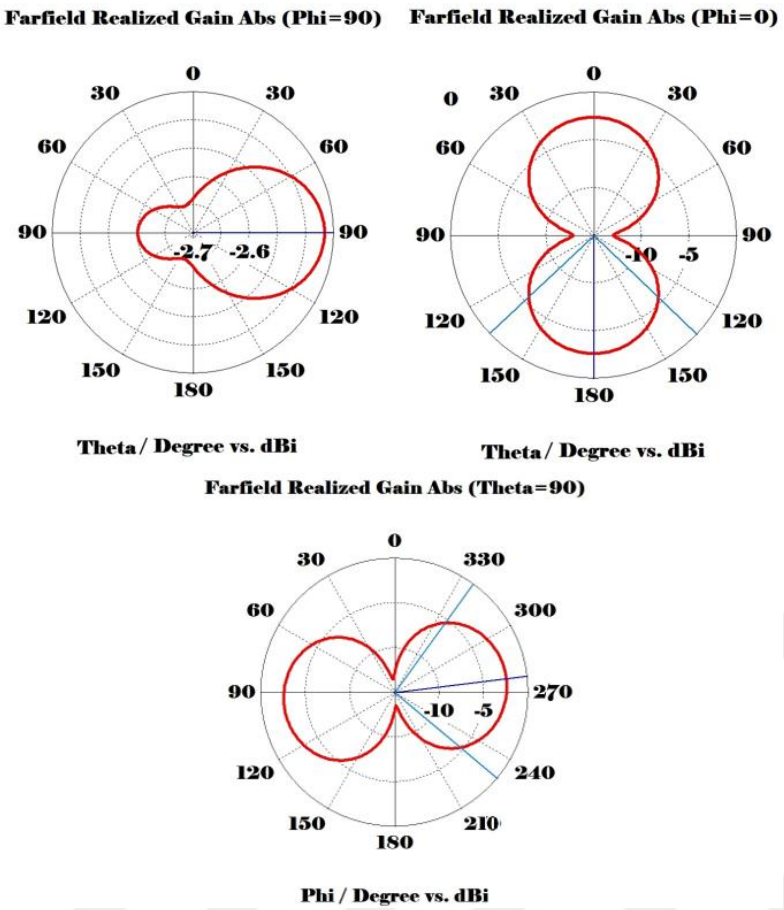

Figure 4.3 : 2D polar radiation patterns for RFID sensor structure.

The surface current distribution in Figure 4.4 shows which sensor sections in the main resonator geometry are more prone to the liquid drops to obtain possibly high value of RSSI value changes between the dry and wet states of RFID wetness sensor. This provides additional practical information on how the relative placement of RFID wetness sensor has to be managed in the adult diaper with the targeted consequence of increased exposure level of wetness sensor to more liquid drops.

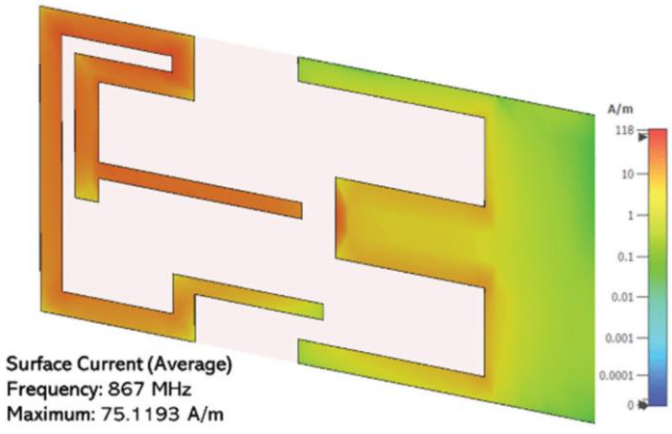

Figure 4.4 : Surface current distribution at 867 MHz.

After the RFID wetness sensor model has been verified through the numerical computations, the fabrication of the sensor has been carried out. To fabricate the RFID sensor structure, according to determined dimensions based on the simulation results, a pad printing method is used and a cliché is prepared. COMEC, EAZY90 pad printing machine has been used in the study. The working principle of the pad printing machine (COMEC, EAZY90) is explained in (Tekcin et al., 2022).

Printing process is carried out using cliché and silver ink for which the prescription is given on the polyamide-based taffeta label fabric. The print pass number has been determined as 3 to increase the conductivity of the RFID sensor. After each print, drying process is applied for 2 minutes in order to avoid print slipping. Finally, the sintering process is applied on the printed RFID sensor in an oven at 150°C for 30 minutes. After this process, the RFID IC must be connected to the RFID sensor in order to make the sensor ready for the measurement with RFID reader. The RFID IC has two contact pads and it has been mounted on the sensor through these contact pads using conductive paste and ready for the measurement. The printed RFID sensor and the chip integrated to the RFID sensor are shown in Figure 4.5.

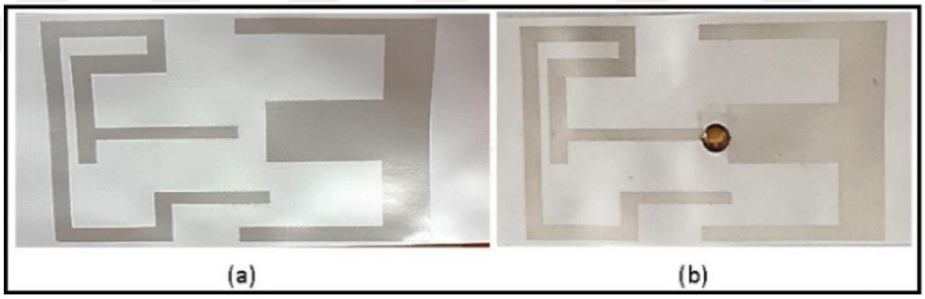

Figure 4.5 : a) Printed RFID sensor structure (b) Printed RFID sensor structure with chip integration.

4.2.3 Integration of the RFID sensor onto adult diaper for RSSI measurements

RFID sensor is printed on adhesive polyamide-based taffeta fabric for easy integration of the RFID sensor onto the adult diaper. The adult diaper consists of many different layers. In order for the RFID sensor not to come into direct contact with the skin, the sensor must be placed between the layers. Therefore, the top layer of the diaper is removed and the RFID sensor is placed between the top layer of the diaper and the ADL (Acquisition/Distribution Layer). Then, the top layer separated to restore the original form of the diaper is sewn to the diaper with an ultrasonic sewing machine. The schematic view of the process is shown in Figure 4.6.

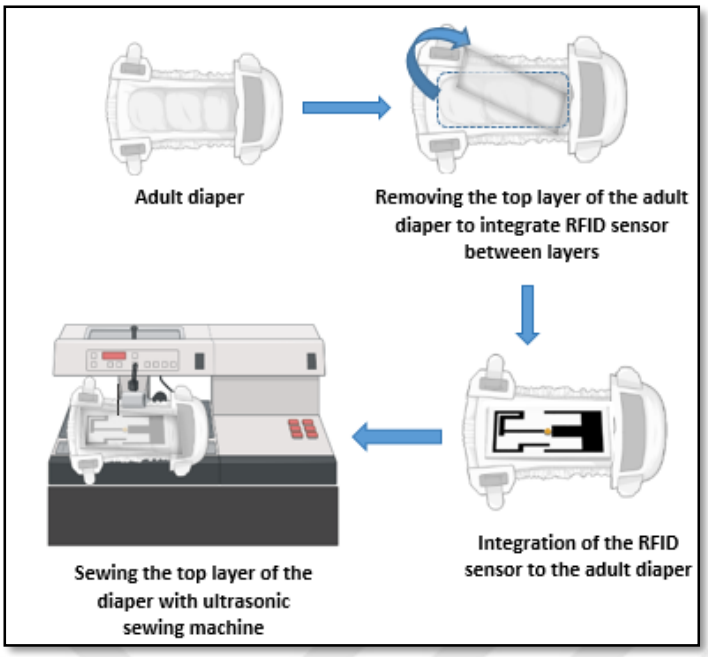

Figure 4.6 : Schematic view of the integration of the RFID sensor into the diaper.

For RSSI measurements, different amounts of water, saline, and urea solutions have been dropped onto the RFID sensor integrated into the adult diaper, and RSSI values are measured with the help of a near field RFID reader through near field communication. Figure 4.7 indicates the schematic view of the near-field RSSI measurement setup. The near-field RSSI measurements are performed as preliminary test and validation steps in the scope of proof of concept in order to observe whether the detectable amount of changes in RSSI levels could be obtained between the wet and dry states of RFID wetness sensor in near field reading ranges.

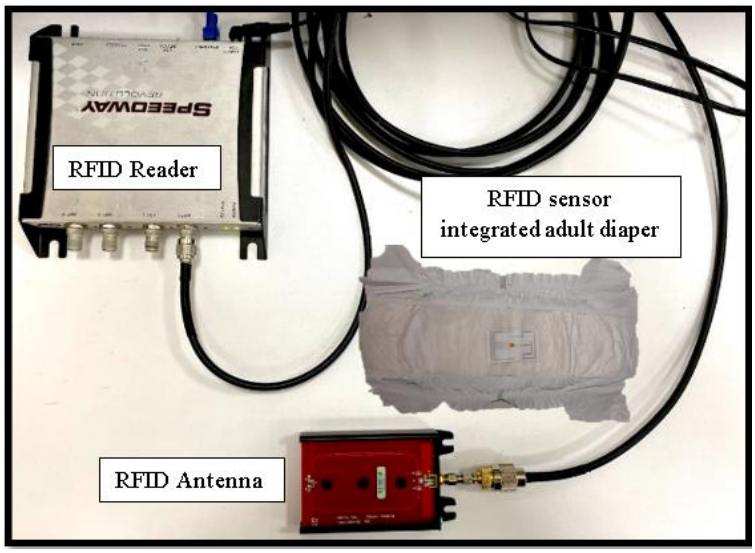

Figure 4.7 : RSSI near field measurement setup.

Near field RSSI measurement results can be basically affected by the relative positioning of the RFID sensor with respect to reader antenna on which the RFID wetness sensor has been directly located in addition to other nearby substances in the environment and ambient conditions (Nilsson et al., 2011; Tajin, Mongan, et al., 2021). For these reasons, attention is paid to ensure that the substances in the environment are at the same distance and position in each measurement to preserve the same measurement conditions. However, in order to investigate the wetness detection performance of the RFID wetness sensor at practical reading distances, in addition to the measurement setup indicated in Figure 4.7, versatile measurements have been carried out by using highly directive antenna array for RFID wetness sensor in salty water at different polarization orientations. The measurement setup shown in Figure 4.8 has been arranged to emulate the RFID wetness sensor embedded patient diaper-reader antenna distances in the real-life environment.

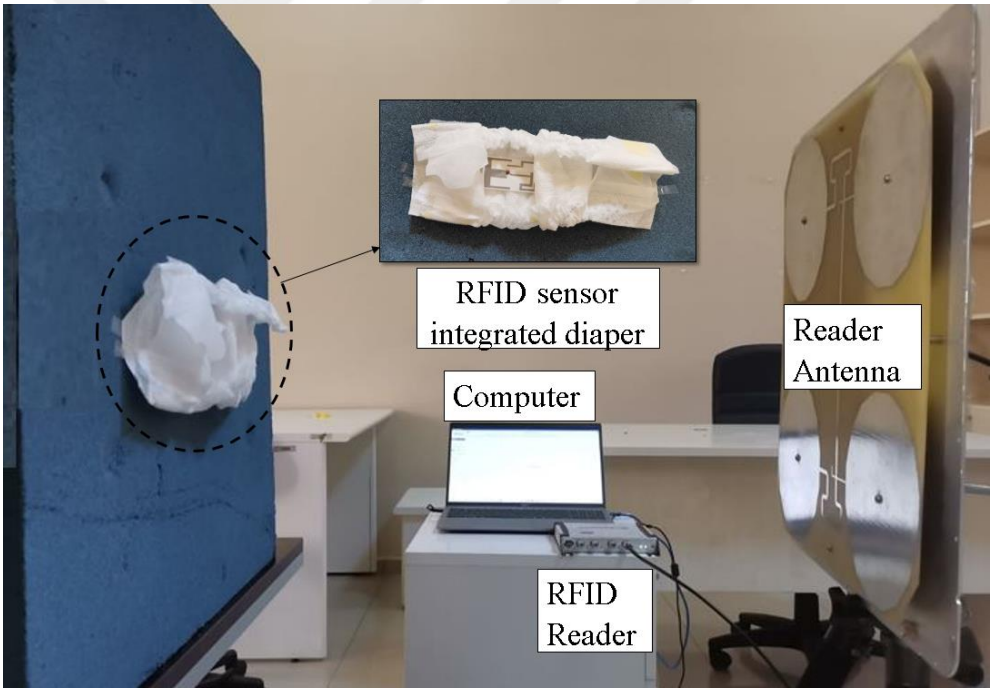

Figure 4.8 : RSSI measurement setup with highly directive 2 × 2 antenna array at practical separation distances emulating the real life.

In real life, it is appropriate to locate the reader antenna at a practical separation distance of 40 cm from the diaper under the patients bed at right antenna orientation. Moreover, in order for the proposed RFID wetness sensor to be used in real life, the RSSI values obtained from the RFID reader have to be firstly calibrated with previously measured data in the wetness detection environment as in other sensor

applications. Based on the laboratory measurement results, it can be deduced that the circular polarized antenna can be conveniently used as a reader antenna to increase the RSSI level for the better detection of wetness level in large amounts of urine in addition to the utilization of new generation RFID systems with lower reading sensitivity levels.

4.2.4 Bending simulation and bending measurement of RFID sensor structure

In order to make the RFID sensor structure printed on the flexible label fabric wearable, the proposed structure should be resistant to bending, stretching, and other deformations (Xu et al., 2020). For this, bending simulations and deformation tests have been applied to the sensor structure.

The performance of the RFID sensor against different bending conditions has been simulated in the CST Studio (Nie et al., 2022). During the simulations, different bending angles, 15°, 45°, 90°, −15°, −45°, and −90°, were applied to the structure. Apart from the numerical computation, a manual deformation test has been carried out by combining the right and left edges of the RFID sensor integrated adult diaper at the middle point (Ozek et al., 2021). This process has been done 10 times.

The proposed RFID wetness detection sensor can be subject to different bending states in practical applications when it is placed into the adult diaper, which has been worn on the human body. A human body phantom has been therefore modelled to gain more information about the change in the input impedance of the RFID sensor affecting the measured RSSI values under these bending conditions.

Considering four-layered human body model, parametric numerical computations of RFID sensor have been conducted for varying bending angles. The four-layered human body model consists of skin (σ_{sk} = 0.85 S/m and ε_{sk} = 41.58), fat (σ_{fat} = 0.05 S/m and ε_{fat} = 5.46), muscle (σ_{mus} = 0.93 S/m and ε_{mus} = 55) and bone (σ_{b} = 0.14 S/m and ε_{b} = 12.48) (Colella et al., 2023; *Dielectric Properties of Body Tissues*, 2023). The RFID wetness sensor has been located on the top of all these four layers with the bending angles ranging from 15° up to 90° with 15° steps. The schematic view of four layered human body model is shown in Figure 4.9.

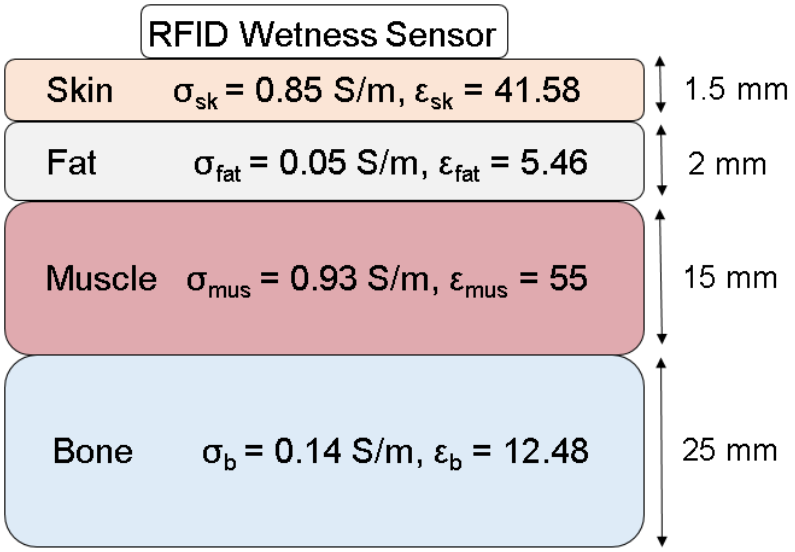

Figure 4.9 : Four layered human body phantom model.

4.3 Results and Discussion

The proposed RFID sensor structure shows the varying sensing performance due to the input impedance change and respective degradation in gain as a result of nearfield coupling to the exposed liquid drops and the corresponding change in RSSI value to be deduced from the Friis Transmission equation shown below:

$$P_R = P_T \frac{G_T(\theta_T, \emptyset_T) G_R(\theta_R, \emptyset_R) \lambda^2}{(4\pi r)^2} (1 - |\Gamma_T|^2)(1 - |\Gamma_R|^2)|\hat{p}_T . \hat{p}_R|^2 \quad (4.1)$$

The term P_R in the equation represents the power received by RFID sensor structure, P_T term is the power transmitted by RFID reader antenna, whereas the G_T indicates RFID reader antenna gain and the G_R represents RFID sensor structure gain and r denotes the distance between the reader antenna and the RFID sensor structure. The term $(1 - |\Gamma_T|^2)(1 - |\Gamma_R|^2)$ represents the transmission loss due to the reflection, $|\hat{p}_T . \hat{p}_R|^2$ term indicates the losses due to the polarization mismatch. For a reliable communication to be realized between the RFID reader and the RFID wetness sensor, the reading sensitivity of the whole reader system imposed by the RFID chip used in the sensor structure is extremely important. The RFID reader in the current study can achieve the reading capability up to −84 dBm RSSI level. However, since distance and environmental factors influence the sensing capability of the proposed sensor

structure, these parameters have been tried to be kept constant in all near field measurements for different situations.

In the measurement process, RSSI values have been obtained with the measurement software of the RFID reader. To detect the wetness, different amounts of salt water mixture have been dropped onto different points of the sensor structure by using a dropper, and the response of the structure for these different situations has been determined through RSSI measurements. Figure 4.10 shows the variation of RSSI values according to different salt water amounts in near field measurements. When Figure 4.10 is examined, the RSSI value of the designed sensor structure is −35.31 dBm in the dry state, while a certain amount of degradation in RSSI value is then observed when water and saltwater mixtures are dropped in different amounts. Measurements have been made using a reader antenna with a gain of 2 dBi in the near field. When water has been dropped over 100 mL on the sensor structure, it could not be read from RFID reader because the sensitivity of the RFID reader is −84 dBm. Since all environmental values are kept constant during the measurement, the reason for the RSSI change is that water and saltwater drops affect the gain of the RFID sensor structure.

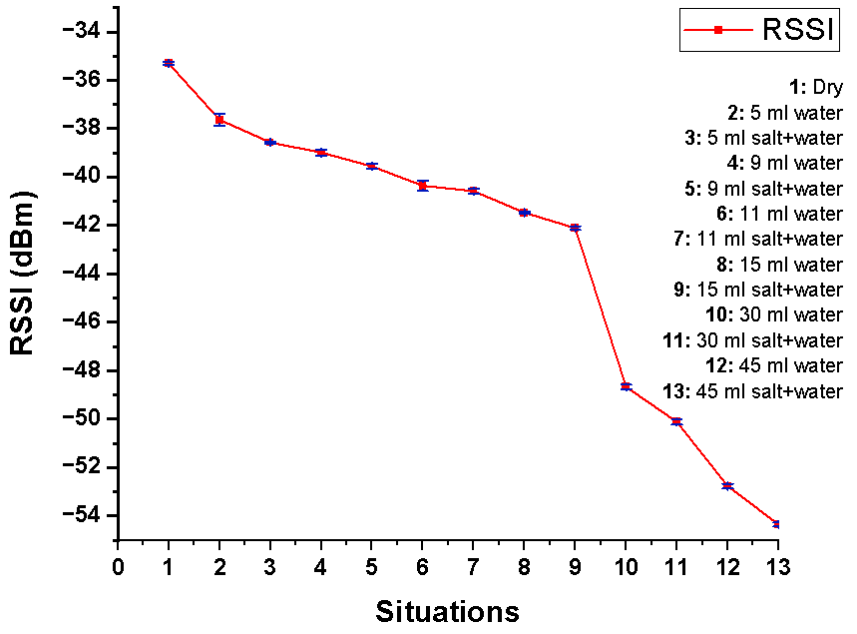

Figure 4.10 : RSSI levels for different salt water amounts on RFID sensor structure.

Especially in health monitoring applications, both the health personnel and the patient have difficulties in determining the urinary incontinence status of adult patients. In order to prevent this situation, an easy-to-fabricate RFID wetness sensor providing

remote warning and directly integrable to diaper is needed. In order to test RFID sensor performance with a diaper, different solutions containing saline, and urine have been prepared and poured onto diaper where the RFID sensor is hidden between diapers' layers. Urine solution is prepared with 20 mL of distilled water, 0.4 g of urea, and 0.2 g of NaCl. Table 4.2 shows the RSSI values measured in the sensor structure for different situations.

When Table 4.2 is examined, it is seen that the RFID sensor structure responds to different wetness conditions in the direction of lower RSSI value as observed in previous measurements. Since the purpose of the sensor is to detect wetness, it is seen that it meets the main purpose of use. The sensor structure is thought to be suitable for detecting the wetness of any textile-based product in different situations.

Table 4.2 : RSSI levels for different situations on RFID sensor structure.

RFID sensor situation	Average RSSI (dBm)
Dry	-35.49
12 ml water	-41.19
Between moist nonwoven surface	-48.52
Between very wet nonwoven surface	-52.77
Between salty and moist nonwoven surface	-49.22
Between salty and very wet nonwoven surface	-54.35
Between nonwoven surfaces moistened with urine solution	-42.00
Between nonwoven surfaces wetted with urine solution	-50.50

On the other hand, in more practical situations realized in the measurement setup shown in Figure 4.8, the maximum RSSI level received by the reader antenna for the RFID sensor immersed in 6 mg / mL salt water from a distance of 50 cm is −55.24 dBm. Therefore, the maximum reliable reading range of the RFID sensor is considered to be 50 cm. The minimum RSSI level received for the different polarizations is −68.24 dBm. The maximum and minimum RSSI levels received by the reader antenna are still higher than the sensitivity of the RFID reader module, whose reading sensitivity level is −84 dBm.

Moreover, the reading ranges have been checked through versatile RSSI measurements while changing orientation angles of RFID sensor with respect to RFID

reader antenna set at fixed orientation. RSSI values obtained at different orientation angles for reading ranges of 32 cm, 40 cm and 50 cm have been indicated in the Figure 4.11. Different orientation angles from 0° to 360° with 45° increments have been selected to change the position of the RFID sensor. These RSSI measurements have been carried out by placing the RFID sensor in 6 mg / mL salt water. According to the Figure 4.11, RFID sensor gives permissible RSSI results for different orientations at all reading distances between 32 cm and 50 cm to detect the wetness state. Therefore, it has been determined that the different orientation of the RFID sensor with respect to the reader antenna is not a major disadvantage at the reading ranges up to 50 cm. When the effect of different reading distances has been examined at fixed relative orientation of 90° between RFID wetness sensor and reader antenna for maximum RSSI value, the measured RSSI values at the separation distances of 32 cm, 40 cm, and 50 cm are −47.50 dBm, −50.18 dBm, and −55.24 dBm, respectively.

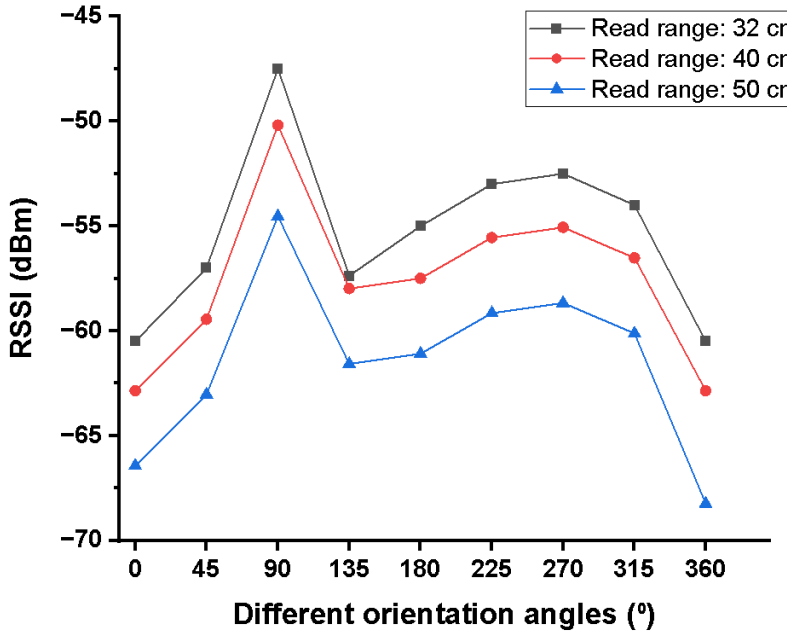

Figure 4.11 : RSSI values of RFID sensor structure for different orientation angles with the separation distance of 32 cm, 40 cm, and 50 cm.

$|S_{11}|$ results of the RFID wetness sensor placed on four layered human body model against different bending angles ranging from 15° to 90° with 15° steps have been shown in the Figure 4.12. According to the Figure 4.12, the input impedance of RFID wetness detection sensor is severely affected due to the nearfield coupling of resonating sensor sections with the stacked human body model layers having different electric permittivity and conductivity parameters. This can be deduced from the

numerically computed radiation patterns shown in Figure 4.3. However, the effect of different bending angles on the reflection parameter is in negligible amount.

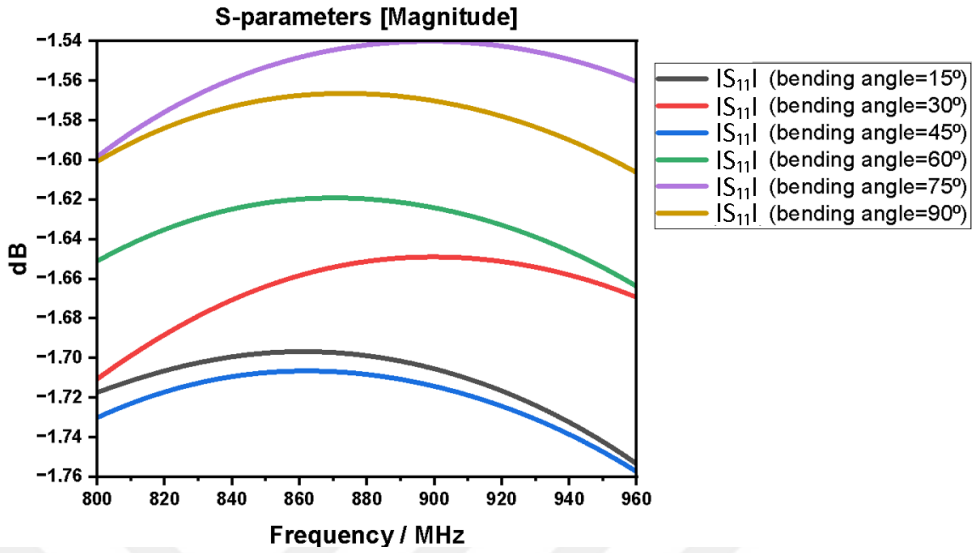

Figure 4.12 : $|S_{11}|$ values of RFID sensor structure placed on the human body model against different bending angles.

In addition, in order to figure out the input impedance behavior of RFID sensor structure in free space without human body phantom model against different bending conditions, the reflection parameter results for different bending angles are shown in Figure 4.13. According to $|S_{11}|$ graphs given in Figure 4.13, when positive bending angles are applied to the structure, it is concluded that the resonance frequency of RFID sensor structure shifts to the lower frequencies with smaller than 2.3% frequency change with reference to the resonance frequency in the unbent condition. Likewise, the tendency of the structure to shift in the resonant frequency is similar when negative bending angles are applied. When the shifts in the resonance frequencies in both graphs are examined, it is seen that the shifts are quite low. Therefore, the resistance of the RFID sensor structure to bending is good.

In addition to the numerical computations, a deformation test has been applied to the RFID sensor structure integrated onto the adult diaper. The RSSI values of the RFID sensor structure in the dry and wetted with water state before and after deformation are measured in near field measurement setup shown in Figure 4.7. The RSSI values measured after a total of 10 deformation cycles are shown in Table 4.3.

Table 4.3 : Near field RSSI measurement results of RFID sensor structure before and after deformation test.

RFID sensor situation	Average RSSI before bending (dBm)	Average RSSI after bending (dBm)	RSSI change (%)
Dry	- 35.45	- 35.48	0.09
5 mL water	- 37.60	- 37.97	0.98
9 mL water	- 38.90	- 39.23	0.86
11 mL water	- 40.28	- 40.95	1.68
15 mL water	- 42.09	- 42.56	1.12
30 mL water	- 48.98	- 49.62	1.30
45 mL water	- 53.02	- 54.92	1.69

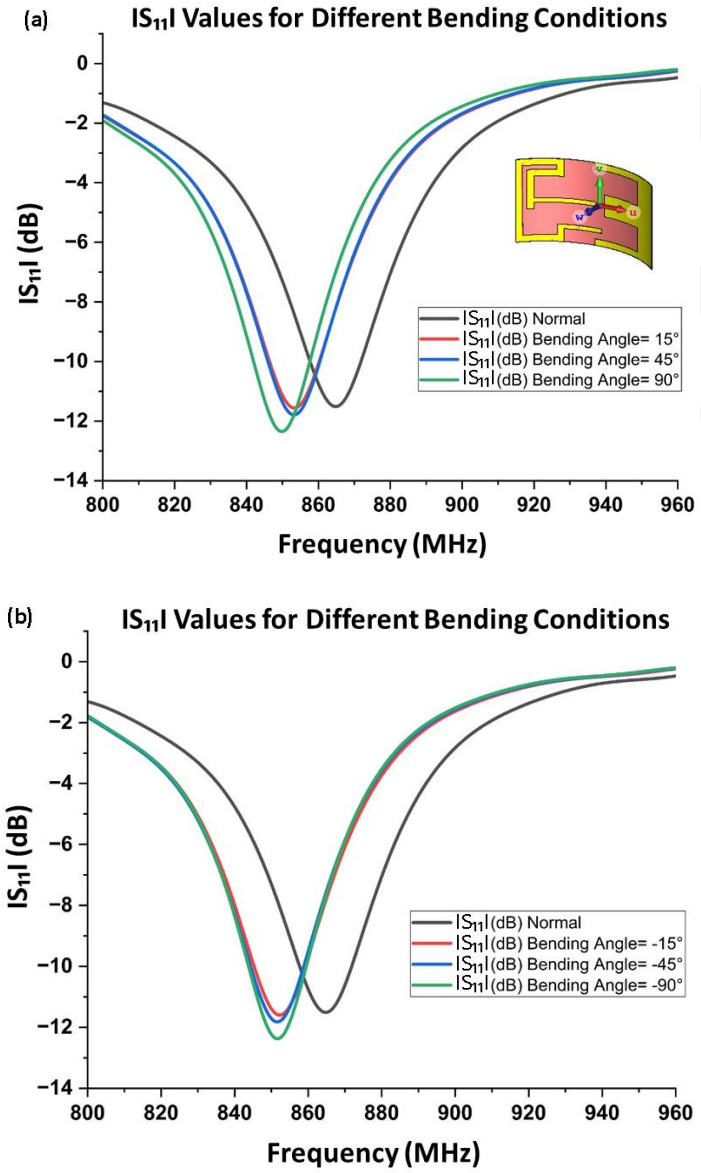

Figure 4.13 : (a) $|S_{11}|$ values of RFID sensor structure against positive bending angles (b) $|S_{11}|$ values of RFID sensor structure against negative bending angles.

According to the percent RSSI changes given in Table 4.3, it is seen that the difference between the RSSI values measured before and after deformation for each condition is quite small. This situation shows that the RFID sensor structure performs well even after 10 cycle deformation. The main purpose of the deformation test is to have an idea of how the stress resulting from bending the RFID sensor can affect the solders of the chip integrated onto the RFID sensor. While applying different bending angles to the chip integrated sensor, it has been determined that the soldered chip could be disconnected from the attached points at angles above 30°. Therefore, the threshold bending angle is determined to be 30°. In addition to these studies, a bending test has been applied to the RFID sensor integrated diaper in the dry state. The RSSI values measured according to the bending at different angles applied to the diaper have been indicated in the Table 4.4. Table 4.5 indicates the comparison of this study with the other studies on diaper wetness sensor. When other passive RFID wetness sensor for urinary incontinence are evaluated in the literature, polarization is considered in very few studies and it is generally linear polarization. Although it can be implied that the polarization mismatch effect can cause approximately 20 dBm signal degradation in RSSI level, the reliable reading performance can be still accomplished at maximum reading range of 50 cm in wet state.

Table 4.4 : RSSI values of RFID sensor structure with diaper for different bending angles at 30 cm.

Bending angles (°)	Maximum RSSI after bending (dBm)
0	- 23.50
15	- 26.00
20	- 28.50
25	- 28.50
30	- 29.00
40	- 29.50

Table 4.5 : Comparison of passive RFID diaper wetness sensors.

Wireless Technology	Sensing Principle	Fabrication Method	Dimensions	Detection	Reading Range	Polarization	Flexible	Disposable	User Testing	Ref.
Passive UHF RFID	Received signal strength indicator (RSSI)	Hand fabrication (Hydrogel-metal hybrid tags)	<100 × 80 × 20 mm^3	Dry/wet	1.0 m	NA	Yes	Yes	Testing with doll	(Sen et al., 2020)
Semi-passive HF RFID	Built-in energy conversion sensor (Action-Activated Tag)	Screen printing	<5 × 5 mm^2 (for sensor) ~25 × 35 mm^2 (for tag)	Dry/wet	1.5 m	NA	NA	Yes	NA	(Sidén et al., 2004)
Passive HF RFID	Near-field inductive coupling of the transponder tag	Attaching the tag antenna, metal sheet and paper	~3×3 mm^2	Dry/wet	0.12 m	NA	Yes	NA	Testing with adult	(Ziai & Batchelor, 2015)
Passive UHF RFID	Received signal strength indicator (RSSI)	Commerciall y available (Monza E64 Viper tag antenna)	105 × 6 × 0.1 mm^3	Dry/wet	4.4 m (adult) 3.6 m (baby)	Considered	Yes	Disposable/ Reusable	Testing with human avatar	(Tajin, Mongan, et al., 2021)

Table 4.5 (continued) : Comparison of passive RFID diaper wetness sensors.

Wireless Technology	Sensing Principle	Fabrication Method	Dimensions	Detection	Reading Range	Polarization	Flexible	Disposable	User Testing	Ref.
Passive HF RFID	Received signal strength indicator (RSSI)	Conductive tracks	550 × 300 mm^2	Dry/wet	0.263 m	NA	NA	Yes	Testing with adult man	(Yamada et al., 2010)
Passive UHF RFID	Degradation of the antenna performance	Commercially available (Gen-2 RFID tags)	NA	Wet	1.4 m	NA	NA	NA	Testing in laboratory	(Nilsson et al., 2011)
Passive UHF RFID	Received signal strength indicator (RSSI)	Pad printing	75 × 38 × 0.12 mm^3	Dry/wet	NA	NA	Yes	Yes	Testing in laboratory	This work

4.4 Conclusion

In this study, wearable and flexible RFID sensor structure that operates in UHF RFID band has been designed and then fabricated using pad printing machine. Two different types of RSSI measurements have been carried out to determine the behavior of the RFID sensor structure against wetness to point out the technical applicability potential of the proposed wetness sensor. Water, saline, and urine solutions are dropped onto the RFID sensor to simulate different wetting conditions while conducting the multiple RSSI measurements in the near field with the result of at least 17 dBm signal difference in measured RSSI values between the dry and wet states. RF performance of the proposed RFID wetness detection sensor has been investigated in more practical applications with three different separation distances ranging from 32 cm up to 50 cm. The maximum reliable reading range of the RFID sensor is determined to be 50 cm under the different polarization angles with respect to the reader antenna in wet state. According to the results obtained, the proposed RFID sensor structure can detect wetness with varying RSSI values. At the same time, the bending test has been applied to the RFID sensor integrated onto the adult diaper to evaluate the performance of the RFID sensor structure against bending. As a result, it is implied that the RSSI values of the structure after bending are changed quite little compared to the RSSI values before the bending. In addition, the dimensions of the developed sensor are very suitable for the integration onto adult diapers or pads. It is thought that the proposed sensor structure can be used to detect wetness situations such as urinary incontinence.

5. CONCLUSIONS AND RECOMMENDATIONS

This thesis consists of three articles that add novelty to the literature. These articles include the designs determined by taking into account the end use of the thesis, the ink formulations used, different fabrication methods, applied tests and their results, and performance evaluations of the proposed sensor and antenna structures. In addition, the unique value that the structures proposed in the articles provide to the literature is emphasized by comparing them with the existing structures in the literature.

In the first article, a humidity sensor that can detect relative humidity and wetness was designed, taking into account the design criteria determined according to literature research. By examining humidity-sensitive polymers and structures in the literature, it was determined that PEDOT:PSS polymer was suitable for the scope of the thesis. Then, the inkjet printing technique, which is the simple and fast method, was selected and formulation and characterization studies were carried out to make the PEDOT:PSS polymer suitable for inkjet printing. The humidity sensor was fabricated by inkjet printing on taffeta label fabric, which is a thin and smooth surface. To evaluate the performance of the humidity sensor against change in relative humidity, a closed humidity chamber was created and the electrical resistance change of the sensor was measured. The relative humidity in the chamber was increased in 5% intervals from 40% to 100%. The electrical resistance of the sensor against increasing relative humidity decreased almost linearly. At the same time, the amount of moisture on the substrate was measured using a moisture meter. It was observed that the amount of moisture on the substrate increased with increasing relative humidity in the chamber. Then, response and recovery times were measured, repeatability and wrist bending tests were also applied to the sensor. The response and recovery times of the fabricated humidity sensor were measured as 42 and 82 seconds, respectively. To conduct the repeatability test, 50 cycles were implemented, involving the elevation of relative humidity in the chamber from 35% to 100%, followed by its subsequent reduction back to 35% RH. The results show that the sensor has good repeatability. In the wrist bending test, the sensor underwent 16 bending cycles. The test results indicated a

maximum resistance change of 1%. Demonstrating the applicability of the moisture sensor for wetness detection involved initially integrating the sensor onto the diaper. Subsequently, the resistance change was assessed by applying varying volumes of urine like water solution to the sensor. The findings revealed that the humidity sensor, as proposed in the study, could detect even the slightest wetness of 0.1 mL. For the proposed humidity sensor to exhibit antenna performance, it necessitates significantly higher conductivity. The PEDOT:PSS polymer's conductivity, employed in the initial article, proved insufficient to ascertain the structure's functionality as an antenna. Consequently, the ink used in the study underwent modification. Despite attempts to employ inkjet printing for the revised sensor, the presence of metal nanoparticles in the ink clogged the nozzles. As a result, the pad printing method was employed in the subsequent phases of the study.

In the second article, silver nanoparticle ink, which has much higher conductivity, was used instead of the conductive PEDOT:PSS polymer used in the first article. The presence of metal nanoparticles in the ink led to nozzle clogging in the inkjet printing method, necessitating a change in the printing technique. Moreover, considering the use of ink containing silver nanoparticles, an examination was conducted to assess the impact of the sintering process on conductivity. In the second article, formulation studies of silver nanoparticle ink were carried out to make the ink suitable for pad printing method. The humidity sensor design used in the first article was printed according to the pad printing method using silver ink. In order to investigate the effects of the sintering process on conductivity and performance, the sintering process was applied to one group of samples, while the sintering process was not applied to the other group. Additionally, to understand the effect of print pass numbers on conductivity, humidity sensors were produced with print pass numbers ranging from 1 to 5. Vector network analyzer was used to measure the antenna performance of humidity sensors. The impedance measurement results of both sintered and unsintered sensor-antennas revealed that the sintered samples exhibited UHF-RFID antenna performance. Gain and bending measurements were conducted on the sintered sensor-antenna structure with 5 print passes, demonstrating the highest conductivity and optimal performance. Based on the gain measurement results, a deviation of approximately -10 dB at 943 MHz is deemed typical, given the dimensions of both the reference antenna and the fabricated antenna. In addition, according to the bending

result applied to 10 mm diameters in the x and y directions, there is no resonance frequency shift compared to the flat state of the sample. Thus, it has been shown that the proposed structure exhibits antenna performance, it is wearable and flexible against bending.

In the final stage of the study, a system that detects wetness wirelessly is needed. For this reason, the humidity sensor design presented in the first and second articles has been modified. Since the conductivity of the silver ink used in the second article was sufficient to demonstrate the antenna performance and the silver ink was compatible with the pad printing method used, printing of silver ink with the pad printing method was continued in the third article.

In the third article, UHF RFID sensor design was done to ensure wireless data transfer. The design was determined to be compatible with the available chip. The proposed structure was printed on polyamide-based taffeta label fabric with three print passes according to the pad printing method using silver conductive ink. Then, the structure was sintered at 150°C for 30 minutes, and the chip was integrated onto the RFID sensor. Then the fabricated RFID sensor was embedded onto the diaper. Different amounts of water, saline and urine solutions were prepared and RSSI measurements were performed. Near-field RSSI measurements were conducted to illustrate distinctions between wet and dry conditions. Omnidirectional measurements were performed utilizing a high antenna array. Reflecting real-life scenarios, bending simulations and bending tests were administered to the RFID sensor tag.

In a dry condition, the RSSI value of the sensor structure is -35.31 dBm. However, when 45 mL of water and 45 mL of saltwater are applied to the sensor, the respective values recorded are -52.77 dBm and -54.35 dBm. To simulate varying wetness levels, the RFID sensor was positioned between nonwoven surfaces soaked with saltwater. The RSSI value for the dry state was measured at -35.49 dBm, while the RSSI value between wet nonwovens was recorded as -54.35 dBm.

In the experimental setup created using a high antenna array, the RFID sensor was immersed in salt water with a concentration of 6 mg/mL and a maximum of -55.24 dBm was measured from a reading range of 50 cm. Therefore, the maximum reading range of the proposed RFID sensor is 50 cm. The minimum measured RSSI value for different polarizations is -68.24 dBm. Since it is known that the reading sensitivity

level of the reader antenna is -84 dBm, the measured values are higher than the sensitivity of the RFID reader. Additionally, different orientations were applied to the RFID sensor in 45° increments from 0° to 360°. By placing the RFID sensor in 6 mg/mL salt water, the maximum RSSI values measured for reading ranges of 32 cm, 40 cm, and 50 cm are −47.50 dBm, −50.18 dBm, and −55.24 dBm, respectively. According to these results, it appears that different orientations of the RFID sensor are not a disadvantage up to a reading range of 50 cm.

The anticipated performance of the RFID sensor when positioned on the human body was forecasted through simulation on a four-layer human body model. The impact of various bending angles on the reflection parameter of the RFID sensor was found to be negligible. Furthermore, in addition to these simulations, the RFID sensor integrated into the diaper underwent physical testing involving 10 instances of deformation. It can be seen that the difference between the RSSI values measured before and after the deformation of the RFID sensor, both dry and wetted with different amounts of water, is quite small. Thus, it was stated that the RFID sensor showed good performance even after deformation. According to all test results, the proposed RFID sensor is a structure that performs well in the human body, is resistant to bending and polarization, and can detect wetness with RSSI changes.

The results of all articles included in this thesis contribute individually to the literature. Upon assessing the findings presented in the articles, it becomes evident that the pad printing method yields rapid and commendable results. The antenna performance is notably high, attributed to the excellent conductivity of the silver ink. Consequently, the suggested structures hold potential for application in wetness detection scenarios, particularly for detection of urinary incontinence. In addition, it is envisaged that users will not experience any discomfort because the proposed structures are thin, light, disposable and easy to integrate onto the diapers. As a result, an RFID sensor structure has been formulated for solution of the problems and to tackle the challenges delineated in the thesis.

In future studies, the proposed structures and systems can be investigated using different types of conductive inks and different printing techniques. Considering the users' well-being, the printed structures situated on the lower layer of the diaper can be coated using the encapsulation method without compromising their performance. Exploring the feasibility of employing these structures in the top layer of the diaper is

warranted. Enhancing the structure design holds the potential to extend the wireless reading distance. Furthermore, the suggested structures and control system could undergo testing in actual environments with numerous patients experiencing urinary incontinence. This approach would enable the assessment of the proposed structures' performance in real-world scenarios.

REFERENCES

A. M., T., Moon, H., Cho, G., & Lee, J. (2022). Fully roll-to-roll gravure printed electronics: challenges and the way to integrating logic gates. *Japanese Journal of Applied Physics*, *61*(SE), SE0802. https://doi.org/10.35848/1347-4065/ac575e

Ahmed, S., Qureshi, S. T., Sydanheimo, L., Ukkonen, L., & Bjorninen, T. (2019). Comparison of Wearable E-Textile Split Ring Resonator and Slotted Patch RFID Reader Antennas Embedded in Work Gloves. *IEEE Journal of Radio Frequency Identification*, *3*(4), 259–264. https://doi.org/10.1109/JRFID.2019.2926194

Ajmeri, J. R., & Ajmeri, C. J. (2016). Developments in the use of nonwovens for disposable hygiene products. In *Advances in Technical Nonwovens*.

Akdag, I., Gocen, C., Palandoken, M., & Kaya, A. (2022). A novel circularly polarized reader antenna design for UHF RFID applications. *Wireless Networks*, *28*(6), 2625–2636. https://doi.org/10.1007/s11276-022-02998-8

Alizadeh, A., Mohammah-Alizadeh-Charandabi, S., Khodaie, L., & Mirghafourvand, M. (2023). Effect of Nigella sativa L. seed oil on urinary incontinence and quality of life in menopausal women: A triple-blind randomized controlled trial. *Phytotherapy Research*, *55*(August 2022), 2012–2023. https://doi.org/10.1002/ptr.7725

Alizadeh, A., Montazeri, M., Shabani, F., Bani, S., Hassanpour, S., Nabighadim, M., & Mirghafourvand, M. (2023). Prevalence and severity of urinary incontinence and associated factors in Iranian postmenopausal women: a cross-sectional study. *BMC Urology*, *23*(1), 1–9. https://doi.org/10.1186/s12894-023-01186-w

Aoki, Y., Brown, H. W., Brubaker, L., Cornu, J. N., Daly, J. O., & Cartwright, R. (2017). Urinary incontinence in women. *Nature Reviews Disease Primers*, *3*. https://doi.org/10.1038/nrdp.2017.42

Aziz, S., Chang, D. E. U. I., Doh, Y. H. O. I., Kang, C. U. N. G., & Choi, K. H. (2015). *Humidity Sensor Based on PEDOT : PSS and Zinc Stannate Nano-composite*. *44*(10), 3992–3999. https://doi.org/10.1007/s11664-015-3914-2

Bariya, M., Shahpar, Z., Park, H., Sun, J., Jung, Y., Gao, W., Nyein, H. Y. Y., Liaw, T. S., Tai, L. C., Ngo, Q. P., Chao, M., Zhao, Y., Hettick, M., Cho, G., & Javey, A. (2018). Roll-to-Roll Gravure Printed Electrochemical Sensors for Wearable and Medical Devices. *ACS Nano*, *12*(7), 6978–6987. https://doi.org/10.1021/acsnano.8b02505

Barmpakos, D., Tsamis, C., & Kaltsas, G. (2020). Multi-parameter paper sensor fabricated by inkjet-printed silver nanoparticle ink and PEDOT : PSS. *Microelectronic Engineering*, *225*(November 2019), 111266. https://doi.org/10.1016/j.mee.2020.111266

Beltrão, M., Duarte, F. M., Viana, J. C., & Paulo, V. (2022). A review on in-mold electronics technology. *Polymer Engineering and Science*, *62*(4), 967–990. https://doi.org/10.1002/pen.25918

Bodenstein, C., Sauer, H. M., Hirmer, K., & Dörsam, E. (2019). Printing process and characterization of fully pad printed electroluminescent panels on curved surfaces. *Journal of Coatings Technology and Research*, *16*(6), 1673–1681. https://doi.org/10.1007/s11998-019-00243-0

Bracco, G., & Holst, B. (2013). Surface science techniques. In *Springer Series in Surface Sciences* (Vol. 51, Issue 1). https://doi.org/10.1007/978-3-642-34243-1

Brooke, R., Wijeratne, K., Hübscher, K., Belaineh, D., & Andersson Ersman, P. (2022). Combining Vapor Phase Polymerization and Screen Printing for Printed Electronics on Flexible Substrates. *Advanced Materials Technologies*, *2101665*. https://doi.org/10.1002/admt.202101665

Caccami, M. C., Amendola, S., & Occhiuzzi, C. (2019). Method and system for reading RFID tags embedded into tires on conveyors. *2019 IEEE International Conference on RFID Technology and Applications, RFID-TA 2019*, 141–144. https://doi.org/10.1109/RFID-TA.2019.8892245

Cao, Q., Jones, D. R., & Sheng, H. (2014). Contained nomadic information environments: Technology, organization, and environment influences on adoption of hospital RFID patient tracking. *Information and Management*, *51*(2), 225–239. https://doi.org/10.1016/j.im.2013.11.007

Casula, G. A., Montisci, G., & Rogier, H. (2020). A Wearable Textile RFID Tag Based on an Eighth-Mode Substrate Integrated Waveguide Cavity. *IEEE Access*, *8*, 11116–11123. https://doi.org/10.1109/ACCESS.2020.2964614

Chen, X., He, H., Khan, Z., Sydanheimo, L., Ukkonen, L., & Virkki, J. (2020). Textile-Based Batteryless Moisture Sensor. *IEEE Antennas and Wireless Propagation Letters*, *19*(1), 198–202. https://doi.org/10.1109/LAWP.2019.2957879

Cheng, Y., Wang, K., Xu, H., Li, T., Jin, Q., & Cui, D. (2021). Recent developments in sensors for wearable device applications. *Analytical and Bioanalytical Chemistry*, *413*(24), 6037–6057. https://doi.org/10.1007/s00216-021-03602-2

Cho, J. H., Choi, J. Y., Kim, N. H., Lim, Y., Ohn, J. H., Kim, E. S., Ryu, J., Kim, J., Kim, Y., Kim, S. W., & Kim, K. Il. (2021). A smart diaper system using bluetooth and smartphones to automatically detect urination and volume of voiding: Prospective observational pilot study in an acute care hospital. *Journal of Medical Internet Research*, *23*(7). https://doi.org/10.2196/29979

Choi, K. H., Sajid, M., Aziz, S., & Yang, B. S. (2015). Wide range high speed relative humidity sensor based on PEDOT:PSS-PVA composite on an IDT printed on piezoelectric substrate. *Sensors and Actuators, A: Physical*, *228*, 40–49. https://doi.org/10.1016/j.sna.2015.03.003

Colella, R., Sabina, S., Mincarone, P., & Catarinucci, L. (2023). Semi-Passive RFID Electronic Devices With On-Chip Sensor Fusion Capabilities for Motion Capture and Biomechanical Analysis. *IEEE Sensors Journal*, *23*(11), 11672–11681. https://doi.org/10.1109/JSEN.2023.3267540

Cooper, C., & Hughes, B. (2020). Aerosol Jet Printing of Electronics: An Enabling Technology for Wearable Devices. *2020 Pan Pacific Microelectronics Symposium, Pan Pacific 2020*. https://doi.org/10.23919/PanPacific48324.2020.9059444

Costa, F., Genovesi, S., Borgese, M., Michel, A., Dicandia, F. A., & Manara, G. (2021). A review of rfid sensors, the new frontier of internet of things. *Sensors*, *21*(9). https://doi.org/10.3390/s21093138

Cummins, G., Desmulliez, M. P. Y., Marc, P., & Desmulliez, Y. (2012). Inkjet printing of conductive materials: A review. *Circuit World, November 2012*. https://doi.org/10.1108/03056121211280413

Das, D. (2014). Composite nonwovens in absorbent hygiene products. In *Composite Non-Woven Materials: Structure, Properties and Applications* (pp. 74–88). Woodhead Publishing Limited. https://doi.org/10.1533/9780857097750.74

***Diaper Market: Global Industry Trends, Share, Size, Growth, Opportunity and Forecast 2021-2026*.** (n.d.). Retrieved November 14, 2023, https://www.researchandmarkets.com/reports/5311866/diaper-market-global-industry-trends-share#src-pos-7 https://www.researchandmarkets.com/reports/5062057/global-adult-diaper-market-2020-2024%23src-pos-14

***Dielectric Properties of Body Tissues*.** (n.d.). Retrieved November 14, 2023, http://niremf.ifac.cnr.it/tissprop/htmlclie/htmlclie.php

***EDANA*.** (n.d.). Retrieved November 14, 2023, https://www.edana.org/

El Hajjaji, C., Delhote, N., Verdeyme, S., Piechowiak, M., Boyer, L., & Durand, O. (2021). Optimization of the conductivity of microwave components printed by inkjet and aerosol jet on polymeric substrates by IPL and laser sintering. *International Journal of Microwave and Wireless Technologies*, *13*(7), 652–662. https://doi.org/10.1017/S175907872100043X

Fischer, M., Renzler, M., & Ussmueller, T. (2019). Development of a Smart Bed Insert for Detection of Incontinence and Occupation in Elder Care. *IEEE Access*, *7*, 118498–118508. https://doi.org/10.1109/ACCESS.2019.2931041

Frigerio, M., Barba, M., Cola, A., Marino, G., Volontè, S., Melocchi, T., De Vicari, D., & Maruccia, S. (2023). Flat Magnetic Stimulation for Stress Urinary Incontinence: A Prospective Comparison Study. *Bioengineering*, *10*(3), 1–10. https://doi.org/10.3390/bioengineering10030295

Gao, M., Li, L., & Song, Y. (2017). Inkjet printing wearable electronic devices. *Journal of Materials Chemistry C*, *5*(12), 2971–2993. https://doi.org/10.1039/c7tc00038c

Gaspar, C., Olkkonen, J., Passoja, S., & Smolander, M. (2017). Paper as active layer in inkjet-printed capacitive humidity sensors. *Sensors (Switzerland)*, *17*(7). https://doi.org/10.3390/s17071464

Gaspari, F., & Quaranta, S. (2019). Nanostructured Materials for RFID Sensors. In *Nanomaterials Design for Sensing Applications*. Elsevier Inc. https://doi.org/10.1016/B978-0-12-814505-0.00003-5

Global Adult Diaper Market 2020-2024. (n.d.). Retrieved November 14, 2023, https://www.researchandmarkets.com/reports/5062057/global-adult-diaper-market-2020-2024#src-pos-14

Gray, M. (2010). Optimal management of incontinence-associated dermatitis in the elderly. *American Journal of Clinical Dermatology*, *11*(3), 201–210. https://doi.org/10.2165/11311010-000000000-00000

Hassan, G., Sajid, M., & Choi, C. (2019). *Highly Sensitive and Full Range Detectable Humidity Sensor using PEDOT : PSS , Methyl Red and Graphene Oxide Materials*. 1–10. https://doi.org/10.1038/s41598-019-51712-w

Hassan, S., & Shehab, S. H. (2016). Evaluation of an Ultra Wideband (UWB) textile antenna in the vicinity of human body model for WBAN applications. *2015 IEEE International WIE Conference on Electrical and Computer Engineering, WIECON-ECE 2015*, 195–198. https://doi.org/10.1109/WIECON-ECE.2015.7443895

Htwe, Y. Z. N., Abdullah, M. K., & Mariatti, M. (2021). Optimization of graphene conductive ink using solvent exchange techniques for flexible electronics applications. *Synthetic Metals*, *274*(January), 116719. https://doi.org/10.1016/j.synthmet.2021.116719

Htwe, Y. Z. N., & Mariatti, M. (2022). Printed graphene and hybrid conductive inks for flexible, stretchable, and wearable electronics: Progress, opportunities, and challenges. *Journal of Science: Advanced Materials and Devices*, *7*(2), 100435. https://doi.org/10.1016/j.jsamd.2022.100435

Izdebska, J., & Thomas, S. (2015). Printing on polymers: fundamentals and applications. *William Andrew*.

Jaafar, A., Schoinas, S., & Passeraub, P. (2021). Pad-printing as a fabrication process for flexible and compact multilayer circuits. *Sensors*, *21*(20). https://doi.org/10.3390/s21206802

Jaekel, A. K., Rings, T. M., Schmitz, F., Knappe, F., Tschirhart, A., Winterhagen, F. I., Kirschner-Hermanns, R. K. M., & Knüpfer, S. C. (2023). Urinary and Double Incontinence in Cognitively Impaired Patients: Impacts on Those Affected and Their Professional Caregivers. *Journal of Clinical Medicine*, *12*(10). https://doi.org/10.3390/jcm12103352

Jerez-Roig, J., Santos, M. M., Souza, D. L. B., Amaral, F. L. J. S., & Lima, K. C. (2016). Prevalence of Urinary Incontinence and Associated Factors in Nursing Home Residents. *Neurourology and Urodynamics*, *107*(August 2014), 102–107. https://doi.org/10.1002/nau

Johnson, T. M., Ouslander, J. G., Uman, G. C., & Schnelle, J. F. (2001). Urinary incontinence treatment preferences in Long-Term Care. *Journal of the American Geriatrics Society*, *49*(6), 710–718. https://doi.org/10.1046/j.1532-5415.2001.49146.x

Kamyshny, A., & Magdassi, S. (2019). Conductive nanomaterials for 2D and 3D printed flexible electronics. *Chemical Society Reviews*, *48*(6), 1712–1740. https://doi.org/10.1039/c8cs00738a

Karakaya, İ. Ç., Yenişehir, S., & Karakaya, M. G. (2019). Nursing Home Residents' Level of Knowledge About Urinary Incontinence. *Annals of Geriatric Medicine and Research*, *23*(1), 20–26. https://doi.org/10.4235/agmr.19.0003

Khan, T. (2019). A noninvasive smart wearable for diaper moister quantification and notification. *International Journal of Electrical and Computer Engineering*, *9*(4), 2848–2862. https://doi.org/10.11591/ijece.v9i4.pp2848-2862

Kim, S., Park, J. H., Ahn, H., Lee, S., Yoo, H. J., Yoo, J., & Won, C. W. (2017). Risk factors of geriatric syndromes in Korean population. *Annals of Geriatric Medicine and Research*, *21*(3), 123–130. https://doi.org/10.4235/agmr.2017.21.3.123

Kutzner, C., Lucklum, R., Torah, R., Beeby, S., & Tudor, J. (2013). Novel screen printed humidity sensor on textiles for smart textile applications. *2013 Transducers and Eurosensors XXVII: The 17th International Conference on Solid-State Sensors, Actuators and Microsystems, TRANSDUCERS and EUROSENSORS 2013*, *June*, 282–285. https://doi.org/10.1109/Transducers.2013.6626757

Kuzubasoglu, B. A., Sayar, E., & Bahadir, S. K. (2021). Inkjet-printed CNT/PEDOT: PSS temperature sensor on a textile substrate for wearable intelligent systems. *IEEE Sensors Journal*.

Long, F., Zhang, X. D., Bjorninen, T., Virkki, J., Sydanheimo, L., Chan, Y. C., & Ukkonen, L. (2015). Implementation and wireless readout of passive UHF RFID strain sensor tags based on electro-textile antennas. *2015 9th European Conference on Antennas and Propagation, EuCAP 2015*.

Lukacs, P., Pietrikova, A., Vehec, I., & Provazek, P. (2022). Influence of Various Technologies on the Quality of Ultra-Wideband Antenna on a Polymeric Substrate. *Polymers*, *14*(3). https://doi.org/10.3390/polym14030507

Luo, C., Gil, I., & Fernandez-Garcia, R. (2022a). Electro-Textile UHF-RFID Compression Sensor for Health-Caring Applications. *IEEE Sensors Journal*, *22*(12), 12332–12338. https://doi.org/10.1109/JSEN.2022.3172506

Luo, C., Gil, I., & Fernandez-Garcia, R. (2022b). Textile UHF-RFID Antenna Embroidered on Surgical Masks for Future Textile Sensing Applications. *IEEE Transactions on Antennas and Propagation*, *70*(7), 5246–5253. https://doi.org/10.1109/TAP.2022.3145477

Luo, C., Gil, I., & Fernandez-Garcia, R. (2022c). Textile UHF-RFID Antenna Embroidered on Surgical Masks for Future Textile Sensing Applications. *IEEE Transactions on Antennas and Propagation*, *XX*(XX), 1–9. https://doi.org/10.1109/TAP.2022.3145477

Luo, C., Gil, I., & Fernández-García, R. (2020). Wearable textile UHF-RFID sensors: A systematic review. *Materials*, *13*(15). https://doi.org/10.3390/ma13153292

Luo, C., Gil, I., & Fernández-García, R. (2022). Experimental comparison of three electro-textile interfaces for textile UHF-RFID tags on clothes. *AEU - International Journal of Electronics and Communications*, *146*, 1–6. https://doi.org/10.1016/j.aeue.2022.154137

Marc, M. E., Ignacio, G., & Raul, F. G. (2021). A smart textile system to detect urine leakage. *IEEE Sensors Journal*, *XX*(XX), 1–10. https://doi.org/10.1109/JSEN.2021.3080824

Marmur, A. (2006). Soft contact: Measurement and interpretation of contact angles. *Soft Matter*, *2*(1), 12–17. https://doi.org/10.1039/b514811c

Mecnika, V., Hoerr, M., Jockehoefel, S., Gries, T., Krievins, I., & Schwarz-Pfeiffer, A. (2015). Preliminary study on textile humidity sensors. *Smart SysTech 2015 - European Conference on Smart Objects, Systems and Technologies*, 1–9.

Meng, W., Ma, Y., Tian, C., & Su, D. (2022). An Ultra-long Range, Wideband Planar UHF RFID Tag with Two Split-arcs. *IEEE Antennas and Wireless Propagation Letters*, *21*(5), 1017–1021. https://doi.org/10.1109/LAWP.2022.3155191

Merilampi, S. L., Björninen, T., Ukkonen, L., Ruuskanen, P., & Sydänheimo, L. (2011). Characterization of UHF RFID tags fabricated directly on convex surfaces by pad printing. *International Journal of Advanced Manufacturing Technology*, *53*(5–8), 577–591. https://doi.org/10.1007/s00170-010-2869-y

Mersani, A., Lotfi, O., & Ribero, J. M. (2018). Design of a textile antenna with artificial magnetic conductor for wearable applications. *Microwave and Optical Technology Letters*, *60*(6), 1343–1349. https://doi.org/10.1002/mop.31158

Michel, M. C., Cardozo, L., Chermansky, C. J., Cruz, F., Igawa, Y., Lee, K.-S., Sahai, A., Wein, A. J., & Andersson, K.-E. (2023). Current and Emerging Pharmacological Targets and Treatments of Urinary Incontinence and Related Disorders. *Pharmacological Reviews*, *75*(4), 554–674. https://pharmrev.aspetjournals.org/content/75/4/554.abstract

Milsom, I., & Gyhagen, M. (2019). The prevalence of urinary incontinence. *Climacteric*, *22*(3), 217–222. https://doi.org/10.1080/13697137.2018.1543263

Moon, K. S., Dong, H., Maric, R., Pothukuchi, S., Hunt, A., Li, Y. I., & Wong, C. P. (2005). Thermal behavior of silver nanoparticles for low-temperature interconnect applications. *Journal of Electronic Materials*, *34*(2), 168–175. https://doi.org/10.1007/s11664-005-0229-8

Najeeb, M. A., Ahmad, Z., & Shakoor, R. A. (2018). Organic Thin-Film Capacitive and Resistive Humidity Sensors: A Focus Review. *Advanced Materials Interfaces*, *5*(21), 1–19. https://doi.org/10.1002/admi.201800969

Nie, H. K., Xuan, X. W., Shi, Q., Guo, A., Li, M. J., Li, H. J., & Ren, G. J. (2022). Wearable Antenna Sensor Based on EBG Structure for Cervical Curvature Monitoring. *IEEE Sensors Journal*, *22*(1), 315–323. https://doi.org/10.1109/JSEN.2021.3130252

Nilsson, H. E., Sidén, J., & Gulliksson, M. (2011). An incontinence alarm solution utilizing RFID based sensor technology. *2011 IEEE International Conference on RFID-Technologies and Applications, RFID-TA 2011*, 359–363. https://doi.org/10.1109/RFID-TA.2011.6068662

Ozek, E. A., Tanyeli, S., & Yapici, M. K. (2021). Flexible Graphene Textile Temperature Sensing RFID Coils Based on Spray Printing. *IEEE Sensors Journal*, *21*(23), 26382–26388. https://doi.org/10.1109/JSEN.2021.3075902

Park, J., Kang, T., Kim, B., Lee, H., Choi, H. H., & Yook, J. (2018). Real-time Humidity Sensor Based on Microwave Resonator Coupled with PEDOT : PSS Conducting Polymer Film. *Scientific Reports*, *December 2017*, 1–8. https://doi.org/10.1038/s41598-017-18979-3

Pietrikova, A., Ruman, K., Rovensky, T., & Vehec, I. (2015). Impact analysis of LTCC materials on microstrip filters' behaviour up to 13 GHz. *Microelectronics International*, *32*(3), 122–125. https://doi.org/10.1108/MI-01-2015-0003

Prather, J. C., Meng, Y., Bolt, M., Horton, T., & Adams, M. (2019). Wireless head impact monitoring system utilizing eye movement as a surrogate for brain movement. *AEU - International Journal of Electronics and Communications*, *105*, 54–61. https://doi.org/10.1016/j.aeue.2019.04.003

Qi, X., Ha, H., Hwang, B., & Lim, S. (2020). Printability of the screen-printed strain sensor with carbon black/silver paste for sensitive wearable electronics. *Applied Sciences (Switzerland)*, *10*(19), 1–10. https://doi.org/10.3390/app10196983

Qing, X., Chean, K. G., & Zhi, N. C. (2009). Measurement of UHF RFID tag antenna impedance. *2009 IEEE International Workshop on Antenna Technology, IWAT 2009*, *2*(2), 25–28. https://doi.org/10.1109/IWAT.2009.4906968

Rittersma, Z. M. (2002). Recent achievements in miniaturised humidity sensors - A review of transduction techniques. *Sensors and Actuators, A: Physical*, *96*(2–3), 196–210. https://doi.org/10.1016/S0924-4247(01)00788-9

Salvado, R., Loss, C., Gon, & Pinho, P. (2012). Textile materials for the design of wearable antennas: A survey. *Sensors (Switzerland)*, *12*(11), 15841–15857. https://doi.org/10.3390/s121115841

Seekaew, Y., Lokavee, S., Phokharatkul, D., & Wisitsoraat, A. (2014). Low-cost and flexible printed graphene – PEDOT : PSS gas sensor for ammonia detection. *ORGANIC ELECTRONICS*, *15*(11), 2971–2981. https://doi.org/10.1016/j.orgel.2014.08.044

Sen, P., Kantareddy, S. N. R., Bhattacharyya, R., Sarma, S. E., & Siegel, J. E. (2020). Low-Cost Diaper Wetness Detection Using Hydrogel-Based RFID Tags. *IEEE Sensors Journal*, *20*(6), 3293–3302. https://doi.org/10.1109/JSEN.2019.2954746

Shafiq, Y., Gibson, J. S., Kim, H., Ambulo, C. P., Ware, T. H., & Georgakopoulos, S. V. (2019). A Reusable Battery-Free RFID Temperature Sensor. *IEEE Transactions on Antennas and Propagation*, *67*(10), 6612–6626. https://doi.org/10.1109/TAP.2019.2921150

Shan, L., & Xiao, H. (2015). Impedence characterization of RFID tag antennas and application in conformal tag antenna. *Proceedings - 7th Asia-Pacific Conference on Environmental Electromagnetics, CEEM 2015*, 140–142. https://doi.org/10.1109/CEEM.2015.7368649

Shao, S., Kiourti, A., Burkholder, R. J., & Volakis, J. L. (2015). Broadband textile-based passive UHF RFID tag antenna for elastic material. *IEEE Antennas and Wireless Propagation Letters*, *14*, 1385–1388. https://doi.org/10.1109/LAWP.2015.2407879

Shuaib, D., Ukkonen, L., Virkki, J., & Merilampi, S. (2017). The possibilities of embroidered passive UHF RFID textile tags as wearable moisture sensors. *2017 IEEE 5th International Conference on Serious Games and Applications for Health, SeGAH 2017*. https://doi.org/10.1109/SeGAH.2017.7939286

Sidén, J., Koptioug, A., & Gulliksson, M. (2004). The "smart" diaper moisture detection system. *IEEE MTT-S International Microwave Symposium Digest*, *2*(iii), 659–662. https://doi.org/10.1109/mwsym.2004.1336073

Simik, M. Y. E., Chi, F., & Wei, C. L. (2019). Design and Implementation of a Bluetooth-Based MCU and GSM for Wetness Detection. *IEEE Access*, *7*, 21851–21856. https://doi.org/10.1109/ACCESS.2019.2897324

Skotnes, L. H., Omli, R., Romild, U., Hellzèn, O., & Kuhry, E. (2012). Urinary incontinence in Norwegian nursing home residents. *Open Journal of Nursing*, *2*(4), 116–122. https://doi.org/10.1111/j.1532-5415.1998.tb02483.x

Stauffer, C. E. (1965). ***The Measurement of Surface Tension by the Pendant Drop Technique.*** *69*(6), 1933–1938.

Stoppa, M., & Chiolerio, A. (2014). Wearable electronics and smart textiles: A critical review. *Sensors (Switzerland)*, *14*(7), 11957–11992. https://doi.org/10.3390/s140711957

Su, P. G., & Wang, C. S. (2007). Novel flexible resistive-type humidity sensor. *Sensors and Actuators, B: Chemical*, *123*(2), 1071–1076. https://doi.org/10.1016/j.snb.2006.11.015

Sun, J., Sun, Y., Jia, H., Bi, H., Chen, L., Que, M., Xiong, Y., Han, L., & Sun, L. (2022). A novel pre-deposition assisted strategy for inkjet printing graphene-based flexible pressure sensor with enhanced performance. *Carbon*, *196*(February), 85–91. https://doi.org/10.1016/j.carbon.2022.04.021

Tafoya, R. R., Gallegos, M. A., Downing, J. R., Gamba, L., Kaehr, B., Coker, E. N., Hersam, M. C., & Secor, E. B. (2022). Morphology and electrical properties of high-speed flexography-printed graphene. *Microchimica Acta*, *189*(3). https://doi.org/10.1007/s00604-022-05232-6

Tajin, M. A. S., Amanatides, C. E., Dion, G., & Dandekar, K. R. (2021). Passive UHF RFID-Based Knitted Wearable Compression Sensor. *IEEE Internet of Things Journal*, *8*(17), 13763–13773. https://doi.org/10.1109/JIOT.2021.3068198

Tajin, M. A. S., Mongan, W. M., & Dandekar, K. R. (2021). Passive RFID-Based Diaper Moisture Sensor. *IEEE Sensors Journal*, *21*(2), 1665–1674. https://doi.org/10.1109/JSEN.2020.3021395

Tekcin, M., Kuzubasoglu, B. A., Sayar, E., Yalcin, M. K., & Bahadir, S. K. (2021). *Performance Analysis of Wearable and Flexible Humidity Sensor Integrated to Face Mask for Respiration Monitoring*. 663–666.

Tekcin, M., Paker, S., & Bahadir, S. K. (2022). UHF-RFID enabled wearable flexible printed sensor with antenna performance. *AEU - International Journal of Electronics and Communications*, *157*(September), 154410. https://doi.org/10.1016/j.aeue.2022.154410

Tekcin, M., Sayar, E., Yalcin, M. K., & Bahadir, S. K. (2022). Wearable and Flexible Humidity Sensor Integrated to Disposable Diapers for Wetness Monitoring and Urinary Incontinence. *Electronics*, *11*(7), 1025. https://doi.org/10.3390/electronics11071025

Ueda, T., Tamaki, M., Kageyama, S., Yoshimura, N., & Yoshida, O. (2000). Urinary incontinence among community-dwelling people aged 40 years or older in Japan: Prevalence, risk factors, knowledge and self-perception. *International Journal of Urology*, *7*(3), 95–103. https://doi.org/10.1046/j.1442-2042.2000.00147.x

Vena, A., Sorli, B., Saggin, B., Garcia, R., & Podlecki, J. (2019). Passive UHF RFID sensor to monitor fragile objects during transportation. *2019 IEEE International Conference on RFID Technology and Applications, RFID-TA 2019*, 415–420. https://doi.org/10.1109/RFID-TA.2019.8892033

Wang, Y., Huang, Y., Li, Y. ze, Cheng, P., Cheng, S. yuan, Liang, Q., Xu, Z. quan, Chen, H. jun, & Feng, Z. sheng. (2021). A facile process combined with roll-to-roll flexographic printing and electroless deposition to fabricate RFID tag antenna on paper substrates. *Composites Part B: Engineering*, *224*(July), 109194. https://doi.org/10.1016/j.compositesb.2021.109194

Wang, Z., Zhao, T., Liang, X., Zhu, P., & Sun, R. (2017). A low cost method to synthesize silver nanoparticles for the screen printing conductive inks. *18th International Conference on Electronic Packaging Technology, ICEPT 2017*, 1121–1124. https://doi.org/10.1109/ICEPT.2017.8046638

Wanhua, W. (2020). Design and Research of Logistics Distribution System Based on RFID. *Journal of Physics: Conference Series*, *1544*(1). https://doi.org/10.1088/1742-6596/1544/1/012193

Xie, S., Ma, C., Feng, R., Xiang, X., & Jiang, P. (2022). Wireless Glucose Sensing System Based on Dual-Tag RFID Technology. *IEEE Sensors Journal*, *22*(13), 13632–13639.

Xiong, Y., & Qu, Z. (2011). Antenna 3D Pad printing solution evaluation. *IEEE Antennas and Propagation Society, AP-S International Symposium (Digest)*, 2773–2776. https://doi.org/10.1109/APS.2011.5997101

Xu, L., Chen, X., Tan, S., Hu, Z., Ying, B., Ye, T. T., & Li, Y. (2020). Characterization and Modeling of Embroidered NFC Coil Antennas for Wearable Applications. *IEEE Sensors Journal*, *20*(23), 14501–14513. https://doi.org/10.1109/JSEN.2020.3008594

Yalduz, H., Tabaru, T. E., Kilic, V. T., & Turkmen, M. (2020). Design and analysis of low profile and low SAR full-textile UWB wearable antenna with metamaterial for WBAN applications. *AEU - International Journal of Electronics and Communications*, *126*(May), 153465. https://doi.org/10.1016/j.aeue.2020.153465

Yamada, K., Toshiaki, N., Ishihara, K., Takahashi, R., Ohno, Y., Ishii, A., Shimizu, S., Takahashi, H., Shimizu, E., & Araki, T. (2010). Development of new type incontinence sensor using RFID tag. *Conference Proceedings - IEEE International Conference on Systems, Man and Cybernetics*, 2695–2700. https://doi.org/10.1109/ICSMC.2010.5641889

Zhang, X., Maddipatla, D., Bose, A. K., Hajian, S., Narakathu, B. B., Williams, J. D., Mitchell, M. F., & Atashbar, M. Z. (2020). Printed carbon nanotubes-based flexible resistive humidity sensor. *IEEE Sensors Journal*, *20*(21), 12592–12601. https://doi.org/10.1109/JSEN.2020.3002951

Zhu, H., Ko, Y. C. A., & Ye, T. T. (2010). Impedance measurement for balanced UHF RFID tag antennas. *2010 IEEE Radio and Wireless Symposium, RWW 2010 - Paper Digest*, 128–131. https://doi.org/10.1109/RWS.2010.5434202

Ziai, M. A., & Batchelor, J. C. (2015). Smart radio-frequency identification tag for diaper moisture detection. *Healthcare Technology Letters*, *2*(1), 18–21. https://doi.org/10.1049/htl.2014.0098

CURRICULUM VITAE

PHOTO

Name Surname **:** Meltem TEKÇİN

Place and Date of Birth **:**

E-Mail **:**

EDUCATION **:**

- **B.Sc.** **:** 2014, İstanbul Technical University, Textile Technologies and Design Faculty, Textile Engineering Department
- **M.Sc.** **:** 2016, İstanbul Technical University, Textile Technologies and Design Faculty, Textile Engineering Department

PROFESSIONAL EXPERIENCE AND REWARDS:

- 2016-2017 Matesa Textile, Merchandiser.
- 2018-2023 İstanbul Technical University, Research Assistant.

PUBLICATIONS, PRESENTATIONS AND PATENTS ON THE THESIS:

- **Tekcin, M.,** Palandoken, M., Kursun, S. 2023. Wearable UHF-RFID sensor for wetness detection, *IEEE Access*, 11, 115179-115189.
- **Tekcin, M.,** Paker, S., Bahadir, S.K. 2022. UHF-RFID enabled wearable flexible printed sensor with antenna performance. *AEU*, 157, 154410.
- **Tekcin, M.,** Sayar, E., Yalcin, M.K., Bahadir, S.K. 2022. Wearable and Flexible Humidity Sensor Integrated to Disposable Diapers for Wetness Monitoring and Urinary Incontinence. *Electronics*, 11, 1025.
- **Tekcin, M.,** Sayar, E., Bahadır, S. K. 2022: Wearable and Flexible Humidity Sensor Fabrication using Pad Printing Technique. International Conference on Advanced Electrical and Electronics Engineering (ICAEEE), July 25, 2022 Athens, Greece.

- **Tekcin, M.,** Kuzubasoglu, B. A., Sayar, E., Yalcin, M. K., Bahadır, S. K. 2021: Performance Analysis of Wearable and Flexible Humidity Sensor Integrated to Face Mask for Respiration Monitoring. IEEE 3rd Eurasia Conference on IOT, Communication and Engineering (ECICE), October 29-31, 2021 Yunlin, Taiwan.

OTHER PUBLICATIONS, PRESENTATIONS AND PATENTS:

- **Tekcin, M.,** Hamzaoglu, D.R.T., Kursun, S. 2023. Flexible humidity sensor for smart agricultural applications, *Flex. Print. Electron*, 8 (3), 035003.
- Kuzubasoglu, B. A., **Tekcin, M.,** Bahadır, S. K. 2021. Chapter: Electronic Textiles (E-Textiles): Fabric Sensors and Material-Integrated Wearable Intelligent Systems, Encyclopedia of Sensors and Biosensors, vol. 3, Elsevier, pp. 80 – 100.
- **Tekçin, M.,** Atakan R., Mittilineos, S., Erben, T., Bahadır, S. K. 2019: Design of RFID Antennas using Embroidery Technique, EEMKON 2019-Electrical Electronics Engineering Congress, November 14-16, 2019 İstanbul, Turkey.
- Altay, P., Özcan, G., **Tekçin, M.,** Şahin, G., Çelik, S. 2018. Comparison of conventional and ultrasonic method for dyeing of spunbond polyester nonwoven fabric, *Ultrasonics Sonochemistry*, 42, 768-775.